

Master's Program in Chemical, Biochemical and Materials Engineering

Electrically Conductive Metal Organic Polymer: Synthesis and Characterization

Harambage Koshila Hiruni

Copyright ©2024 Harambage Koshila Hiruni

Author Harambage Koshila Hiruni		
Title of thesis Electrically conductive metal organic polymer: synthesis and characterization		
Programme Chemical, Biochemical and Materials Engineering		
Major Chemistry		
Thesis supervisor Prof. Maarit Karppinen		
Thesis advisor(s) Dr Malar Auxilia Francis and Mari Heikkinen, MSc		
Date 18.03.2025	Number of pages 93	Language English
<p>Abstract</p> <p>Thermoelectric materials are emerging as an important type of material that address the most critical topics today, such as energy efficiency and sustainability. They are used in various applications like power generation, thermal imaging, automobiles, solar cells, electronics cooling and wireless sensors. When a metal organic polymer is crystalline and extremely porous, it is referred to as a metal organic framework (MOF). The unique properties of metal organic materials, such as low thermal conductivity, high electrical conductivity and tunability make them suitable for use as thermoelectric materials.</p> <p>In this work, two synthesis methods were used to fabricate copper-ethylenetetra-thiolate (Cu-ETT), which is recognized as a metal organic polymer with thermoelectric properties. Atomic Layer Deposition (ALD)/Molecular Layer Deposition (MLD) technique was used to fabricate Cu-ETT thin films. Chemical synthesis method used to synthesize Cu-ETT bulk material. Literature on synthesis methods has discussed the importance of these methods. Also, the results were understood and interpreted by using existing literature.</p> <p>Bulk Cu-ETT material was synthesized using copper chloride dihydrate ($\text{CuCl}_2 \cdot 2\text{H}_2\text{O}$) as the secondary building unit (SBU) source, sodium methoxide (NaOMe) as the base and 1,3,4,6-tetrathiapentalene-2,5-dione (TPD) as the organic linker source. Thermoelectric properties of the synthesized Cu-ETT bulk material were studied in varying experimental conditions such as number of Cu equivalents, reaction temperature, and solvent. Clear differences in electrical conductivity, thermal conductivity and Seebeck coefficient were observed under various experimental conditions.</p> <p>Cu-ETT thin films were fabricated using two different lithium precursors as bases: lithium <i>tert</i>-butoxide ($\text{Li-O}t\text{Bu}$) and lithium bis(trimethylsilyl)amide (Li-HMDS). 1,3,4,6-tetrathiapentalene-2,5-dione (TPD) was used as the organic linker source and copper acetyl acetonate ($\text{Cu}(\text{acac})_2$) used as the SBU source. In ALD/MLD process, the optimized deposition temperature was 220 °C and precursor pulse/purge lengths were 4/16 s for $\text{Cu}(\text{acac})_2$ and Li-HMDS, 7/28 s for TPD. The electrical resistivity of the deposited Cu-ETT thin films was studied.</p>		
Keywords Metal organic polymer, ALD, MLD, chemical synthesis, electrical conductivity, thermoelectricity		

Table of contents

Preface and acknowledgements.....	3
Symbols and abbreviations	4
Symbols	4
Abbreviations	4
1 Introduction.....	6
2 Literature Section	8
2.1 Metal Organic Framework	8
2.1.1 Structural properties	9
2.1.2 Physical properties	11
2.1.3 Classification	12
2.2 Electrically Conductive MOFs.....	14
2.2.1 Mechanisms of electrical conductivity of EC-MOF	15
2.2.2 Design strategies and in situ modifications.....	22
2.2.3 Post synthetic modifications.....	28
2.2.4 Applications of electrically conductive MOFs	30
2.3 Synthesis of EC-MOFs	36
2.3.1 Chemical Synthesis of EC-MOF.....	36
2.3.2 Thin film fabrication of EC-MOF.....	38
3 Research goals	43
4 Experimental Section.....	45
4.1 Chemical synthesis.....	45
4.1.1 Reactant preparation.....	45
4.1.2 Synthesis methodology	45
4.2 ALD/MLD.....	47
4.2.1 Precursor preparation.....	47
4.2.2 ALD/MLD process.....	49
5 Characterization.....	50
5.1 Infrared Spectroscopy.....	50
5.2 X-ray methods	51
5.3 Spectroscopic ellipsometer	52
5.4 Thermoelectric measurements.....	52
5.5 Microscopy	53

5.6	Inductive Coupled Plasma- Optical Emission Spectroscopy	53
5.7	Elemental analyser	54
6	Results and discussion	55
6.1	Chemical synthesis.....	55
6.1.1	Purity and crystallinity phase.....	55
6.1.2	Chemistry of Cu-ETT bulk material	57
6.1.3	Thermoelectrical properties.....	61
6.2	ALD/MLD.....	66
6.2.1	Deposition process optimization for Cu-ETT.....	66
6.2.2	Chemistry of fabricated thin films	68
6.2.3	Thermoelectric properties of Cu-ETT thin films	74
6.2.4	Stability of Cu-ETT thin films	76
7	Conclusions and research suggestions	79
	References.....	83

Preface and acknowledgements

The research done in this thesis was conducted in Laboratory of Inorganic Chemistry at Aalto University School of Chemical Engineering during May-November 2024.

First and foremost, I want to express my gratitude to my supervisor, Aalto distinguished professor Maarit Karppinen for giving me this opportunity to work in her research group and for her guidance during the thesis. Secondly, I would like to thank my advisors Dr. Malar Francis and M.Sc. Mari Heikkinen for their assistance throughout this work and to get GI-XRD, Elementary analyzer measurements.

I also wish to thank Dr.Girish Tewari and M.Sc Ilkka Valimaa for their assistance with thermoelectric and ICP-OES measurements.

Special thanks to my husband Sameera for always being encouraging, patient and supportive.

Espoo, 18 March 2025
Harambage Koshila Hiruni

Symbols and abbreviations

Symbols

d	Dimensionality of the sample
e	elementary charge
n_e	charge density of electrons
n_h	charge density of holes
T	Temperature
T_o	Constant specific to material
S	Seebeck coefficient
s	Electrical conductivity
σ_o	Constant specific to material
σ	Electrical conductivity
m_e	charge mobility of electrons
m_h	charge mobility of holes
k	Thermal conductivity

Abbreviations

ALD	Atomic layer deposition
AT	Aminothiolo
ATR	Attenuated Total Reflectance
BDC	1,4-benzodicyclohexane-1,4-dicarboxylate
BHT	Benzene hexathiol
BTC	Benzene tricarboxylic acid
CP	Coordination polymer
CuPc	Copper phthalocyanine
DABCO	1,4-diazabicyclo-[2.2.2] octane
DFT	Density Functional Theory
DMF	Dimethylformamide
dhbq ^{2-/3-}	2,5-dioxidobenzoquinone
DSBDC ²⁻	2,5-disulfhydrylbenzene-1,4-dicarboxylate
DOBDC ²⁻	2,5-dihydroxybenzene-1,4-dicarboxylate
EC-MOF	Electrically conductive metal organic framework
ED-EPMA	Energy Dispersive Electron Probe X-ray Microanalysis
FET	Field effect transistors
FT-IR	Fourier Transform- Infrared
GIXRD	Grating Incidence X-ray Diffraction
GO	Graphene oxide
HAB	Hexaaminobenzene
HATP	Hexaaminotriphenylene
HER	Hydrogen evolution reaction
HHTC	2,3,8,9,14,15-hexahydroxyltribenzocyclyne
HHTP	2,3,6,7,10,11-hexahydroxytriphenylene

HAB	Hexaaminobenzene
HHTC	2,3,8,9,14,15-hexahydroxyltribenzocyclyne
HHTP	2,3,6,7,10,11-hexahydroxytriphenylene
HIB	Hexaiminobenzene
HITT	2,3,7,8,12,13-hexaiminotetraazanaphthotetraphene
HITP	2,3,6,7,10,11-hexaiminotriphenylene
HKUST-n	Hong Kong University of Science and Technology
HSAB	Hard and Soft Acid and Base theory
HTTP	2,3,6,7,10,11- hexathiol triphenylene
ICP-OES	Inductively Coupled Plasma- Optical Emission Spectroscopy
IT	Iminothiolato
IRMOF	Isorecticular metal organic framework
MeOH	Methanol
MIL MOF	Materials of Institute Lavoisier metal organic framework
MLD	Molecular layer deposition
MOF	Metal organic framework
NDI	Naphthalenediimide
NiDI	bis(diimino)nickel framework
NOTT- <i>n</i> MOF	University of Nottingham metal organic frameworks
NU MOF	Northwestern university metal organic framework
OER	Oxygen evolution reaction
OLED	Organic light emitting diodes
ORR	Oxygen reduction reaction
R.T	Room Temperature
RGO	Reduced graphene oxide
SBU	Secondary building unit
SEM	Scanning Electron Microscope
TTF	Tetrathiafulvalene
TTFTB	Tetrathiafulvalene tetra benzoate
Pc	Phthalocyanine
PCP	Porous coordination polymer
PCN	Porous coordination network
pdt	2,3-pyrazinedi- thiolate
PF	Power factor
POST- <i>n</i> MOF	Pohang University of Science and Technology metal organic framework
PSM	Post synthetic modifications
pyrazol-NDI	1,4-bis[(3,5-dimethyl)-pyrazol-4-yl]naphthalenediimide
UiO MOF	University of Oslo metal organic framework
XAFS	X-ray absorption fine structure
XPS	X-ray photoelectron spectroscopy
XRD	X-ray Diffraction
ZIF	Zeolitic Imidazolate Framework

1 Introduction

Thermoelectric materials are one of the specialized materials that can convert waste heat into electricity (Seebeck effect) or electricity into heat (Peltier effect). These materials address the most critical topics today, due to their energy efficiency and sustainability. Thermoelectric materials are used in various applications, such as power generation, thermal imaging, automobiles, solar cells, electronics cooling and wireless sensors.

Metal organic polymers are hybrid materials with characteristics that cannot be observed in either pure organic compounds or pure inorganic compounds. The unique properties of metal organic polymers such as low thermal conductivity, high electrical conductivity and tunability make them suitable as thermoelectric materials. Poly metal ethylenetetra-thiolate (poly(M-ETT)), where M stands for Cu or Ni, is a metal organic polymer with high electrical conductivity. This metal organic polymer compounds can be synthesized easily without any doping process, and they have low thermal conductivity due to their amorphous nature.[1] High electrical conductivity and low thermal conductivity are crucial properties for optimizing the performance of thermoelectric materials. The precursors for synthesizing Cu-ETT are comparatively less toxic, and p-type semiconductor behaviour can be observed with this compound.

Metal organic polymers with high porosity and crystallinity are known as metal organic frameworks (MOF).[2] Most of MOFs are considered as electrical insulators with electrical conductivity less than 10^{-10} S cm^{-1} at room temperature because of having no low energy pathways for charge transport and no free charge carriers.[3] In the literature, several design strategies have been proposed to introduce or enhance the electrical conductivity of MOFs.

The literature section of this thesis comprises two sections. The first section provides a general overview of MOFs, and a specific type of MOF called electrically conductive MOFs (EC-MOFs). EC-MOFs exhibit high electrical

conductivity in the range of 10^{-10} - 10^2 S cm^{-1} . [3] There are several approaches to designing EC-MOFs with different electrical conductivity mechanisms. The second section describes methods to synthesize EC-MOFs in the form of thin films and bulk materials.

In the experimental section of this thesis, two synthesis methods discussed in the literature section were used to fabricate Cu-ETT. Atomic Layer Deposition (ALD)/ Molecular Layer Deposition (MLD) technique has been used to fabricate Cu-ETT thin films. Thin films of thermoelectric materials have flexibility which is an important property for applications like wearable devices, microelectronic cooling. [4] Electrical conductivity of deposited Cu-ETT thin films was studied. Chemical synthesis method used to synthesize Cu-ETT bulk material. The thermoelectric properties of the synthesized Cu-ETT bulk material were studied under various experimental conditions.

2 Literature Section

2.1 Metal Organic Framework

Metal Organic Framework (MOF) is a material with crystallinity, high porosity, tunable structure, and large surface area.[5] [6] [7] MOFs are included into a large family of materials which is called coordination polymers (CPs) and the term MOF is used when the material is crystalline and highly porous.[2] MOFs consist of metal ions and organic ligands. Because of its organic-inorganic nature, MOF is considered as hybrid organic-inorganic material.

In 1995, a unique class of crystalline porous material was named ‘metal organic framework (MOF)’ by Omar Yaghi.[8] The golden era of MOF started in the late 1990s by exploring the synthesis pathway, X-ray single crystal determination, and gas absorption properties of MOF-5($Zn_4O(BDC)_3$) which is the first robust and porous metal organic framework.[9] The components and structure of MOF can be dictated to achieve the expected functionality used in a large array of applications like catalysis, gas sorption and separation, proton conductivity, and chemical sensors. These reasons have allowed to explore many MOF structures over the past decades and the amount of research publications related to MOF is continuously increasing.[6]

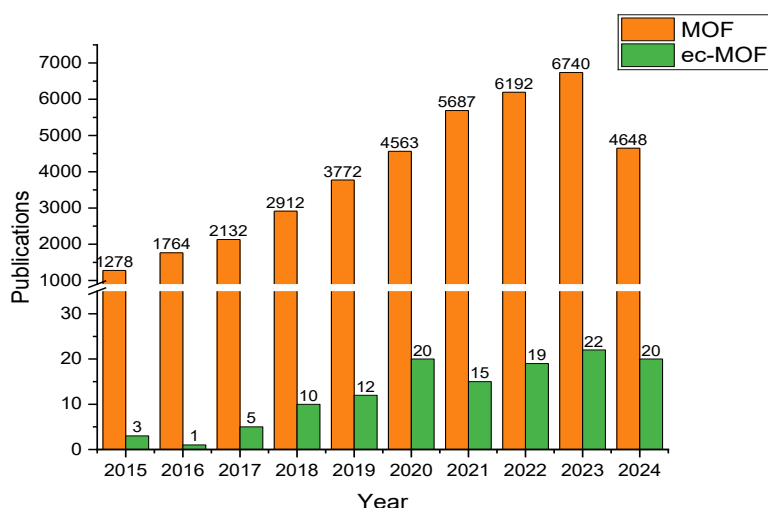


Figure 01. Annually published papers on MOFs and EC-MOFs. From Thomson Reuters Web of Science on 30.08.2024

2.1.1 Structural properties

The two main components of MOF are organic ligands and metal ions. They form strong chemical bonds to generate a periodic network of crystalline structures with permanent porosity of 1 dimension, 2 dimensions, or 3 dimensions. The properties of MOF not only depend on the type of organic ligand or metal ion but also on the way they connect with each other. An example of the MOF structure is shown in figure 02.

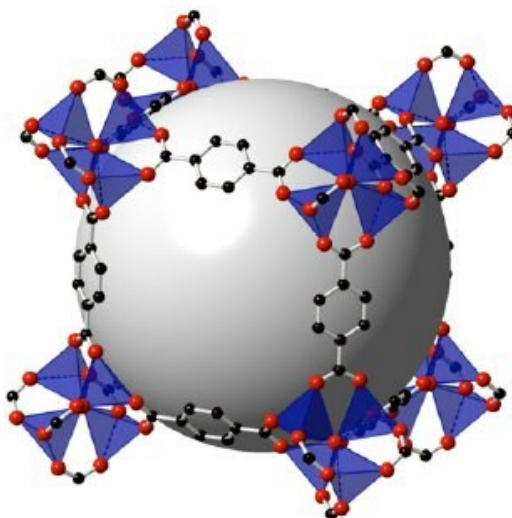


Figure 02. The structure of MOF-5, where the gray color sphere represents the porous space. The tetrahedron represents the coordination of 1,4-benzodicyboxylate (BDC) into zinc atom. Zn-O-C clusters at the corners are interconnected through benzene group. [10]

The organic ligand which is also known as organic linker is generally a bi, tri, or tetra dentate ligand. It includes a conjugate base of a carboxylic acid or an anion such as a heterocyclic compound, salt of sulfonic acid, or organophosphorus compound. [11]

Metal ions like Ti(IV), Sr(IV), Fe(III), Cr(III), Cu(II), Zn(II) and Ni(II) are frequently used as metal ions. Tetravalent metal ions like Ti(IV) and Zr(IV) form strong coordination bonds with organic linkers and these tetravalent metal ions are widely used to synthesize water stable MOFs. Trivalent metal ions like Fe(III), Cr(III) with oxygen containing ligands form more coordination bonds

resulting in high thermal and chemical stability of the MOF. Divalent metals like Cu(II), Ni(II), Zn(II) form weak coordination bonds with carboxylic acid ligands. Due to that reason, the water stability of the resulting MOF is very low. [12] Metal clusters consist of a group of metal ions connected by multi-tooth functional groups. These metal clusters are known as Secondary Building Unit (SBU).[13] Figure 03 shows some common SBUs used for MOF preparation.

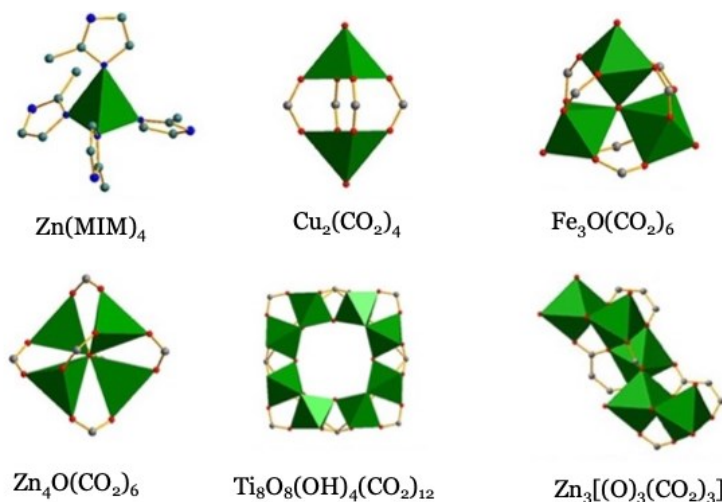


Figure 03. Some common SBUs used for MOF preparation[6]

The geometry of MOF is dependent on the ligancy, character of the organic linker, and analytical geometry of the metal ion or cluster. Different types based on shapes can be seen in MOFs like triangle, square paddle wheel, trigonal prisms, and octahedron. [11]

On comparison to zeolite and other porous materials, MOFs are especially superior due to high surface area, tunability, and exceptional porosity. The surface area of MOF ranges beyond Langmuir surface area of 10,000 m²/g. This high surface area is important in applications like sensors, storage, separation, and drug delivery. [14] The geometry and the size of the secondary building unit and size of the organic linker can dictate the pore size, shape and functionality to a certain degree for a specific application. [12]As an example, Yaghi et al. in their article have explored that isoreticular series of MOF(IRMOF)-74 can be constructed by systematic expansion of the ligand structure, from its original link of one phenylene ring (IRMOF-74-I) to eleven phenylene rings

(IRMOF-74-XI) respectively with pore size ranging from 14 to 98 Å. In this series, microporous IRMOF-74-I can accommodate small gas molecules like N₂, and macroporous IRMOF-74-VII and IRMOF-74-IX can accommodate protein molecules. [16]

The inner pore of the MOF can be filled with guest molecules such as nano particles, organic dyes, polymers and small enzymes. The applications of MOF can extend with guest molecules which cannot be reached with a single MOF. [6] This concept plays a crucial role in applications like gas storage and separation.

2.1.2 Physical properties

Because of organic-inorganic nature, MOF has achieved special characteristics which cannot be observed in either in pure organic or inorganic compounds. For example, higher thermal stability can be observed in MOFs than pure organic polymers and a higher degree of mechanical stability than in pure inorganic materials. Due to the porosity, MOFs have high mechanical stability to a certain extent under applied pressure. But under high compressive loading, MOF can undergo phase changes and even amorphization. [14]

The research studies towards increasing the MOF stability under water and heat have achieved progress during recent years. During the degradation of MOF in the presence of water, metal-coordinated linkers of MOF are replaced by water or hydroxide. By increasing the strength of the coordination bonds between SBU and organic linker, the stability of MOF can be improved. As an example, chromium based MIL (Materials of Institute Lavoisier)-101 series have high water stability due to strong coordination bonds between Cr(III)-O in the carboxylate group of terephthalate ligands. Another example is, UiO(University of Oslo)-66 has achieved higher water stability by having a strong coordination bond between Zr(IV)-O in terephthalate dicarboxylate linker. Another approach is to create hydrophobic surfaces or interfaces in MOF to increase water stability. [15]

Most MOFs are stable up to 400 °C and some MOFs like MIL-53 is stable even at higher temperatures of about 500 °C. The thermal stability of MOF depends on the bond strength of metal node-organic linker and the number of organic linkers connected to a metal node. MOFs with high valence metal ions such as Al³⁺, Ti⁴⁺ have high thermal stability. [6]

2.1.3 Classification

To date, tens of thousands of MOFs with various structures and compositions have been synthesized. MOFs have been classified based on different methods to utilize them more efficiently and rapidly.[19]MOF can be divided into categories based on the dimension of the skeleton, component unit, and application.

2.1.3.1 Classification based on dimension of the skeleton

Based on the composition of the complex skeleton, MOF can be classified as 1-dimensional(1D), 2-dimensional(2D), and 3-dimensional (3D) skeletons. Figure 04 shows the examples of different structural dimensionalities of MOF skeletons.

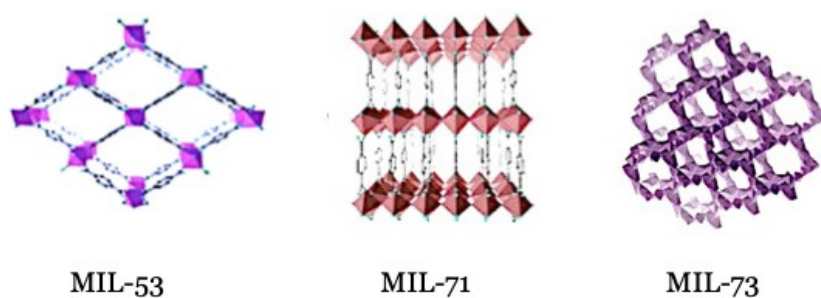


Figure 04. Schematic diagram of MOFs, MIL-53, MIL-71 and MIL-73 as examples for 1 D, 2 D and 3 D MOFs respectively [20]

1D MOFs exist as fibers or nanorods and they can extend to infinity along one direction. 2D MOFs exist as membranes or thin films. Advances in MOFs are

more focused on 2D MOFs due to highly ordered pore structure and processing of abundant active sites. 3D MOFs exist as continuous and extended materials. There are various types of 3D MOFs, and the structure is more complex like cubic type, molecular sieve type, and diamond like.

Although this classification method summarizes the structural characteristics of MOFs, only the skeleton information cannot distinguish the composition of MOF, type of SBU, and organic linker.[19]

2.1.3.2 Classification based on component unit

Based on the component unit, MOFs can be divided into various categories like IRMOF, Zeolitic Imidazolate Frameworks (ZIF), MIL MOFs, Porous Coordination Polymers (PCPs), and UiO MOFs.

Isorecticular MOFs are octahedral microporous materials. They have the same structural topology as zeolite. The structure of these compounds consists of nitrogen containing tetrahedrons connected to imidazole rings with various functional groups surrounding the metal ions like Fe, Cu, and Zn. MIL MOFs contain two carboxylic functional groups as organic linker. PCPs have transition metal ions as secondary building units and carboxylic acid, pyridine and its derivatives as organic linkers. [11] UiO MOFs consist of Zr^{4+} as the secondary building units and carboxylic acid as the organic linkers. UiO MOF series have active Zr-O clusters. [21]

Other than the above compounds various MOFs like Porous Coordination Network (PCN), Northwestern University (NU), Pohang University of Science and Technology (POST-*n*), University of Nottingham (NOTT-*n*) and Hong Kong University of Science, and Technology (HKUST-*n*) have been reported recently. [11]

2.2 Electrically Conductive MOFs

Electrically conductive metal organic frameworks (EC-MOFs) have the intrinsic ability of electrical conduction with the tunability and high porosity. Most of MOFs are considered as electrical insulators with electrical conductivity less than 10^{-10} S cm^{-1} at room temperature because of having no low energy pathways for charge transport and no free charge carriers. Normally, electrical conductivity of reported MOFs ranged from 10^{-10} - 10^2 S cm^{-1} . [3]

The first EC-MOF has been reported by Takaishi et al. in 2009. They have synthesized MOF $\text{Cu}[\text{Cu}(\text{pdt})_2]^-$ (pdt = 2,3-pyrazinedi-thiolate) as a 3D porous MOF with electrical conductivity of 6×10^{-4} S cm^{-1} at 300 K. To achieve the electrically conductive property Takaishi et al. have used electron donors and acceptors as building unit, Cu(I) as electron donor and $[\text{Cu}^{\text{III}}(\text{pdt})_2]$ as electron acceptor. A significant improvement in EC-MOF can be observed recently with the development of molecular designing. [22][23] Different metals such as transition metals, lanthanides are used as SBUs in EC-MOFs. Figure 05 shows number of publications of various metals as SBUs in electrically conductive MOFs.

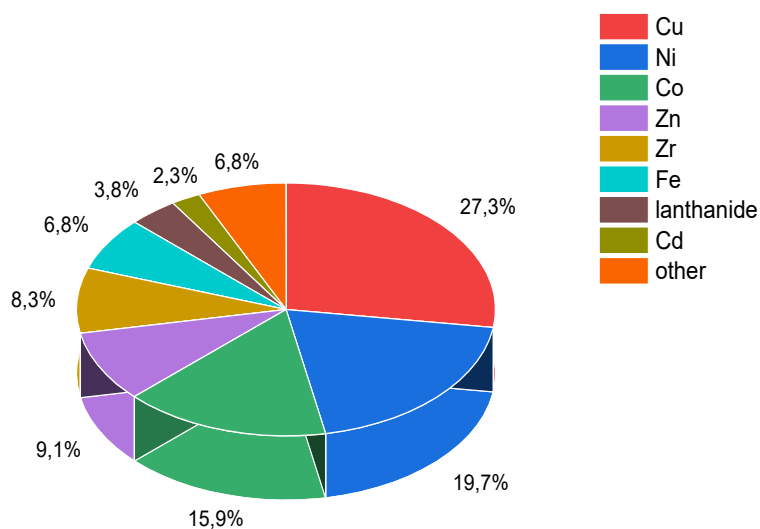


Figure 05. Division of number of publications of metals as SBUs in electrically conductive MOFs. From Thomson Reuters Web of Science on 16.08.2024

2.2.1 Mechanisms of electrical conductivity of EC-MOF

The electrical conductivity of a material quantifies the ability to transfer electrical charge. The SI unit of electrical conductivity is Siemen's per meter ($S m^{-1}$). Electrical conductivity (σ) is usually defined as follows[24]:

$$\sigma = e(\mu_e n_e + \mu_h n_h) \quad (1)$$

Where e is elementary charge ($1.602 \times 10^{-19} C$), n_e is the charge density of electrons, n_h is charge density of holes, μ_e is charge mobility of electrons and μ_h is the charge mobility of holes.

According to this equation, to achieve a higher electrical conductivity, both high charge density and high charge mobility are required. The charge density of a material is increased when increasing the concentration of loosely bound charge carriers. Both SBU and organic ligand can be source of charge carriers in MOF. When the SBU is the charge carrier, metal ion should have high energy electrons or holes. As an example, square planar d^9 Cu^{II} metal ion centre has high energy unpaired electrons. When organic linker is the charge carrier, it should have stable radicals to provide unpaired electrons or should be a redox active molecule to makes charge transfer between metal ions.[24]

Band theory figure out the approaches to enhance the charge density of MOF and helps to understand the electronic structure. Generally, band structures for MOFs are computed with Density Functional Theory (DFT) calculations and they are referenced to the electrostatic potential of the pore. In metallic MOFs, conduction band and valence band have overlapped or have a small band gap enabling easy movement of charge carriers(electrons) from valence band to conduction band resulting high charge density which leads to high electrical conductivity. Figure 06 shows electronic structure of metallic MOF, $Ni_3(HIB)_2$. In semiconducting and insulating MOFs, Fermi level lies in the band gap between conduction band and valence band, where $Zn_4O(BDC)_3$ with

a large band gap which is 4.6 eV as an example for insulator and less band gap $Zn_2(TTFTB)$ as an example for semiconductor.[24] [25]

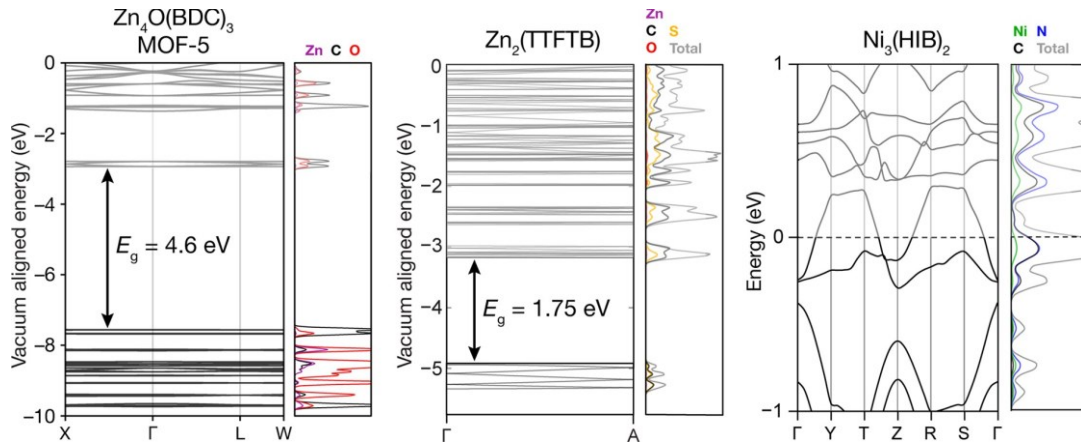


Figure 06. Calculated band structure and density of states of insulator, semiconductor and metallic MOF respectively $Zn_4O(BDC)_3$ [26], $Zn_2(TTFTB)$ [27] and $Ni_3(HIB)_2$ [25]

Charge mobility indicates the efficiency of charge transport. Mainly there are 3 types of charge transport mechanisms can be operative in MOFs which are hopping transport, through bond approach and through space approach as shown in figure 07.

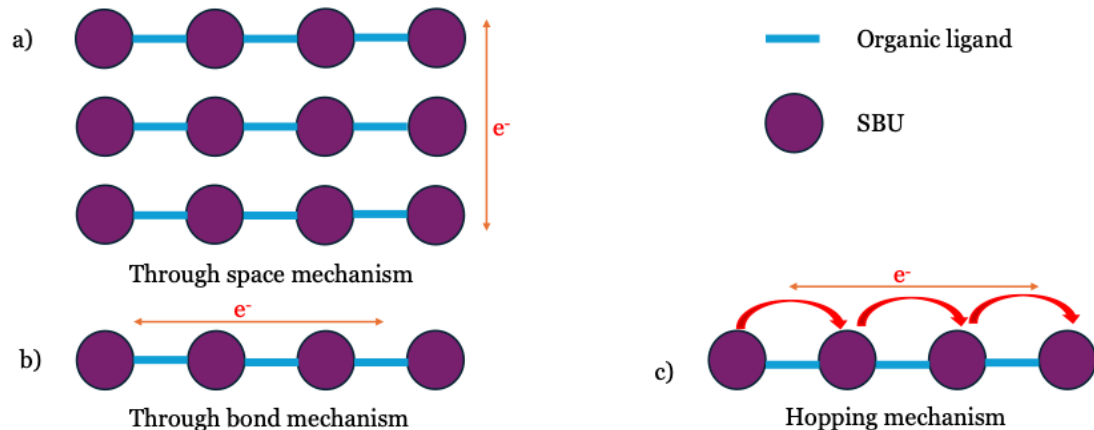


Figure 07. Schematic diagram of through space, through bond and hopping charge transport mechanisms[28]

Through bond approach and through space approach are based on band transport.[27] Band transport can be both thermally activated and deactivated dependant on the type of material. In metals with higher concentration of charge carriers, different types of scattering processes occur with high

temperature which leads to less efficiency in charge transport. This makes to decrease electrically conductivity while increasing temperature. Only few of MOFs have been identified as metallic. In semiconductors, conductivity is limited by carrier concentration which are free electrons or holes. When the temperature is increasing, more free electrons and holes are generated resulting high electrical conductivity. [3]

2.2.1.1 Through bond approach

Through bond approach for electron transport can be seen in MOFs with $(-M-X-)_n$ lattices (where M is the metal ion and X is the donor atom of the functional group of organic linker). Through bond electron transport mechanism is independent of the ligand backbone. In this approach, charge transport occurred by favourable energetic and spatial overlap of metal and donor atom of the ligand orbitals. Charge is moved through continuous chains of coordination and covalent bonds in the lattice. By combining soft donor atoms such as S, P and Se with transition metal ions, it can promote electrical conductivity via through bond approach. Through bond approach can be observed in 2D MOFs with extended π conjugated system and MOFs with redox active organic linker and metal ion. [27]

As an example, Figure 08 shows 3 D structure of $Cu[Cu(pdt)]$ and $Cu[Ni(pdt)]$ MOFs which are highly electrically conductive due to covalent character of metal-sulphur bond that contributes for charge transport. In the first reported conductive MOF, $Cu[Cu(pdt)_2]$, Cu(II) ions are bridged to each other through pdt ligand forming 2-D sheet. These 2 D sheets are interconnected with each other via copper bis(dithiolene) while forming a 3 D structure.[24] [23]Figure 08(b) shows single Cu(pyrazine) 2D sheet in $Cu[Ni(pdt)]$.[23]

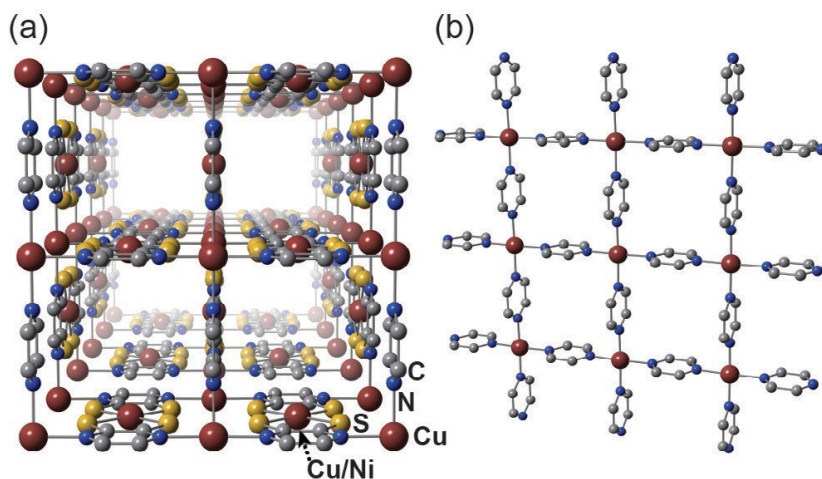


Figure 08. a) 3D structure of Cu[Ni(pdt)₂] and Cu[Cu(pdt)₂], b) Single Cu(pyrazine) 2D sheet in Cu[Ni(pdt)][21]

The shortest length between two parallel pdt ligands is 6.82 Å which is higher than Van der Waals bond distance. Because of that it makes impossible for through space charge transfer. d⁹ Cu(II) has high energy unpaired electrons and it increase the charge density of this MOF. Due to that, charge transfer occurs through Cu(pyrazine) 2D sheets via Cu(II) bis(dithiolene) generating high electrical conductivity. [22]

Kobayashi et al. have replaced Cu(pdt)₂²⁻ with Ni(pdt)₂²⁻ in Cu[Cu(pdt)₂] and synthesized Cu[Ni(pdt)₂]. For Cu[Cu(pdt)₂] electrical conductivity was observed as 1 x 10⁻⁴ S cm⁻¹ and a huge reduction in electrical conductivity for Cu[Ni(pdt)₂] MOF as 1 x 10⁻⁸ S cm⁻¹ at room temperature. This low electrical conductivity is a result of lower charge density which arise by replacing half of Cu(II) d⁹ sites with Ni(II) d⁸. Also, Kobayashi et al. have observed a lower electrochemical potential for [Ni(pdt)₂]^{2-/1-} as 0.257 V which is a less negative value than for [Cu(pdt)₂]^{2-/1-}. It indicates that the weak oxidizing capability makes Ni(II) d⁸ to not provide high energy electrons as charge carriers. [30]

2.2.1.2 Through space approach

In through space approach, charge transport promotes through non-covalent interactions like π - π stacking between organic ligands by overlapping orbitals of ligands while creating extended charge transport pathway. Through space charge transport can be observed in MOFs with metal-ligand bonds with interplanar distance less than 3.5 Å. Stable organic radicals have identified as the most suitable component as organic linker because they provide free charge carriers and induce the charge density. [24], [32]

Park et al. have developed $M_2(\text{TTFTB})$ ($M = \text{Mn, Zn, Co}$ and Cd). As shown in figure 09, all these 4 types of MOFs are isostructural, and TTF molecules form π - π stacked 1D helical columns with short S-S distances between neighbouring TTF moieties. [27]

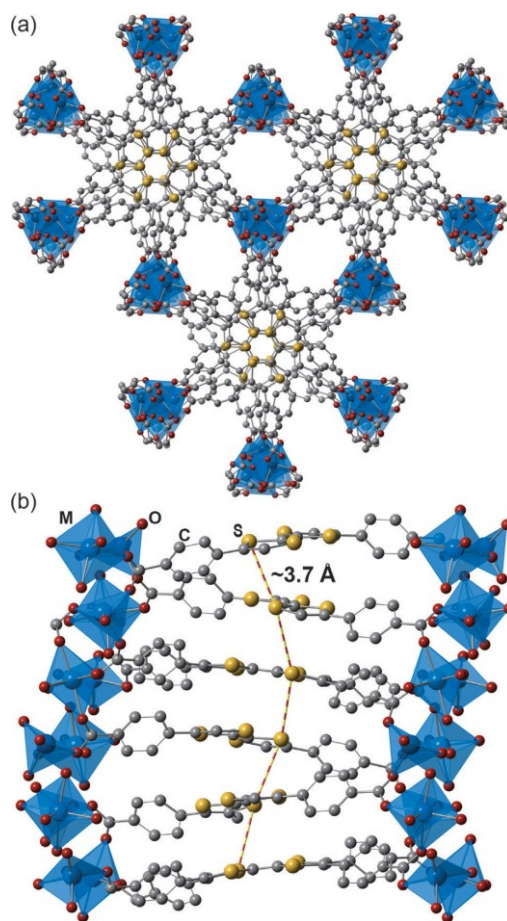


Figure 09. (a) structure of $M_2(\text{TTFTB})$ ($M = \text{Mn, Zn, Co}$ and Cd) (b) side view of 1D helical columns of TTF moieties with short S-S distance. [24]

In the as-synthesized material in $M_2(\text{TTFTB})$, TTF groups can be partially oxidized to radical cations which leads to increasing charge density. Single crystal conductivity values for $\text{Zn}_2(\text{TTFTB})$ $3.95 \times 10^{-6} \text{ S cm}^{-1}$ and, $\text{Co}_2(\text{TTFTB})$ $1.49 \times 10^{-5} \text{ S cm}^{-1}$, for $\text{Mn}_2(\text{TTFTB})$ $8.64 \times 10^{-5} \text{ S cm}^{-1}$ and for $\text{Cd}_2(\text{TTFTB})$ $2.86 \times 10^{-4} \text{ S cm}^{-1}$ at room temperature. The conductivity is correlated with the ionic radii of the metal cations. When increasing the ionic radii, conductivity value also increases. But metal carboxylate chains do not contribute to the charge transfer. Park et al. have explained in their article, when increasing the ionic radii of the metal cation, the length of the metal-carboxylate chain is increased and thereby TTF stack is pinched leading to shorter S...S distance. S...S distances have been observed for $\text{Zn}_2(\text{TTFTB})$ 3.75 \AA and $\text{Co}_2(\text{TTFTB})$ 3.77 \AA , for $\text{Mn}_2(\text{TTFTB})$ 3.69 \AA and for $\text{Cd}_2(\text{TTFTB})$ 3.65 \AA . By decreasing the S...S distance between neighbouring TTF moieties, the orbital overlap of $3p_z$ orbitals of sulphur can be increased which involve in charge transport, resulting higher electrical conductivity. [27]

2.2.1.3 Hopping transport

In the absence of band like transport mechanism, charge transport by electron hopping between molecular sites with various redox states. This mechanism is promoted in the presence of weak metal-ligand overlap or metal-orbital overlap nature is ionic. During hopping transport, localized electrons jump between redox active sites. [33] To achieve a higher redox conductivity equal amount of reduced and oxidized sites need to be present at the standard potential according to the Nernst equation. Because the probability of a single electron hopping depend on the availability of a neighbouring acceptor site. [34] Hopping transport is always thermally activated indicating that high temperature leads to high conductivity. This temperature dependency can be explained by the exponential law as follows:

$$\sigma = \sigma_0 \exp [-(T_0/T)^{1/d}] \quad (2)$$

Where T is the temperature, d is the dimensionality of the sample, T_0 and σ_0 are constants specific to the material.[3]

As an example, Li et al. in their work have selected Zn(pyrazol-NDI) (where pyrazol-NDI stands for pyrazol-NDI = 1,4-bis[(3,5-dimethyl)-pyrazol-4-yl]naphthalenediimide) as the model to investigate the redox hopping mechanism and they have deposited Zn(pyrazol-NDI) thin film on FTO. Figure 10 shows schematic diagram of the structure of Zn(pyrazol-NDI). This MOF consists of tetrahedral d^{10} Zn(II) and redox active NDI as the organic linker. Due to coordination environment of this MOF, π - π orbital overlap between neighbouring organic linker or metal-ligand orbital overlap(d - π) are not possible. It makes the charge transport mechanism of this MOF to become redox hopping transport. During the charge transport, NDI organic linker undergo 2 sequential one electron reduction reactions such as half of NDI reduced to $\text{NDI}^{\cdot-}$ or half of $\text{NDI}^{\cdot-}$ reduced to NDI^{2-} resulting high redox conductivity. [34]

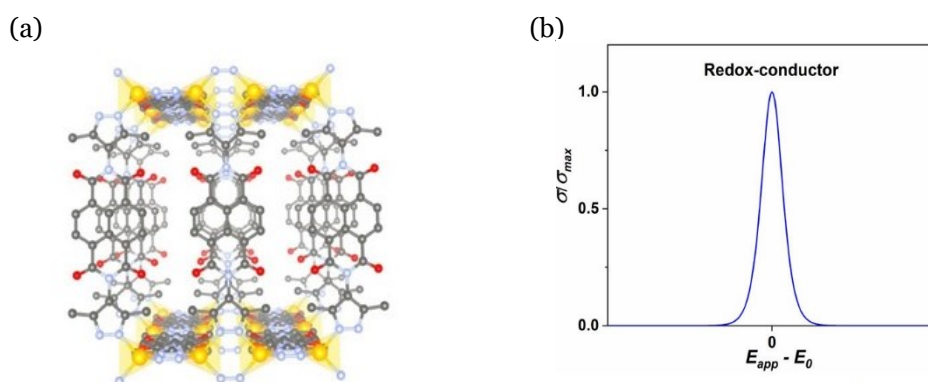


Figure 10. (a) Diagram of Zn(pyrazol-NDI) MOF with organic linker to linker localized redox hopping; C, N, O, and Zn atoms presented by gray, blue, red, and brown color spheres, respectively. (b) Bell-shaped distribution of redox conductivity of Zn(pyrazol-NDI) MOF.[34]

In this study using UV visible Spectro electrochemistry, Li et al. monitored the redox states of the thin film and experimentally demonstrated the potential dependent bell-shaped distribution of conductivity as a function of redox state of the MOF. As shown in figure 10(b), characteristic bell-shaped curve can be

observed only in the materials which charge transport occurred through redox hopping mechanism. [34]

2.2.2 Design strategies and in situ modifications

Design strategies and in situ modifications play important roles when synthesizing electrically conductive MOFs. According to the mechanisms discussed in section 2.1.1, to be an electrically conductive MOF it requires delocalization of charges within the MOF while promoting long range charge transport pathway. Charge delocalization can be generated by delocalized ligand or charge hopping between adjacent metal node and organic linker. [35]

Electrical conductivity of MOF is also depended on the metal ion, because the size and electronic structure of metal ion are capable to change the intermolecular contacts and thereby electrical conductivity. Generally, transition metal ions with unpaired electrons such as Fe, Cu, Co, Ni, Zn are used as metal component in electrically conductive MOFs to generate π interactions with organic linker. To show the dependency of electronic structure of metal ion for electrical conductivity, Ziebel et al. have carried out research in 2018. They have synthesized 3 isostructural 2 D MOFs which are $(\text{H}_2\text{NMe}_2)_2[\text{M}_2(\text{C}_6\text{O}_4\text{Cl}_2)_3]$ where $\text{M}=\text{Ti}$, V and, $(\text{H}_2\text{NMe}_2)_{1.5}[\text{Cr}_2(\text{C}_6\text{O}_4\text{Cl}_2)_3]$. Electrical conductivities for Ti, V and Cr containing MOFs reported as $2.7 \times 10^{-3} \text{ S cm}^{-1}$, 0.45 S cm^{-1} , and $1.2 \times 10^{-4} \text{ S cm}^{-1}$ respectively at room temperature. Thermal dependency of conductivity with temperature have shown that conductivities of Cr and Ti have generated because of redox hopping between neighbouring organic ligand in various valence states. Comparatively high conductivity of V containing MOF is due to variable range hopping mechanism for charge transport. [36]

Valence state of metal ion also has an impact on electrical conductivity by facilitating the electron transfer. As an example, metal ions with lower valence state have more free electrons (Fe^{2+} compared to Fe^{3+}) to charge transfer, thereby enhance the electrical conductivity. [37]

Organic linkers with extended π conjugated system have excellent electron transport pathways and ability to enhance long range charge mobility. Organic ligands based on coronene, phthalocyanine, benzene, anthracene, naphthalene and tri-phenylene which consist of conjugated π electron system are commonly used as organic linkers in EC-MOFs. [28]

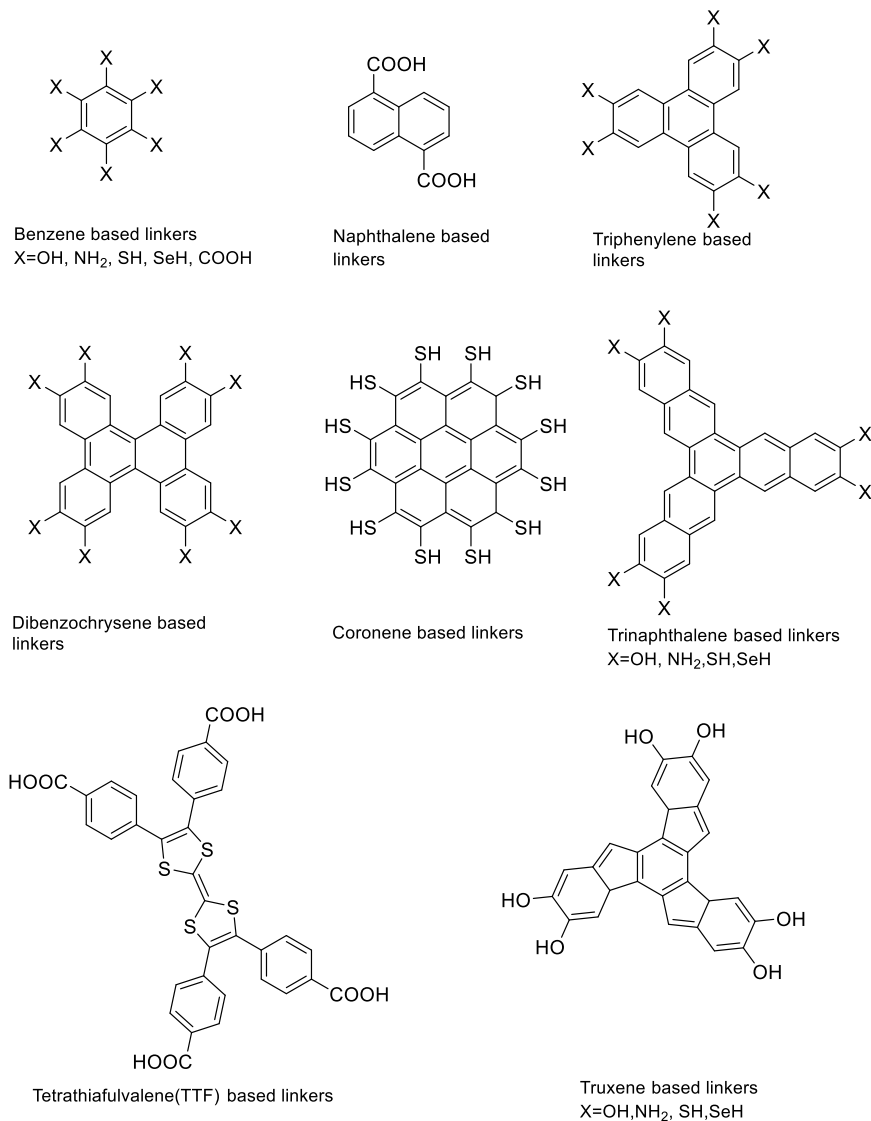


Figure 11. Representative organic linkers for electrically conductive MOFs[28]

According to the hopping transfer mechanism which discussed in chapter 2.2.1.3, it can enhance the electrical conductivity of MOF by improving charge transport and modulating the charge transfer. By introducing metal ions with different oxidation states as the metal nodes or varying oxidation states of

organic linkers help to increase the electrical conductivity. This concept is called as mixed valency and when mixed valency is present, it induces the hopping type of charge mobility and charge mobility on neighbouring atoms. Fe(II)/(II) and Cu(I)/(II) are some of commonly used redox couples as mixed valence metal ions. As an example for mixed valency in metal nodes, Feng et al. have explored mixed valence Cu-BHT (where BHT stands for benzenehexathiols) with a higher electrical conductivity of 95 S cm^{-1} at room temperature. In Cu-BHT, Cu atom shows mixed valency of $\text{Cu}^+/\text{Cu}^{+2}$ due to the defect state. In the conjugated structure, Cu^+ existed because of partial reduction of Cu^{2+} . According to the XAFS (X-ray absorption fine structure) and XPS (X-ray photoelectron spectroscopy) studies, Cu atoms are coordinated with S atoms in benzene rings and form a π -d conjugated structure. This π -d conjugated structure allows delocalization of charge carriers in the plane. Due to the mixed valency of $\text{Cu}^+/\text{Cu}^{+2}$, carrier mobility of neighbouring atoms is increased resulting high electrical conductivity. [38] As an example for mixed valency in organic ligand, Darago et al. have synthesized $(\text{NBu}_4)_2[\text{Fe}^{\text{III}}_2(\text{d}(\text{h}(\text{b}(\text{q}))_3)]$ ($\text{d}(\text{h}(\text{b}(\text{q}))_3^{2-}/3^- = 2,5$ -dioxidobenzoquinone) MOF and $\text{Na}_{0.9}(\text{NBu}_4)_{1.8}[\text{Fe}^{\text{III}}_2(\text{d}(\text{h}(\text{b}(\text{q}))_3]$ as oxidized and reduced species respectively. $\text{D}(\text{h}(\text{b}(\text{q}))_3^{n-}$ is the organic ligand in this MOF. According to the conductivity measurements, conductivity of oxidized species and reduced species are 0.16 and 0.0062 S cm^{-1} at 298 K respectively. The reason for it is the number of $\text{d}(\text{h}(\text{b}(\text{q}))_3^{2-}$ vacancies increases due to reduction and then unpaired electron of $\text{d}(\text{h}(\text{b}(\text{q}))_3^{3-}$ hop into the neighbour $\text{d}(\text{h}(\text{b}(\text{q}))_3^{2-}$ vacancies. These results lowering carrier mobility and thereby low electrical conductivity. [29]

Dimension is another parameter which affects to the electrical conductivity of MOF. Dimension determines the pathway of moving charge carriers. Most of 2D MOFs have shown higher electrical conductivity compared to other dimensions due to extended π conjugations in the 2D layers which mediated by electron moving through the metal ions and in plane charge delocalization. [39] 2D honeycomb lattice exhibit high electrical conductivity due to high charge density in the lattice. These honeycomb structures are formed by coordinating planar metal centres (ex: Cu(II), Ni(II)) to organic linkers which are based on

benzene or triphenylene(ex: HTTP-2,3,6,7,10,11- hexathiol triphenylene). Nickel bis(dithiolene) is an example of 2D honeycomb structure which synthesized from coordination reaction of BHT and Ni(II)acetate.[40]Figure 12 shows the chemical structure and schematic diagram of honeycomb lattice of Ni(II)acetate.

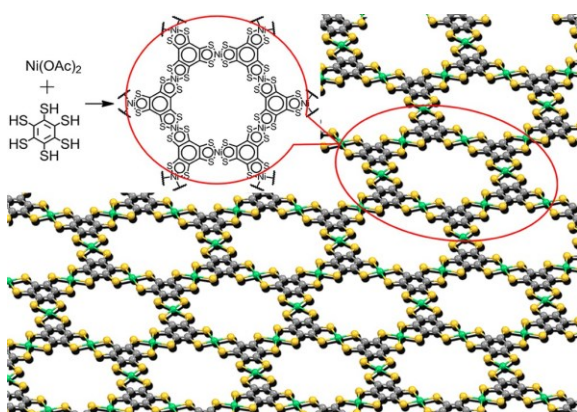


Figure 12. Chemical structure and schematic diagram of Nickel bis(dithiolene)[40]

When designing electrically conductive MOFs it is important to consider about coordinating atom/chelating atom which involve in charge transport. Most commonly N, O and S atoms are used as coordination atoms in MOFs. [41], [42] Incorporating harder chelating atoms (ex: O atom) into a softer metal ion results energy gaps and trapped valence state which reduce the conductivity. Incorporating softer chelating atoms like N, S results covalent bonding and thereby increase the conductivity. Therefore, it is important to control the hardness and softness of metals and chelating atoms. [43]As an example, Sun et al. have synthesized MOF-74 structure (M=Mn and Fe metals) with the formula of $M_2(\text{DOBDC})$, $M_2(\text{DSBDC})$ (where DSBDC²⁻ stands for 2,5-disulfhydrylbenzene-1,4-dicarboxylate and DOBDC²⁻ stands for 2,5-dihydroxybenzene-1,4-dicarboxylate) and the SBU is consisted of $(-M-O)_\infty$ and $(-M-S)_\infty$ chains respectively. There, pair of metal atoms have bridged with a phenolate group and thiophenolate group and the coordinating atom in $M_2(\text{DOBDC})$ is oxygen and in $M_2(\text{DSBDC})$ is sulphur. [42]

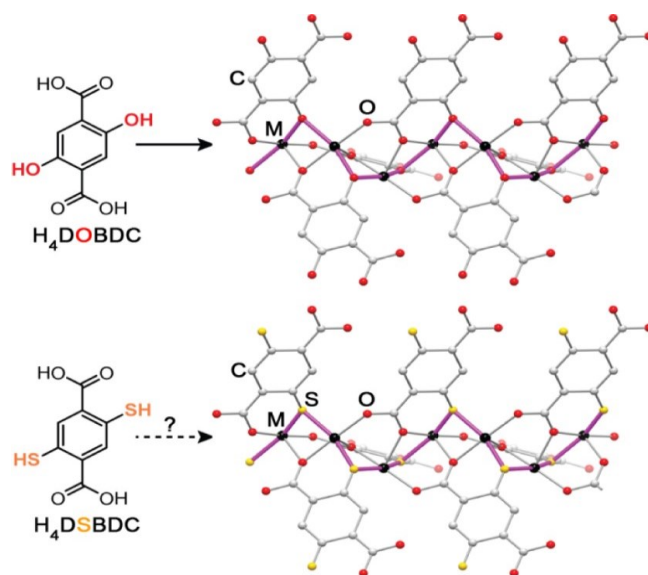


Figure 13. Schematic diagram of $(-M-O)_\mu$ chain and $(-M-S)_\mu$ chain. Purple line indicates infinite $(-M-O)_\mu$ chain in $M_2(\text{DOBDC})$ and $(-M-S)_\mu$ chain in $M_2(\text{DSBDC})$ [42]

The conductivity of $\text{Fe}_2(\text{DOBDC})$ and $\text{Mn}_2(\text{DOBDC})$ were recorded as $3.2 \times 10^{-7} \text{ S cm}^{-1}$ and $3.9 \times 10^{-13} \text{ S cm}^{-1}$ respectively. By substituting hydroxyls with thiols, the conductivity of $\text{Fe}_2(\text{DSBDC})$ and $\text{Mn}_2(\text{DSBDC})$ are $2.5 \times 10^{-12} \text{ S cm}^{-1}$, $3.9 \times 10^{-6} \text{ S cm}^{-1}$ respectively. By replacing phenolate groups with thiophenolate groups result in high charge mobility, thereby high conductivity in $M_2(\text{DSBDC})$ than $M_2(\text{DOBDC})$. Also, in both cases $\text{Fe}_2(\text{DOBDC})$ and $\text{Fe}_2(\text{DSBDC})$ show higher conductive value and the reason for it is, Fe^{2+} has loosely bound β spin d electron which could provide overlap between ligand orbitals and d orbitals in metal resulting efficient electron delocalization. Due to that there is a better charge transfer in the MOF framework generating electrical conductivity. But Mn^{2+} has half-filled d electron configuration resulting localized electron structure and therefore not efficient in charge transport within the MOF. Also, it can observe that, when having sulphur as the coordinating atom it shows high conductivity than oxygen in both cases, $M=\text{Mn}$ and Fe .[42]

Other than the above discussed parameters morphological factors such as size, surface area, crystal structure and orientation affect the electrical conductivity of MOF to some extent. When it is considering about particle size, electrically

EC-MOFs with less particles size can enhance the grain boundaries which act as sites of electron tunnelling and scattering, thereby affect the electrical conductivity of MOF. A higher surface area of MOF leads to incomplete coordination and defects on the surface that serve as scattering centres reducing conductivity. On the other hand, large surface area can increase the impurity doping and thereby enhance the electrical conductivity. [44] Crystal structure and orientation also effects to the conductivity of MOF. When the MOF has single crystalline structure, it has longer electron transfer pathways and lower resistance leading to a high conductivity. When the structure is polycrystalline it has grain boundaries and scattering, and these grain boundaries reduce conductivity. During the MOF synthesise impurities and defects can be introduced which can alter the electron transport and thereby electrical conductivity. [45][46]

Fabricating MOF-Carbon composites is another method to enhance the electrical conductivity. In this method MOF can be hybridized with carbon containing compounds such as graphene, carbon nanotubes or graphene oxide (GO) to enhance the charge transfer reaction. Kim et al. have fabricated composites of ZIF-8 with GO and reduced graphene oxide (RGO) by mixing precursors of ZIF-8 MOF with GO and RGO powder separately. GO/ZIF-8 acts as an insulating material because both GO and ZIF-8 show insulating properties. But ZIF-8/RGO has exhibited 64 S m^{-1} electrical conductivity because of the presence of RGO. According to that, electrical conductivity property has been introduced to an insulating MOF upon combining with a conductive material. Also, they have observed that only 2.5 wt% of RGO can introduce conductivity (2 S m^{-1}) to RGO/ZIF-8. [47]

Introducing guest is considered as one of a charge transport pathway, which is an in-situ modification in MOFs to enhance the electrical conductivity. In the templated in situ modification, guest component is mixed with organic linker and metal ion during the synthesise process of MOF. As shown in figure 14, MOF (the host) build around the guest molecule and the guest molecules remain in the pore of the MOF via weak interactions, coordinated to the

functional groups of the organic linker or metal ions. In situ modification of inserting guest species into MOFs helps to insert guest species larger in size than the pore of MOF, thereby restrict the removal/insertion of guests. [48]

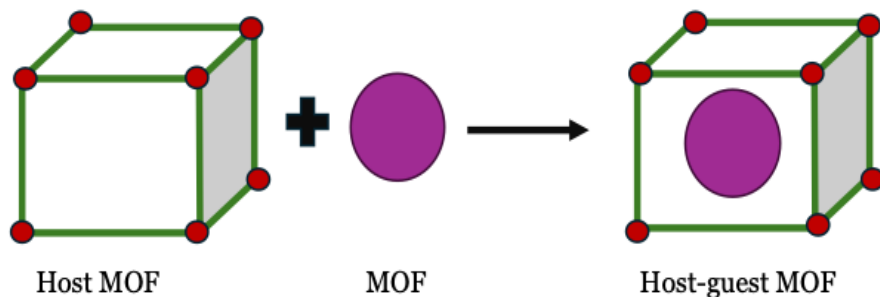


Figure 14. Schematic diagram of host-guest interaction of MOF[49]

2.2.3 Post synthetic modifications

Post synthetic modification (PSM) carried out to enhance or introduce functionality into an already synthesized material. When compared to in-situ modification, post synthetic modification is more beneficial because it allows the functionalization of various types of MOFs. There are various types of post synthetic modifications for MOF to enhance or introduce electrical conductivity.

In section 2.2.2, it was discussed about through guest approach as an insitu modification to enhance the electrical conductivity. Also, this approach can be a post synthetic modification. Different guest species can be inserted into the pore of the already synthesized MOF and encapsulating of guest depend on the host-guest interaction, size of the pore and pore window in MOF for the guest species.[48] Redox active guest molecules have used to convert insulative MOFs into EC-MOFs. I_2 has been used as a most common dopant for this purpose. Kobayashi et al. have exposed $Cu[Ni(pdt)_2]$ film to I_2 vapor at $50\text{ }^\circ\text{C}$ and observed 10^4 fold enhancement of conductivity upon introducing guest (1×10^{-8} to $1 \times 10^{-4} \text{ S cm}^{-1}$). But weight analysis has proved that very less amount of dopant I_2 within the MOF and electrical conductivity due to MOF rather than I_2 . The reason behind the conductivity is partial oxidation of framework by I_2 which gives loosely bound electrons as charge carriers.[30]

Panda et al, have carried out post synthetic guest encapsulation to enhance the electrical conductivity of 2D Cu(I)-Sulfonate MOF consisted of NDI(naphthalenediimide) organic ligand. Guest Li^+ ions can bind to NDI ligand through the oxygen atoms in carbonyl group and sulfonate group in NDI and perchlorate anion in NDI via anion- π bonds at same time. The pristine MOF shows low electrical conductivity of $4.65 \times 10^{-10} \text{ S m}^{-1}$ at room temperature because of low charge carrier density and lack of electron delocalization pathway. After infiltration of LiClO_4 , it shows high ionic conductivity than pristine MOF which is $2.3 \times 10^{-4} \text{ S m}^{-1}$ due to high concentration of Li^+ within the framework which can hop from one binding site to another. [50]

Another method to induce the electrical conductivity is, combining the MOF with carbon based conductive material such as carbon nano tube, graphene oxide and graphene. This combination process can be done by physically mixing MOF with conducting substrate or by growing MOF nano structure on conductive substrate. Lu et al. synthesized HKUST-1, $\text{Zn}_2(\text{BDC})_2\text{DABCO}$ (Where DABCO stands for 1,4-diazabicyclo-[2.2.2] octane) and MIL-68 MOFs on conducting polymer substrates on Pt electrodes. Although HKUST has recognized as an insulator, HKUST/Polyaniline/Pt composite has electrical conductivity of 0.125 S cm^{-1} upon I_2 adsorption.[51]

Post synthetic metalation is one of a method which can be used to enhance the electrical conductivity of MOF. In this method, additional metal ions are introduced into the already synthesized MOF framework. Pham et al. synthesized Ni and Co metalated Cu-HHTC (Where HHTC stands for 2,3,8,9,14,15-hexahydroxyltribenzocyclyne) in their work in 2022. Ni metalated and Co metalated Cu-HHTC have shown electrical conductivity of $4.51 \times 10^{-3} \text{ S cm}^{-1}$ and $3.57 \times 10^{-3} \text{ S cm}^{-1}$ respectively, which are higher than the conductivity of pristine Cu-HHTC, 1.97×10^{-3} . According to the calculations it has revealed that, Ni is in the intrinsic pocket (in plane) and Co is located between 2 pockets (between planes). Figure 15 shows 3D structural simulation of Ni and Co metalated Cu-HHTC. Hence the reason for higher conductivity in metalated Cu-HHTC is,

intervalence charge transfer between inserted metal ions and the Cu-HHTC MOF.[44]

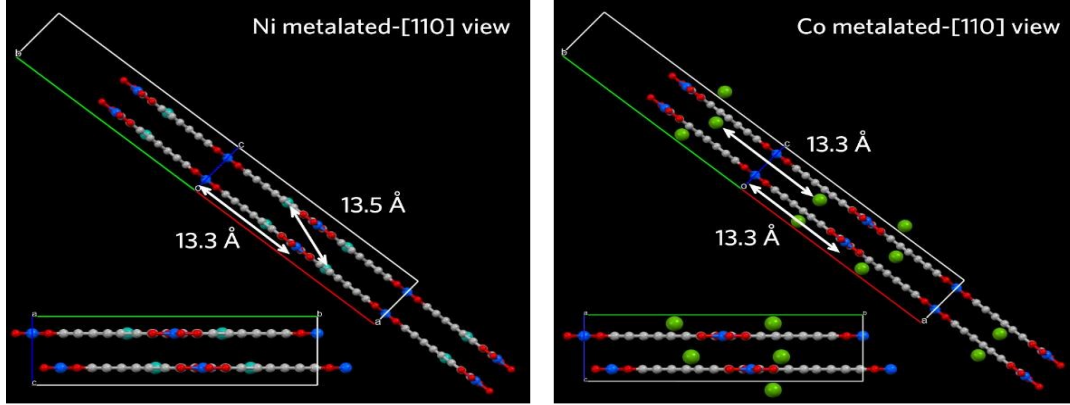


Figure 15. 3D structural simulation of Ni-metalated and Co-metalated Cu-HHTC at [110] view where C, O, Cu, Ni, and Co represent by gray, red, blue, teal, and green atoms respectively[44]

2.2.4 Applications of electrically conductive MOFs

Electrically conductive MOFs are used in many applications due to its specific chemical and physical properties. Some of them are thermoelectric devices, electrocatalysis, batteries, chemiresistive sensors and supercapacitors.

Electrically conductive MOFs are used in thermoelectric devices. Thermoelectric devices are very important because they could convert energy from heat to electricity or vice versa. This property makes to use these materials in power generation, thermoelectric heating and cooling. Inorganic thermoelectric materials are very costly and arise some environmental issues while organic materials are less conductive to use as thermoelectric materials. EC-MOFs with low thermal conductivity have identified as a good candidate for being thermoelectric material because MOF can be simulated to design electron crystal phonon glass material with a high performance in thermoelectric energy conversion. Performance of a thermoelectric material can be measured by a dimensionless figure of merit which is denotes as ZT . ZT can be explained as follows:

$$ZT = S^2\sigma T / k \quad (3)$$

Where S is Seebeck coefficient, T is the absolute temperature, σ is the electrical conductivity, and k is the thermal conductivity. $S^2\sigma$ is called as power factor (PF) and high PF value indicates the capability of generating high voltage and high current.

Sun et al. have observed that microporous $\text{Ni}_3(\text{HITP})_2$ (Where HITP stands for 2,3,6,7,10,11-hexaiminotriphenylene) shows n type thermoelectric behaviour with 58.8 S cm^{-1} electrical conductivity while thermal conductivity is low as $0.21 \text{ W m}^{-1} \text{ K}^{-1}$. The reason for this thermoelectric behaviour is the microporous structure of $\text{Ni}_3(\text{HITP})_2$ which favours phonon scattering. [52]

EC-MOFs act as electrocatalyst for chemical reactions like hydrogen evolution reaction (HER), oxygen reduction reaction (ORR), water splitting and CO_2 reduction. Conductive MOFs have the properties like high electrical conductivity, high surface area and dense active catalytic centre which makes a high performance electrocatalysis. [53] Specially, the permanent porosity of MOF enables mass transfer and diffusion of electrolyte. High electrical conductivity promotes charge transfer during the electrocatalysis reaction and structural tenability used in identifying catalytic active sites. Peryaiah et al. have synthesized Co-Cu-MOF by combining Co with Cu-MOF and H_2BDC as organic linker. They observed better bifunctional activity for water splitting reaction with a 0.21 V (oxygen evolution reaction- OER) lower overpotential and -0.71 V (HER) at 10 mA cm^{-2} of current density. [54]



Figure 16. Schematic diagram of bifunctional electrocatalysis of Cu-Co MOF [54]

Another application of electrically conductive MOF is, chemiresistive sensing. Chemiresistive sensing is a type of chemical sensing which the resistance of a material changes as a response of exposing to certain chemical species. The variation in chemical resistance helps to detect or quantify targeted chemical species in the environment. Campbell et al. have developed 2 D electrically conductive MOF $\text{Cu}_3(\text{HITP})_2$ for ammonia vapor detection in sub ppm level with linearity. But isostructural $\text{Cu}_3(\text{HITP})_2$ does not show any response to ammonia vapor highlighting the importance of structural specificity of MOF. [39]

Electrically conductive MOFs have been identified as a promising candidate for battery material due to its high surface area, electrical conductivity, crystalline porous and tailored structure. Electrically conductive MOFs are used as cathode/anode material, host material or separators in batteries. Nishihara et al. have reported 2D electrically conductive MOF, bis(diimino)nickel framework (NiDI) as a cathode material for Li ion battery. In this MOF, both anion and cation can act as charge carriers to the process of charging and discharging energy. NiDI as an anion/cation material gives high specific capacity of 155 mA h g^{-1} at the current density of 10 mA g^{-1} and it has more stable cycling performance up to 300 cycles. The reason for it is, NiDI consist of $\text{Ni}(\text{L}^{\text{isq}})_2$ (L = o-diiminobenzosemiquinonate) which is a special redox active unit with the ability of up to 4 electron reduction and 2 electron oxidation transfer per metal center. [55]

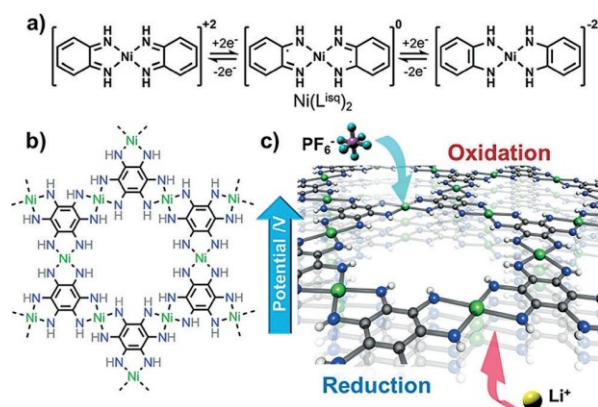


Figure 17. a) Redox reactions of $\text{Ni}(\text{L}^{\text{isq}})_2$ b) Chemical structure of NiDI MOF. c) Oxidation and reduction reactions of NiDI with respective counter ions. [55]

Supercapacitors are widely used for the electrical energy storage purpose because they have high charge/discharge rate, high charge density and high cyclability. Electrically conductive MOFs are more suitable material for supercapacitors because of its ability to offer more redox active sites, high porosity and surface area. Sheberla et al. have synthesized supercapacitor from $\text{Ni}_3(\text{HITP})_2$ MOF without any conductive additives or binders. This MOF exhibit a high-capacity retention of 90% over 10,000 cycles at 2 A g^{-1} of current density and high areal capacitance $18 \mu\text{F cm}^{-2}$ at a discharge rate of 0.05 A g^{-1} . [56]

Electrically conductive MOFs also can be integrated into electronic devices like Field Effect Transistors (FETs) and organic light emitting diodes (OLEDs). Conductive MOFs are used as a novel porous material for FETs because of the specific properties of MOF such as electrical tunability, ability of membrane preparation and high crystallinity. Also, the FET helps to study about charge transport such as carrier type and carrier mobility in electrically conductive MOFs. In 2019, Wu et al. have fabricated a liquid gated FET device by using electrically conductive MOF, Ni_3HITP_2 . There, Ni_3HITP_2 has been synthesized on Si/SiO₂ wafer by in situ growing. This Ni-MOF-FET exhibit $45.4 \text{ cm}^2 \text{ V}^{-1} \text{ s}^{-1}$ and 2.29×10^3 mobility and on/off current ratio respectively. [57] Table 01 and 02 show EC-MOFs prepared with Cu and Ni metal nodes respectively including organic ligand, chelating atom, dimensionality, pore diameter, electrical conductivity and application.

Table 01. EC-MOFs prepared with Cu as metal node

Name of the MOF	Organic ligand	Chelating atom	Dimensionality	BET surface area ($\text{m}^2 \text{ g}^{-1}$)	Pore diameter (\AA)	Electrical conductivity (S cm^{-1})	Application	Reference
$\text{Cu}_3(\text{HITP})_2$	HITP	N	2D		N/A	0.2 (pellet, 2 point probe) at R.T	Chemiresistive sensing of ammonia vapor	[39]
Cu-BHT	BHT	S	2D		N/A	95 at R.T	As a semiconductor in electronic	[38]

							device appli- cations	
Cu-HHTC	HHTC	O	2D		19	1.97×10^{-3} (pellet, 4- point probe method under am- bient con- ditions)	N/A	[44]
Cu-CuPc	CuPc	N	2D		Bi- modal pore struc- ture with 1.4 and 11	1.6×10^{-6} at 80 °C (Pel- let, 2-point probe method)	cathode ma- terial in LIBs	[58]
Cu[Cu(pdt) ₂]	pdt	S	3D		3.4	6×10^{-4} at 300 K	Porous elec- trode mate- rial	[23]
Cu ₃ (HITT) ₂	HITT	N	2D		1.8	$0.05- 10^{-6}$ at 298 K	N/A	[59]
Cu ₃ (HIB)	HIB		2D		N/A	13 at 300 K	Advanced electronic application	[25]
Cu-HHTP	HHTP		2D		18	0.2 at R.T	Supercapac- itor	[60]
Cu-HHB	HHB	O	2D		N/A	7.3×10^{-8} at R.T	Electronics and sensing	[61]
Cu ₃ (HTTP) ₂	HTTP		2D	171		2.4×10^{-8} at R.T	Electro- chemical capture and release of ethylene in solid state	[62]
Cu ₃ (BTC) ₂	BTC		2D	214		4.1×10^{-5} at R.T	Electronic devices and sensors	[63]
TCNQ@Cu ₃ (BTC) ₂	BTC		2D	214		0.04	Electronic devices and sensors	[63]

Table 02. EC-MOFs prepared with Ni as metal node

Name of the MOF	Organic ligand	Chelating atom	Dimensionality	BET surface area (m ² g ⁻¹)	Pore diameter (nm)	Electrical conductivity (S cm ⁻¹)	Application	Reference
Ni ₃ (HITP) ₂	HITP	N	2D		2	2 for bulk 40 for film	Molecular conductor	[64]
Ni ₃ (HITT) ₂	HITT	N	2D		1.8	4.5 at 298 K	N/A	[59]
Ni ₃ (HHTP) ₂	HHTP	O	2D		1.3	0.32 x 10 ⁻⁴	Chemical sensing of metabolites in sweat	[65]
Ni ₃ (BHT) ₂	BHT	S	2D		N/A	0.15 at R.T	Molecular electronics	[40]
Ni ₃ (HIB) ₂	HIB		2D		N/A	8 at 300 K	Advanced electronic application	[25]
Ni-Pc	Pc	N	2D	593	N/A	0.2 at R.T	Water oxidation catalysis	[66]
Ni ₃ (HTTP) ₂	HTTP		2D	166		3.6 x 10 ⁻⁴ at R.T	Electrochemical capture and release of ethylene in solid state	[62]
Ni(IT) ₂	IT ⁶⁻		2D	N/A	N/A	0.1	N/A	[67]
Ni(AT) ₂	AT ³⁻		2D	N/A	N/A	3 x 10 ⁻⁶ at R.T	Electrocatalyst for H ₂ evolution	[68]
Ni-HAB	HAB		2D	130		1.05	Electrocatalyst for ORR	[46]

2.3 Synthesis of EC-MOFs

Synthesis of EC-MOF is a crucial topic as they are applied in number of applications which some of them have discussed in chapter 2.2.4. Synthesis method of EC-MOFs can be varied according to the application, desired conductivity, time and scalability. There are several methods to synthesis EC-MOFs and these methods can be mainly divided into two types as chemical synthesis methods and thin film fabrication methods.

2.3.1 Chemical Synthesis of EC-MOF

In chemical synthesis methods, metal ions and organic linkers are combined mostly in a liquid phase, that is in the presence of a solvent to form EC-MOF under specific conditions such as controlled temperature, PH or pressure. The choice of solvent is depended on its reactivity, redox potential and solubility. The choice of solvent is important in determining activation energy and thermodynamics in reactions. Chemical synthesis methods can be used to synthesize EC-MOFs in large scale. [69]

2.3.1.1 Solvothermal and hydrothermal methods

Solvothermal and hydrothermal methods are widely used in EC-MOF fabrication due to the possibility to achieve scalability and high yield product. In this method, organic molecules, metal salts and solvents are added to a sealed vessel/autoclave and temperature is set up to a specific value to obtain the expected EC-MOF product. The schematic diagram of solvothermal or hydrothermal approach of EC-MOF is shown in figure 18. [70]

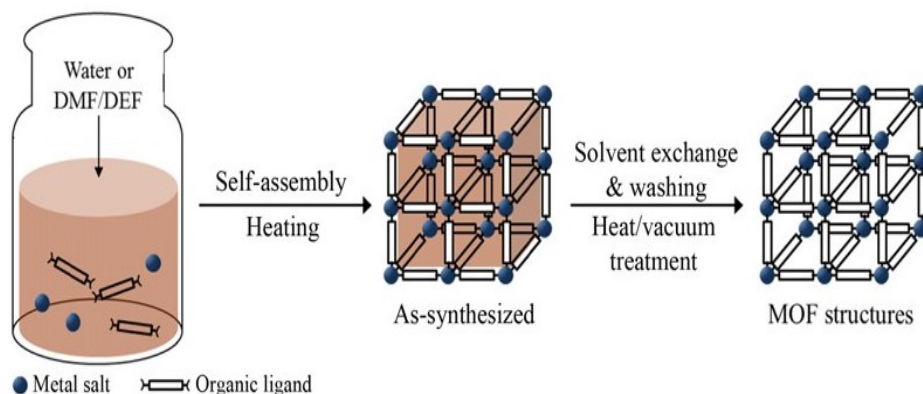


Figure 18. Schematic diagram of solvothermal or hydrothermal approach of EC-MOF [71]

In solvothermal method reaction is carried out in a solvent other than water, typically organic solvent (ex: methanol, dimethylformamide (DMF), ethanol) and solvothermal method is used when organic ligand and metal salt are highly dissolve in organic solvent. Nagatomi et al. have fabricated Cu-CuPc 2D EC-MOF with intrinsic conductivity $1.6 \times 10^{-6} \text{ S cm}^{-1}$ at 80°C by solvothermal method. During the solvothermal synthesis, CuPcOH, $\text{Cu}(\text{C-F}_3\text{acac})_2$, and aqueous NH_3 are heated with DMF/ H_2O to 120°C for 36 hours.[58]

In hydrothermal method, reaction is carried out in water instead of organic solvent. Hmadeh et al. synthesized a series of catecholate based MOFs as $\text{Cu}_3(\text{HHTP})$, $\text{Co}_3(\text{HHTP})$ and $\text{Ni}_3(\text{HHTP})$ which are also called as Cu-CAT-1, Co-CAT-1 and Ni-CAT-1 respectively. During the hydrothermal synthesis of these MOFs, metal acetates and hexahydroxytriphenylene(HHTP) organic linker are hydrated in aqueous solution and heated at 85°C for 24 hours. The electrical conductivity at room temperature on single crystal of Cu-CAT-1 by using 4 probe method was recorded as $2.1 \times 10^{-1} \text{ S cm}^{-1}$.[72]

2.3.1.2 Direct reaction in solution

This method is important when expecting high yield, simple operation and less requirement of equipment in EC-MOF synthesis. In direct reaction in solution method, precursors are directly mixing in reaction solution under ambient conditions.

Hassan et al. synthesized a composite of HKUST-1 MOF and graphene by direct reaction in solution method. Graphene was added to a solution containing ethanol, $\text{Cu}(\text{NO}_3)_2 \cdot 2.5 \text{H}_2\text{O}$ and sonicated for half an hour. Ethanol solution with BTC (1,3,5-benzenetricarboxylic acid) was added to the reaction mixture while stirring at room temperature. After filtration and washing with ethanol, the sample was dried overnight at room temperature to obtain the composite material. The composite material showed $7.6 \times 10^{-6} \text{ S m}^{-1}$ electrical conductivity while pristine MOF comparatively exhibited lower electrical conductivity which was $1.7 \times 10^{-9} \text{ Sm}^{-1}$. [73]

2.3.1.3 Microwave assisted synthesis

In this method microwave radiation is used to heat the reaction mixture uniformly and can achieved fast nucleation, short reaction time. Also, microwave assisted synthesis method helps to modify the properties of synthesized MOF.

Wu et al. have synthesized Ru supported carbonized EC-MOF for hydrogen evolution by microwave assisted synthesis methods. Ultra small Ru nano particles supported $\text{Co}_3(\text{HHTP})_2$ have been synthesized by heating in a microwave oven for 60 seconds which is a quick method. [74]

2.3.2 Thin film fabrication of EC-MOF

Thin film fabrication of EC-MOF is crucial because it is applied in diverse fields and enable to investigate the intrinsic electrical properties with anisotropic structures. The advantage is, that it can reduce the interferences at junctions and contacts and thereby improve the performance of EC-MOF in various applications. In this method it forms continuous layers of EC-MOF on a solid substrate with few nanometres to micrometre thickness and the properties of thin film vary with the thickness. [75]

Thin film fabrication of EC-MOF can be divided into mainly 2 types as gas phase fabrication and liquid phase fabrication. Chemical layer deposition

(CVD) is included into gas phase fabrication. Layer by layer growth and electrochemical growth included into liquid phase fabrication methods. [33]

2.3.2.1 Chemical Vapor Deposition

Chemical Vapor Deposition (CVD) is one of a gas-solid interfacial assisted method which can be used to fabricate EC-MOF thin films on selected substrates. In CVD, volatile precursor gases are introduced into the reaction chamber and these precursors are reacted/decomposed on the heated substrate or/and in the gas phase to form the expected product. CVD allows layer by layer growth as it depended on chemical reaction which take place on the substrate. Although conformality and uniformity of the film can be controlled by CVD, atomic scale conformality is impossible. EC-MOF films can be incorporated into actual devices by CVD because of the unique properties of CVD such as high quality and resulting highly oriented films without solvent disruption. [76]

Choe et al. fabricated thin film of 2D conductive MOF, $\text{Cu}_3(\text{C}_6\text{O}_6)_2$ which exhibited electrical conductivity of 92.95 Scm^{-1} by single step all vapour phase CVD. $\text{Cu}_3(\text{C}_6\text{O}_6)_2$ thin film was synthesized by vapor phase ligand substitution reaction of bis(2,4-pentanedionato) Cu(II) ($\text{Cu}(\text{acac})_2$) and tetrahydroxy-1,4-benzoquinone (THQ). [76]

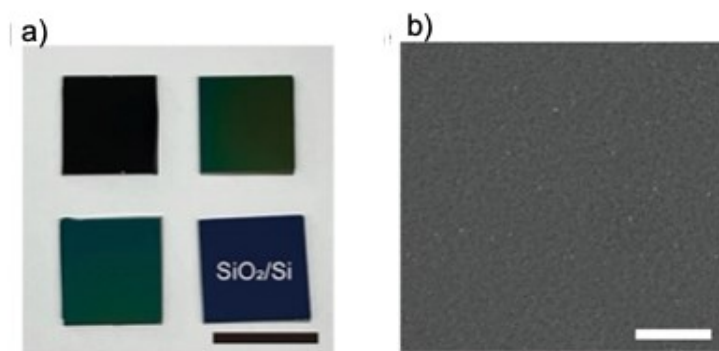


Figure 19. a) Optical image (scale bar: 1 cm) and b) SEM image (scale bar: 2 μm) of $\text{Cu}_3(\text{C}_6\text{O}_6)_2$ thin film on a SiO_2/Si substrate [76]

There is a specialized subset of CVD which is called as atomic layer deposition (ALD). ALD is a well-recognized gas phase deposition method which offers self-limiting reactions to obtain high conformal and thickness-controlled films with atomic level precision. In this technique, two or more gas phase precursors are pulsed to the substrate sequentially by an inert carrier gas to form thin monolayers. Molecular layer deposition (MLD) follows same principle as ALD, but the precursors used for this technique are organic compounds resulting organic thin films. [77]The hybrid of ALD and MLD widely used for organic-inorganic thin film fabrication. But there is no literature available so far for synthesizing EC-MOF from ALD/MLD process.[2]

In ALD/MLD hybrid technique, metal atoms make covalent bonds with organic moieties resulting periodic organic-inorganic thin film structures. This resulted thin film has completely new material properties that cannot be observed in organic or inorganic thin films alone. Figure 20 shows ALD/MLD cycle and resulted organic-inorganic hybrid thin film.[78]

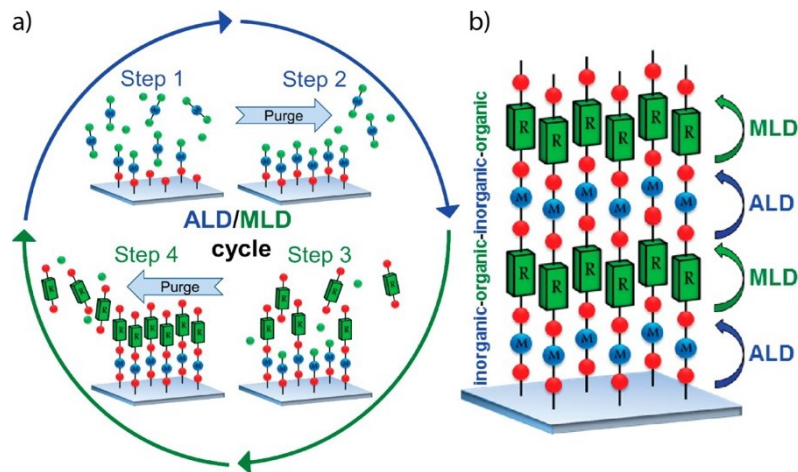


Figure 20. a) Schematic diagram of ALD/MLD cycle, step 1- pulsing of SBU precursor, step 2- purging of SBU precursor with inert gas, step 3- pulsing organic linker precursor, step 4-purging organic linker precursor with inert gas b) Schematic diagram of resulted ALD/MLD hybrid thin film (green: organic, blue: metal, red: oxygen)[79]

2.3.2.2 Electrochemical methods

Electrochemical methods are widely used for thin film fabrication of EC-MOF powder on an industry scale. This is a comparatively quick method that can operate under mild conditions such as under low temperatures. In this method, metal ions are provided into the reaction mixture which contains electrolyte and organic ligand by anodic dissolution.

Liu et al. synthesized $\text{Cu}_3(\text{HHTP})_2$ large area film on Cu foil. When voltage is applied, Cu^{2+} dissociate from Cu foil and combine with the migrating organic linker to form MOF. Dissociation rate of Cu^{2+} and migration rate of organic linker can be varied according to the applied voltage. By that it can control the film thickness and film morphology. They have synthesized $\text{Cu}_3(\text{HHTP})_2$ film with 80nm thickness with 8.7 S cm^{-1} electrical conductivity. Also, this formed $\text{Cu}_3(\text{HHTP})_2$ film with high flexibility which allow them to be used in the fabrication of flexible devices. [80]

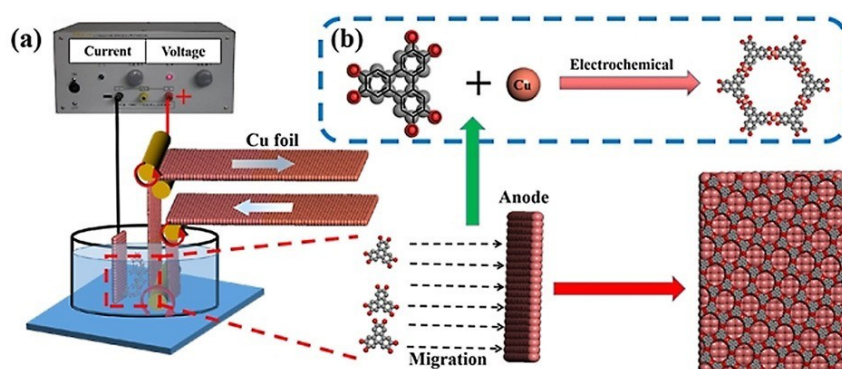


Figure 21. a) Electrochemical synthesis method of $\text{Cu}_3(\text{HHTP})_2$ b) Schematic diagram of coordination reaction between Cu^{2+} ion and the HHTP ligand [80]

2.3.2.3 Layer by layer liquid phase epitaxy method

In this method, surface of a conducting substrate is functionalized with organic molecules like carboxylate, sulphide, hydroxide or with metal ions to form a self-assembled monolayer (SAM). If SAM consists of organic molecules, they react with metal salt and then with organic linker to form MOF on SAM layer. This is achieved by soaking in solution of metal salt and organic linker. The

number of soakings determine the thickness and number of layers of the deposited MOF thin film.[33]

Yao et al. have synthesized EC-MOF thin film of $\text{Cu}_3(\text{HHTP})_2$ with smooth surface, dense packing and well controlled thickness by layer-by-layer assembly for room temperature chemiresistive sensing. Synthesized $\text{Cu}_3(\text{HHTP})_2$ nano film has exhibited electrical conductivity of 0.02 Scm^{-1} at room temperature. [81]

3 Research goals

Metal organic compounds have unique characteristics over pure organic or pure inorganic compounds due to their hybrid structure combining both inorganic and organic components. Some of these characteristics are tuneable structure with tailorable chemical functionality, high porosity and high surface area. Among them metal organic polymer exhibits enhanced electrical conductivity due to presence of extended pathways for electron transport. In this research we aimed to develop reliable synthesis methods for a selected metal organic polymer which exhibits a thermoelectric property with high electrical conductivity and low thermal conductivity. Thermoelectrical property of a metal organic polymer is crucial as it enhance the potential of using them in various applications such as electronic and microelectronic devices, medical and wearable devices, wireless sensor networks. [82]

Recently the interest towards organic thermoelectric materials have risen due to light weight, mechanical flexibility, solution processable and ability to synthesize from abundant resources. When it is compared to inorganic counterpart organic materials exhibit low thermal conductivity which contributes to a high ZT. Transition metal complexes and polymers consist of thiochelatate ligands have shown high electrical conductivity with various oxidation states and easy synthesis methods. Among these compounds poly metal ethylenetetrathiolate (poly(M-ETT)), where M stands for Cu or Ni exhibits high electrical conductivity at room temperature ranging from 10^{-5} -50 S cm⁻¹ and this metal organic polymer can be synthesized easily without any doping process. These compounds are low thermal conductive due to their amorphous nature. [1] [83] From the first site, as it was expected to observe p-type behaviour in the synthesized metal organic polymer compound, copper metal was selected over nickel metal as SBU. These reasons made to focus on synthesizing Cu-ETT. Thermoelectric property of synthesized Cu-ETT bulk material was optimized via chemical synthesis methods and thin film fabrication methods.

As the first part of the experimental work, we focused to synthesize Cu-ETT bulk material and study thermoelectric properties of Cu-ETT by varying reaction parameters, such as source of SBU, base, temperature, number of SBU equivalents, reaction time and oxidation method were varied. We aimed to study the effect of these parameters on thermoelectric behaviour of Cu-ETT material.

As the second part of the experimental work, we aimed to fabricate electrically conductive Cu-ETT thin film via ALD/MLD technique. ALD/MLD are well known thin film synthesizing methods which helps to get conformal layers of thin films with excellent uniformity and precise thickness control. To synthesize Cu-ETT thin film different bases were used. Other than that, we carried out process optimization to ensure the saturation of the thin film and thereby enhance the electrical conductivity. We aimed to study the electrical resistivity of deposited Cu-ETT thin films.

4 Experimental Section

4.1 Chemical synthesis

4.1.1 Reactant preparation

Thermoelectric properties of Cu-ETT bulk material were optimized by several chemical compounds as SBU source and base. Copper acetylacetonate ($\text{Cu}(\text{acac})_2$, *thermo scientific*, 98%) and $\text{CuCl}_2 \cdot 2\text{H}_2\text{O}$ (*thermo scientific*, 99%) were used as the metal ion source. 1,3,4,6-tetrathiapentalene-2,5-dione (TPD, *BLD pharm*, 97%) was used as the organic linker source. Lithium *tert*-butoxide (LiO^tBu , *thermo scientific*, 99%) and sodium methoxide (NaOMe , *thermo scientific*, 98%, 0.5 M in methanol) were used as base. LiO^tBu and TPD are air sensitive compounds and required to handle with care. LiO^tBu and TPD were kept in *Etelux Lab 2000 GP20* Ar filled glove box to avoid from passivation by moisture or oxygen in air where LiO^tBu results lithium hydroxide and lithium carbide respectively. LiO^tBu , $\text{Cu}(\text{acac})_2$ and TPD have very fine powder composition with white, blue and light brown in color respectively. $\text{CuCl}_2 \cdot 2\text{H}_2\text{O}$ is a bright blue color crystalline solid.

As solvents methanol (*thermo scientific*, 99.9%), tetrahydrofuran (THF), dimethylformamide (DMF, *Sigma Aldrich*, 99.8%) were used. To quench the reactions a mixture of methanol and glacial acetic acid (*Supelco*, 100%) were used. I_2 (*Merck*, 99.5%) was used for I_2 oxidation.

4.1.2 Synthesis methodology

Under an inert atmosphere, sodium methoxide (10.0 ml, 5 mmol) solution is added to TPD (208 mg, 1 mmol) in methanol and stirred for 24 hours at required temperature. $\text{CuCl}_2 \cdot 2\text{H}_2\text{O}$ (170 mg, 1 mmol) dissolved in methanol (5.0 ml) was added to the reaction mixture. After 24 hours, the reaction was quenched with a mixture of methanol (4.0 ml) and glacial acetic acid (0.4 ml) under an inert atmosphere to remove any additional base before

oxidation.[84] After 15 minutes of refluxing, I_2 (127 mg, 0.5 mmol) dissolved in methanol (8.0 ml) was added to the reaction mixture for oxidation and reaction continued for 24 hours. The total reaction time was 72 hours. The resulted black colour product was washed with deionized water, methanol and diethyl ether respectively by centrifugation to remove unreacted precursors and/or byproducts.[85] Resulted solid product was dried in vacuum oven for 12 hours. In certain reactions air oxidation was carried out instead of I_2 oxidation, where reaction mixture was exposed to air for 30 minutes before washing the product. For some reactions $CuCl_2 \cdot 2H_2O$ was added initially along with TPD and the reaction time was maintained for only 48 hours.

Thirteen reactions were carried out by varying temperature, reaction time, solvents, concentration of Cu precursor and oxidation method as given in table 03. At high temperatures, reaction was carried out as shown in figure 22.

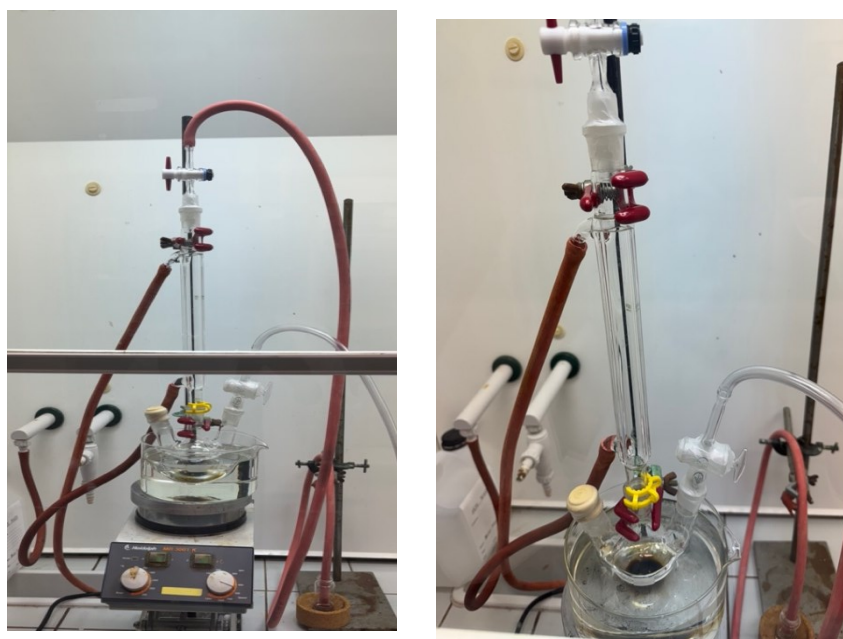


Figure 22. Experimental set up for 60°C reaction of Cu-ETT synthesis

Preliminary experiments of the reaction were carried out with TPD as organic linker source, $Cu(acac)_2$ as SBU source and LiO^tBu as base at room temperature or 60°C with THF/DMF as solvents and I_2 or air oxidation. After washing there was no solid product observed.

Table 03. Reaction parameters for Cu-ETT synthesis

Sample number	SBU source	Reaction time	Cu equivalent	Organic linker source	Base	Solvent	Temperature	Oxidation method
1	CuCl ₂ ·2H ₂ O	72 hours	1	TPD	NaOMe	MeOH	RT	Air oxidation
2	CuCl ₂ ·2H ₂ O	72 hours	1	TPD	NaOMe	MeOH	60°C	Air oxidation
3	CuCl ₂ ·2H ₂ O	48 hours	1	TPD	NaOMe	DMF	RT	I ₂ oxidation
4	CuCl ₂ ·2H ₂ O	48 hours	1	TPD	NaOMe	DMF	50°C	I ₂ oxidation
5	CuCl ₂ ·2H ₂ O	48 hours	1	TPD	NaOMe	DMF	60°C	I ₂ oxidation
6	CuCl ₂ ·2H ₂ O	72 hours	1	TPD	NaOMe	MeOH	60°C	I ₂ oxidation
7	CuCl ₂ ·2H ₂ O	72 hours	1	TPD	NaOMe	MeOH	RT	I ₂ oxidation
8	CuCl ₂ ·2H ₂ O	72 hours	2	TPD	NaOMe	MeOH	RT	I ₂ oxidation
9	CuCl ₂ ·2H ₂ O	72 hours	2	TPD	NaOMe	MeOH	60°C	I ₂ oxidation
10	CuCl ₂ ·2H ₂ O	72 hours	1	TPD	NaOMe	DMF	60°C	I ₂ oxidation
11	CuCl ₂ ·2H ₂ O	72 hours	1	TPD	NaOMe	DMF	RT	I ₂ oxidation
12	CuCl ₂ ·2H ₂ O	72 hours	2	TPD	NaOMe	DMF	RT	I ₂ oxidation
13	CuCl ₂ ·2H ₂ O	72 hours	2	TPD	NaOMe	DMF	60°C	I ₂ oxidation

4.2 ALD/MLD

4.2.1 Precursor preparation

Three precursors were used for Cu-ETT ALD/MLD process which are Lithium bis(trimethylsilyl) amide (Li-HMDS, *Sigma aldrich*, 97%), TPD and Cu(acac)₂. Li-HMDS was an off-white colour powder. Li-HMDS and TPD were stored in *Etelux Lab 2000 GP20* Ar filled glove box. Li-HMDS and TPD were transferred into small glass vials in the glove box to avoid from decomposition or any passivation reactions. These small glass vials added into a large glass bottle for further use outside the glove box. These small glass vials and large glass bottle filled with Ar gas. During the ALD/MLD process, small glass vials were taken out from the large glass bottle and glass bottle flush with N₂ gas. For some

depositions LiO^tBu was used as lithium source instead of Li-HMDS and it was handled same way as Li-HMDS. Also, Ni-ETT was deposited for few depositions and nickel acetylacetonate (Ni(acac)₂, Merck-Schuchardt, 98%), TPD, Li-O^tBu were used as precursors. Ni(acac)₂ was a green color fine powder. Chemical structure of precursors used in Cu-ETT ALD/MLD process is shown in figure 23.

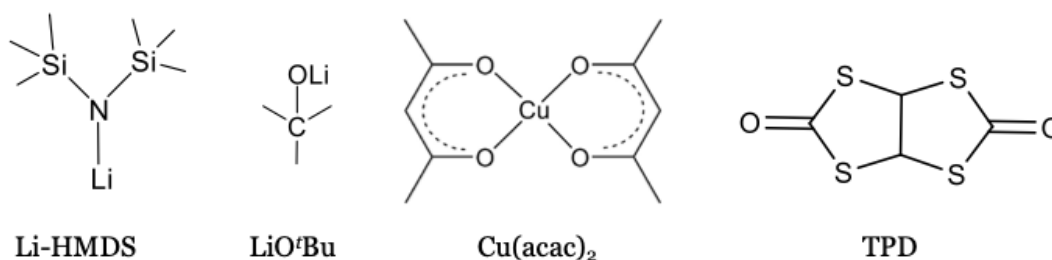


Figure 23. Precursors of Cu-ETT ALD/MLD process

These precursors were filled to glass precursor boats in the ALD reactor (*F-120*, flow-type hot-wall reactor, *ASM Microchemistry LTD.*) Thin films were deposited on borosilicate glass substrate and silicon (100) wafer (400 +/- 25 μm, *Okmetic LTD.*) substrates. Silicon substrates were cut into small pieces by diamond pen. Silicon substrates were washed with distilled water, ethanol and acetone respectively followed by blow drying with pressurized air before kept in the middle of the reaction chamber. Borosilicate glass was kept in the reaction chamber beside silicon substrate for electrical conductivity measurements.

Precursors were kept in the ALD reactor under inert condition and the air exposure time was minimized once the reactor opened to change the substrate. Each precursor was heated to their sublimation temperature which were 60°C, 90°C, 120°C for Li-HMDS, TPD and Cu(acac)₂, respectively. The deposition/substrate temperature was 220°C. Sublimated precursors were carried to the reaction chamber by N₂ gas flow. Figure 24 shows schematic diagram of ALD reactor with temperature zones and precursors. During the depositions primary and secondary N₂ gas flow was 300 sccm, 100 sccm respectively and the pressure inside the reactor was approximately 3-5 mbar.

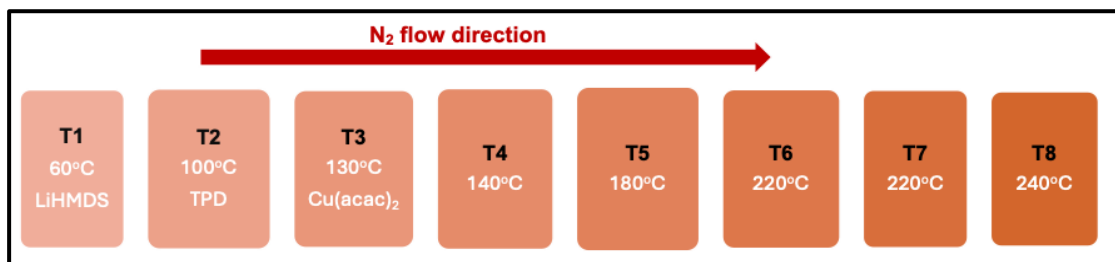


Figure 24. Schematic diagram of ALD reactor with temperature zones and precursors. N₂ flows from T1 to T8 temperature zones.

4.2.2 ALD/MLD process

In ALD/MLD process, depositions were carried out with TPD, Li-HMDS and Cu(acac)₂ as precursors to fabricate electrically conductive Cu-ETT thin films. Process parameters were optimized to ensure the saturation of film and thereby enhance electrical conductivity of films. Pulse optimization for all 3 precursors was carried out with 220°C deposition temperature and 70 cycles. Pulse/purge length of Cu(acac)₂, Li-HMDS, TPD were changed and growth per cycle (GPC) was calculated for each optimized thin film from film thickness value. Results of optimization process is presented in section 6.2.1. Chemical stability of deposited Cu-ETT thin film was investigated under 3 different conditions which were at ambient air, less/no moist environment in desiccator and high moist environment in humidifier.

As a proof of concept, some depositions were carried out to fabricate electrically conductive Ni-ETT thin films with Ni(acac)₂, Li-HMDS and TPD as precursors at 220°C deposition temperature. Number of cycles were 50, 100, 200 and 300. Pulse and purge length of Ni(acac)₂, Li-HMDS and TPD were 3/12 s, 3/12 s and 2/8 s respectively. Preliminary depositions were carried out with LiO^tBu, Cu(acac)₂ and TPD as precursors at 140°C, 150°C, 200°C, 220°C, 230°C, 240°C and 250°C deposition temperatures.

5 Characterization

5.1 Infrared Spectroscopy

Attenuated total reflectance (ATR) is a technique which conjugated with FT-IR. In ATR, IR direct to a crystal with high refractive index which contact with the sample. Directed IR reflect at the crystal/sample interface and some waves penetrate the sample. This allows to absorb IR by molecules in the sample and reflected light generates the spectrum as FT-IR. The chemical structure of $\text{Cu}_x[\text{Cu}(\text{ETT})]$ bulk sample studied with ATR. The chemical structure and stability of $\text{Cu}_x[\text{Cu}(\text{ETT})]$ thin films were studied with Fourier transform infrared spectroscopy (FT-IR). FT-IR was one of a common characterization method for thin film analyses. In this technique, broad spectrum of infrared (IR) radiation generated by FT-IR passes through the sample and specific frequencies of IR radiation absorb by different chemical bonds in molecules which represent by peaks at different wavenumbers as shown in Figure 25. *The Bruker Alpha II* FTIR spectrometer was used to collect ATR/FTIR data of the samples.

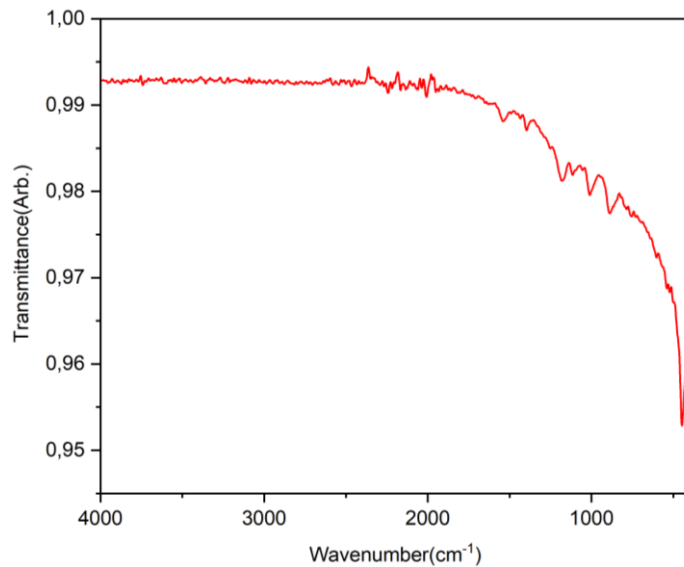


Figure 25. An example of infrared spectrum of Cu-ETT bulk sample

5.2 X-ray methods

X-ray diffraction (XRD) is a powerful, versatile, non-destructive, and one of the most common analytical techniques for identification and quantitative determination of various structural parameters of materials. The purity and the crystallinity phase of synthesized $\text{Cu}_x[\text{Cu}(\text{ETT})]$ bulk material was studied with XRD. Before the analysis Cu-ETT material was crushed into a fine powder. In this technique, X-ray was directed to the sample and atoms in the crystal planes diffract X-ray (according to Bragg's law) at specific angles. These diffracted X-ray collected by the detector and recorded as intensity of X-ray as a function of diffraction angle as shown in Figure 26. *PANalytical X'Pert pro MPD alpha 1* powder XRD was used to collect data of each sample from 10° to 90° . X-ray source of this instrument was Cu monochromator, $\text{K}\alpha_1 1.54060 \text{ \AA}$.

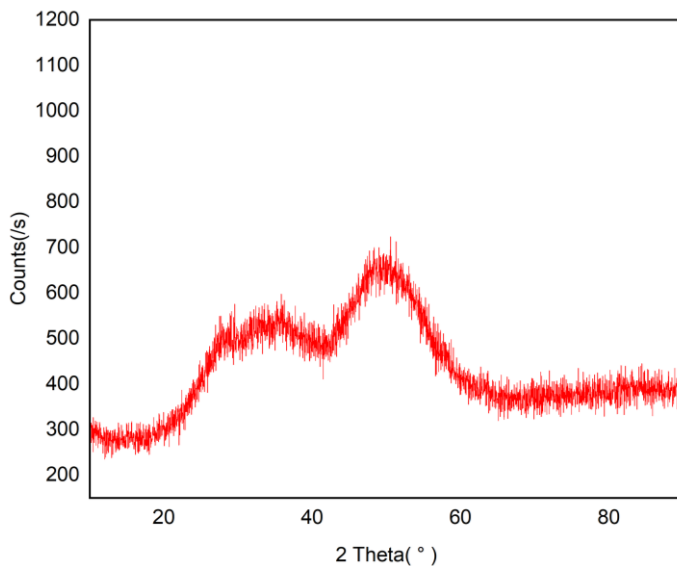


Figure 26. An example of XRD pattern of Cu-ETT bulk sample

Conventional XRD methods are not usable for thin films because a huge interference is generated from the substrate while weak signal generated from the thin film. Grazing Incident X-ray Diffraction (GIXRD) is a non-destructive method which can be used for thin film characterization. In this technique, beam of X-ray directs to the sample at low angle of incidence, and it interacts only with few nanometers of material. The resulted X-ray diffraction pattern gives crystallographic properties of the surface of material. Low angle of

incidence makes only to get measurements from low penetration depth avoiding signals from below surface/substrate. In this thesis, *Rigaku SmartLab diffractometer* was used for measurements. Emitted X-ray source was parallel beam Cu K α 1 radiation with wavelength 1.54059 Å. Two-bounce Ge(220) incidence monochromator was used. Highscore software was used to analyze the XRD data.

5.3 Spectroscopic ellipsometer

Ellipsometry is a non-destructive, non-contact optical technique used in investigating thickness, optical constants of multi-layer and single layer thin films. In this technique, linearly polarized light directs to the sample at specific angle. Upon the reflection from sample the polarization of light changes into elliptically polarized light. Ellipsometer measures φ and Δ parameters which describes the state of the outgoing elliptical polarized light. Thickness and optical constants of thin film is investigated from these parameters through a model built according to the film structure. Thickness can be measured from few angstroms to several microns. For this technique no reference measurement is required. *Horiba UVISSELPLUS Spectroscopic Ellipsometer* was used to measure the thickness of thin films with Tauc-Lorentz model under 400-900 nm range.

5.4 Thermoelectric measurements

Thermoelectric measurements such as thermal conductivity, electrical resistivity and Seebeck coefficient were obtained by physical property measurement system (PPMS) instrument. PPMS is a versatile and highly precise instrument. *Quantum Design PPMS DynacoolTM* was used to measure thermoelectric properties of samples from 1.85 to 400 K. Two probe and four probe methods used for electrical resistivity measurements of bulk samples and thin films respectively. In two probe method, known current pass into the sample through 2 contacts while current pass through 2 contacts and voltage measures

across other 2 contacts in four probe method. Two probe method most used for high resistance bulk samples. Four probe method is more accurate than two probe method because of eliminating error arise from contacts. The voltage across the sample is measured and thereby electrical resistivity can be calculated.

5.5 Microscopy

Scanning electron microscopy (SEM) was used to observe surface morphology and structure of the bulk and thin film samples of $\text{Cu}_x[\text{Cu}(\text{ETT})]$ at high magnification and resolution. SEM images were taken with *Tescan Mira3* scanning electron microscope with acceleration voltages of 15 kV. In this technique, high energy electron beam is directed to the sample and these electrons interact with atoms in the sample while generating secondary electrons to create the image. As SEM images were acquired from secondary electrons, and thus elementary composition was not acquired. Magnification of 40.2 kx to 2 kx was used in SEM images of Cu-ETT samples.

5.6 Inductive Coupled Plasma- Optical Emission Spectroscopy

Inductive coupled plasma-optical emission spectroscopy (ICP-OES) is a technique which used to analyse quantitative and qualitative elemental composition in samples. This technique uses a plasma which has made out from argon gas ionized by electromagnetic field. This high energy plasma is atomized and excited the atoms while emitting light at certain wavelength which specific to each element. The intensity of the of wavelength is directly proportional to the concentration of each element in the sample. Before measuring with ICP-OES, 50 mg of sample was microwave digested with H_2SO_4 (95%, 5.0 ml) and HNO_3 (70%, 5.0 ml) acid solution by *Speed wave analytic jena* instrument under 2 KW microwave power. Sample was topped up to 500 ml with milli-Q water and analysed with *Agilent 5900 ICP-OES* instrument.

5.7 Elemental analyser

C, H, N and S concentrations in Cu-ETT bulk samples were analysed with elemental analyser. Any solid-liquid sample can be analysed with this instrument. In this technique, sample is placed in reduction/oxidation reactor and temperature raise to 950 °C. At high temperature, organic/inorganic compounds in the sample converted into elements in gaseous state with carrier gas He. These elements are separated in a chromatography column and detect by thermal conductive detector (TCD). C, H, N, S in Cu-ETT samples were analysed with *Thermoscientific Flash Smart EA CHNS/O with MV* instrument. Vanadium Pentoxide was used as the standard.

6 Results and discussion

6.1 Chemical synthesis

6.1.1 Purity and crystallinity phase

The purity and crystalline phase of synthesized Cu-ETT bulk material were analysed with powder XRD. Crystallinity of the sample is usually exhibited as sharp peaks in the XRD pattern. XRD patterns of Cu-ETT bulk samples synthesized with 2 Cu equivalents at 60 °C with MeOH and DMF are shown in Figure 27.

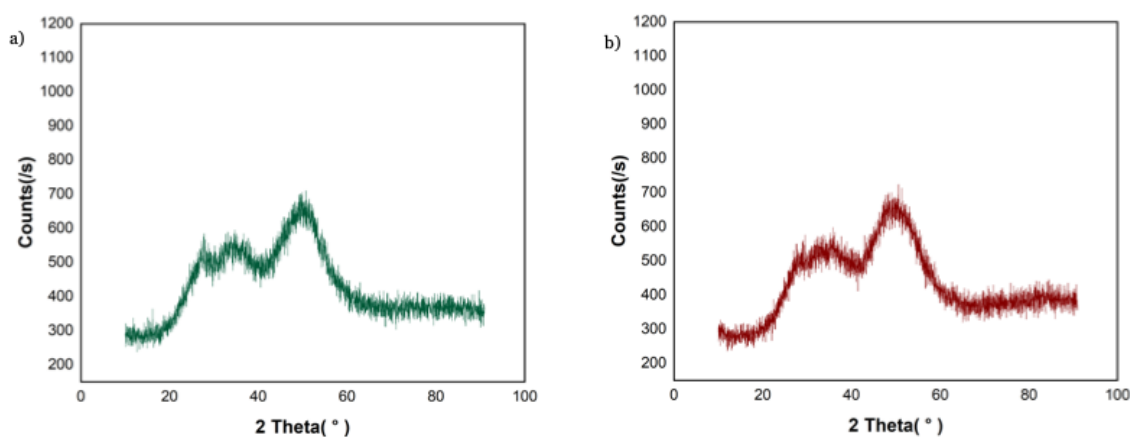


Figure 27. XRD pattern of Cu-ETT samples synthesized with 2 Cu equivalents at 60°C, (a) MeOH as solvent, (b) DMF as solvent

According to above XRD patterns, there are 3 broad peaks around 50°, 35° and 25° in both Cu-ETT samples. XRD spectra of all the other samples also consist of broad peaks. Broad peaks indicate that Cu-ETT is an amorphous material. Sun et al. in their work have mentioned the amorphous nature of metal-ETT polymers.[86]

Comparison in the interplanar distance of synthesized Cu-ETT samples can be performed by d (interplanar spacing) parameter in Bragg equation. For above 2 Cu-ETT samples d spacing is 1.858 Å ($2\theta=50.11$) with MeOH as solvent (sample number 9) and 1.864 Å ($2\theta=48.67$) with DMF as solvent (sample number 13). According to these values, there is no considerable difference in

interplanar distance between samples synthesized with MeOH and DMF as solvents. Similar as these results, variation temperature and number of Cu equivalents result in mostly same interplanar distances.

If the sample contains any crystalline impurities, it can be observed in XRD pattern of the sample as sharp peaks. Figure 28 shows XRD spectrum of Cu-ETT sample synthesized with 48-hour reaction time, 1 copper equivalent, DMF as solvent at 60°C. This Cu-ETT sample contains crystalline peaks indicating that some impurities are present. These impurities may be unreacted precursors/byproducts of the reaction which was not washed out completely during the washing process.

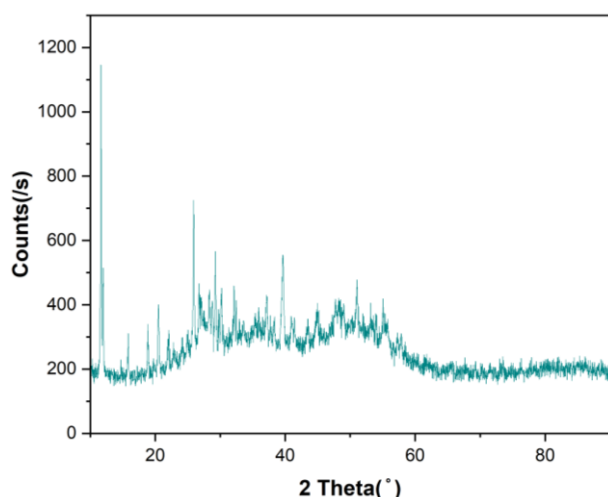


Figure 28. XRD pattern of Cu-ETT sample synthesized with 1 Cu equivalent, DMF as solvent at 60°C

Sun et al. have synthesized Ni-ETT and analysed XRD spectrum of it. They have observed four broad peaks at 14.8°, 27.8°, 40.4° and 52.0° suggesting Ni-ETT is an amorphous powder.[87] Ni and Cu ions have different ionic radii, and possible different electron configurations which can lead to different metal-ligand bond lengths and coordination geometry. The variation of this parameter can cause changes in crystal structure, bonding environment and thereby differences in XRD patterns of Cu-ETT and Ni-ETT.

6.1.2 Chemistry of Cu-ETT bulk material

The elemental composition of synthesized Cu-ETT bulk material was analysed by ICP-OES and elemental analyser. Qualitative and quantitative metal composition was examined by ICP-OES. According to analysed results from ICP-OES, Na and Cu are present in the sample. Qualitative and quantitative carbon, hydrogen, sulphur and nitrogen compositions were analysed by elemental analyser. Analysed Cu, Na, C, H, N and S composition of Cu-ETT synthesized with 2 Cu equivalents, MeOH at R.T is shown in table 04.

Table 04. Elemental composition of Cu-ETT sample synthesized with 2 Cu equivalents, MeOH at R.T (weight %)

Element	Weight percentage (%)
Cu	35.72
Na	0.20
C	5.40
O	2.99
S	25.01
N	0.05
H	0.52

Elemental ratios of S:C, Cu:S, Cu:C are 4.631, 1.428 and 6.615, respectively. According to element ratios one carbon atom bonded to 5 sulphur atoms and seven copper atoms, whereas one sulphur atom bonded to 1 copper atom. According to these elemental ratios, it is not possible to give accurate structure of this polymer since measured data cannot be expressed by the formula, Cu-ETT. Sun et al. have suggested possible reasons for this matter. Due to high rigidity of these polymer molecules, they have low solubility, and it is hard to polymerize as large polymer units with high molecular weight. It makes to precipitate low molecular weight polymer fragments and therefore the fraction of terminal groups in the polymer increases while creating an uncertainty of molecular formula. Another reason is the possibility of centre metal ion becoming

counter ion accidentally making it difficult to analyse the amount of centre metal ion accurately.[86]

The trace amount of sodium may be from NaOMe which was used as base to form Cu-ETT. Sodium can act as counter ion that maintains neutral electric charge. The source of hydrogen may be from water molecules tightly bound to Cu-ETT which cannot be removed completely.[88] The presence of oxygen may be from these water molecules and a contamination from reactant chemicals. There is a negligible amount of nitrogen which also can be a contamination from reactant chemicals.

Functional groups of synthesized Cu-ETT bulk samples were analysed by ATR equipped FT-IR. Figure 29 shows IR transmittance spectrum of Cu-ETT bulk sample synthesized with two Cu equivalents and DMF as solvent at 60 °C.

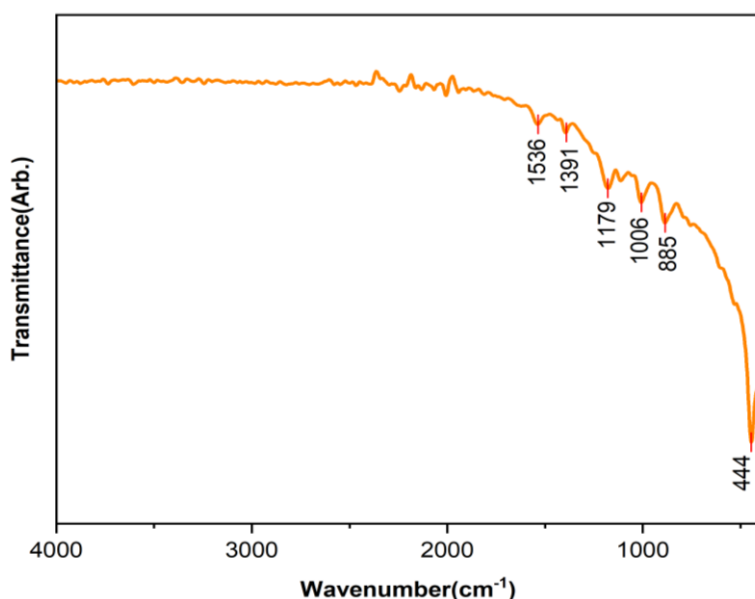


Figure 29.IR transmittance spectrum of Cu-ETT sample synthesized with two Cu equivalents and DMF as solvent at 60°C

In Figure 29, the spectrum is acquired in the region of 4000-400 cm^{-1} . Gupta et al. and Nachimuthu et al. have explained in their articles that peak at wavenumber of 454- 478 cm^{-1} is due to Cu-S stretching in CuS particles.[89], [90] Changes in bonding and molecular environment cause peak shifts in IR spectrum. Because of that, in this spectrum the characteristic peak at 444 cm^{-1} may

belong to Cu-S bond vibration of Cu-ETT. Presence of Cu-S bond in the sample indicates the bond between ligand and metal node which is a sign of existing Cu-ETT. The band at a wavenumber of 885 cm^{-1} is from C-S(aromatic) bond stretching. The peak at a wavenumber of 1536 cm^{-1} indicates C=C (aromatic) stretching. Peaks at 1179 cm^{-1} and 1391 cm^{-1} belong to C-H (aromatic) in plane bending and C-H(methyl) bending vibrations, respectively. Peak at 1006 cm^{-1} belongs to skeletal C-C vibrations. In this spectrum, there are no peaks at $1725\text{--}1705\text{ cm}^{-1}$ indicating that no C=O(ketone) stretching. It confirms unavailability of unreacted TPD molecules in the sample. There is a broad background absorption in Figure 29 which can be observed in other samples as well. Menon et al. have explained in their article about broad background absorption in IR spectrum which is common for conducting polymers.[84],[91],[89], [92]

Figure 30 shows IR transmittance spectrums of Cu-ETT samples synthesized with different numbers of Cu equivalents, solvents and temperatures.

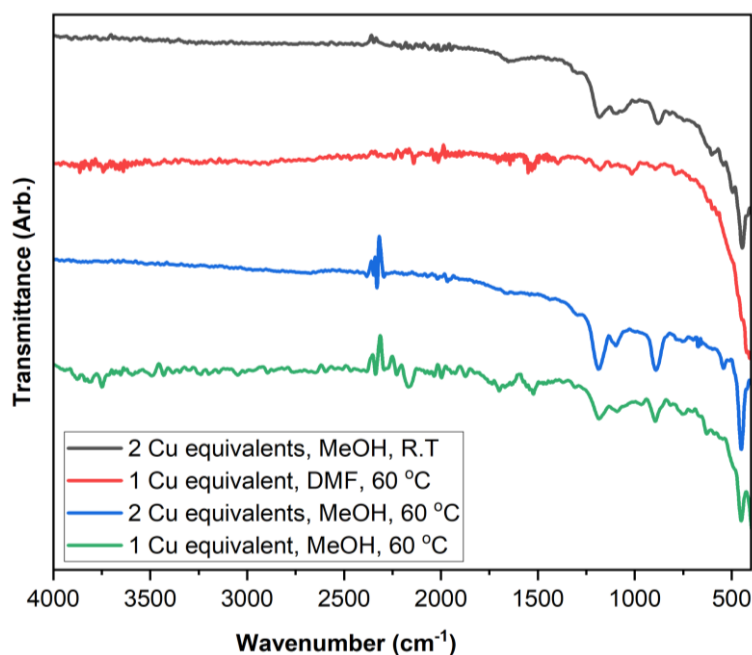


Figure 30. IR transmittance spectrums of Cu-ETT samples synthesized with different number of Cu equivalents, solvents and temperatures

In figure 30, some minor differences of the spectra can be observed when changing the solvent in the samples synthesized with 1 Cu equivalent, DMF at 60 °C and 1 Cu equivalent, MeOH at 60 °C. Both spectra have same peaks, but

the peak intensity and wavenumber of some peaks have changed. The characteristic peak for Cu-S stretching with DMF has shifted to a lower wavenumber. Changes in bond strength and chemical environment around bond cause peak shifting in IR spectrum. Strong bonds result in peaks at high wavenumbers and weak bonds result in peaks at low wavenumbers.[93] The IR spectrum of Cu-ETT synthesized with MeOH has high intensity peaks around 850 cm^{-1} and 1200 cm^{-1} which is responsible for C-S, C-H(aromatic) stretching. The peak at 2200 cm^{-1} may be due to C \equiv C stretching. [92] Having C \equiv C stretching indicates formation of some byproducts containing C \equiv C functional group.

When changing only the reaction temperature in the samples synthesized with 2 Cu equivalents, MeOH at R.T and 2 Cu equivalents, MeOH at $60\text{ }^{\circ}\text{C}$, intensity difference of some peaks could be observed. At $60\text{ }^{\circ}\text{C}$, intensity of peaks at 480 cm^{-1} , 850 cm^{-1} and 1200 cm^{-1} which are responsible for Cu-S, C-S and C-H(aromatic) stretching, respectively have increased when compared to the peaks in the spectra of Cu-ETT at R.T. High intensity of peaks indicate high stoichiometry of chemical bonds.

In figure 30, intensity difference of peaks could be observed when changing only the number of Cu equivalents in the samples synthesized with 2 Cu equivalents, MeOH at $60\text{ }^{\circ}\text{C}$ and 1 Cu equivalent, MeOH at $60\text{ }^{\circ}\text{C}$. With 2 Cu equivalents, peaks around 480 cm^{-1} , 850 cm^{-1} , 1200 cm^{-1} responsible for Cu-S, C-S, C-H(aromatic), respectively high intensity indicating high stoichiometric ratio.

Figure 31 shows SEM images of synthesized Cu-ETT bulk sample with 1 Cu equivalent and MeOH as solvent at $60\text{ }^{\circ}\text{C}$. These SEM images show that the Cu-ETT bulk sample has uniformly distributed particles and the particle size is in a few nanometers(nm) range.

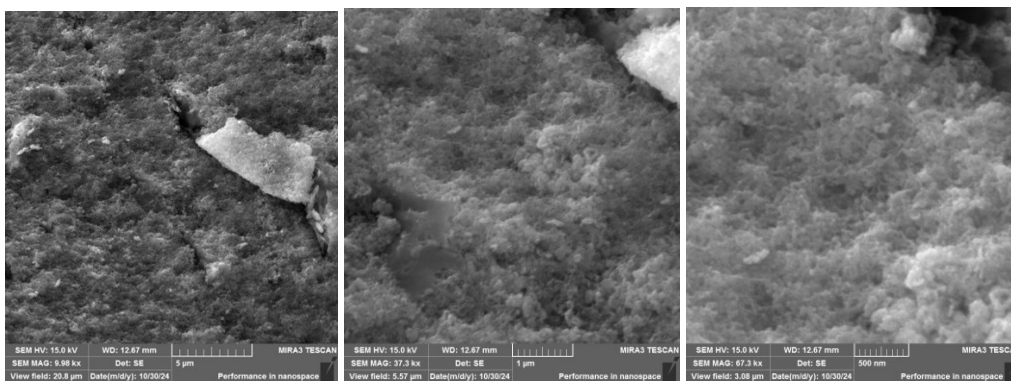


Figure 31. SEM images of synthesized Cu-ETT bulk sample with 1 Cu equivalent and MeOH as solvent at 60 °C, with 9.98 kx(left side), 37.3 kx(middle) and 67.3 kx(right side) magnification

Figure 32 shows macroscopic images of synthesized Cu-ETT bulk sample with 1 Cu equivalent and MeOH as solvent at 60 °C. Cu-ETT bulk sample is a black colour fine powder.

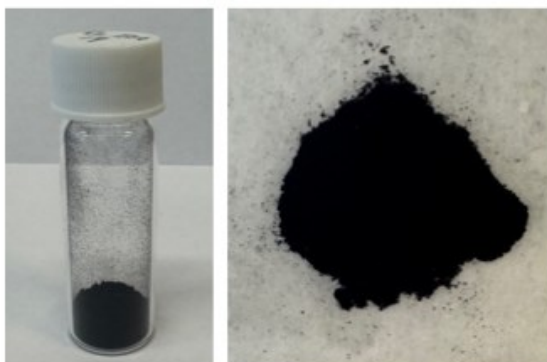


Figure 32. Macroscopic images of synthesized Cu-ETT bulk sample with 1 Cu equivalent and MeOH as solvent at 60 °C

6.1.3 Thermoelectrical properties

Thermoelectrical properties of synthesized Cu-ETT bulk samples were analysed by PPMS. Thermal conductivity, electrical resistivity and Seebeck coefficient were analysed by varying temperature from 0-400 K. Figure 33 shows temperature dependence of thermal conductivity of synthesized Cu-ETT samples.

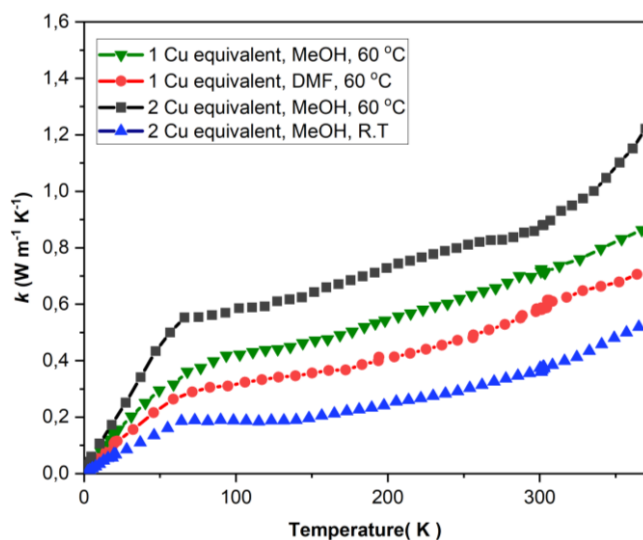


Figure 33. Temperature dependence of thermal conductivity of synthesized Cu-ETT samples

In figure 33, synthesized sample's thermal conductivity has risen with elevated temperature while exhibiting typical behaviour of amorphous compounds. In amorphous materials heat is transported mainly by propagons, diffusons and locons rather than phonons in crystalline materials. These are different types of vibrational modes that contribute to the heat transport in amorphous materials. When the temperature increases, number of thermally activated vibrational modes increase resulting in high thermal conductivity.[94] But amorphous materials have comparatively low thermal conductivity due to short-range ordering which limits the heat transport by vibrations. Thermal conductivity of amorphous materials varies from 0.1- 1 W m⁻¹ K⁻¹.[95] In figure 33, thermal conductivity has varied from 0 to 1.25 W m⁻¹ K⁻¹ between 0-370 K. Sheng et al. have shown in their article the temperature dependency of thermal conductivity of Cu-ETT material has increased when increasing the temperature indicating amorphous nature of the material.[1]

Type of solvent, temperature and number of Cu equivalents can affect the thermal conductivity. In figure 33 when changing only the solvent, Cu-ETT sample synthesized with 1 Cu equivalent, MeOH, 60 °C has exhibited higher thermal conductivity than the sample synthesized with 1 Cu equivalent, DMF, 60 °C. Solvent can affect to chain alignment of amorphous material and thereby

thermal conductivity. Singh et al. have shown that amorphous polythiophene exhibits high thermal conductivity when improving chain alignment.[96] In figure 33 when changing only the temperature, Cu-ETT sample synthesized with 2 Cu equivalents, MeOH at 60 °C have exhibited higher thermal conductivity than the sample with 2 Cu equivalents, MeOH at R.T. High reaction temperature can enhance atomic mobility during synthesizing process resulting in more aligned and compact structure. It reduces voids inside the material leading to high thermal conductivity. [97] In figure 33, when changing only the number of Cu equivalents, Cu-ETT sample synthesized with 2 Cu equivalents, MeOH, 60 °C has exhibited higher thermal conductivity than the sample synthesized with 1 Cu equivalent, MeOH at 60 °C. When the number of Cu equivalents is increased it can enhance the thermal conductivity by electronic components. Because Cu is a metal with high thermal conductivity due to high density of free electrons.

Figure 34 shows temperature dependence of electrical resistivity of synthesized Cu-ETT samples.

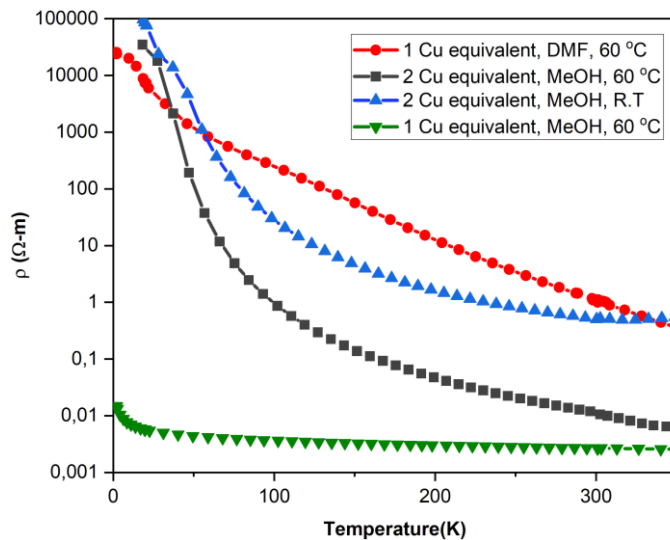


Figure 34. Temperature dependence of electrical resistivity of synthesized Cu-ETT samples

In figure 34, electrical resistivity of synthesized samples is reduced when increasing temperature due to increasing charge carrier (holes) concentration.

As electrical resistivity inversely proportional to electrical conductivity it shows the increment of electrical conductivity when increasing temperature which is a typical behaviour for semiconductor.[83],[1]

Electrical conductivity also affected by solvent, reaction temperature and number of Cu equivalents. In figure 34 when changing only the solvent, Cu-ETT sample synthesized with 1 Cu equivalent, DMF at 60 °C has exhibited low electrical conductivity than the sample synthesized with 1 Cu equivalent, MeOH at 60 °C. Rajab et al. have exhibited the variation of electrical conductivity when using different solvents to synthesize conducting polymer, poly(O-Toluidine). Different solvents make different activation energies for reaction resulting different electrical conductivity with solvent. [98]

In figure 34, when changing only the temperature, Cu-ETT sample with 2 Cu equivalents, MeOH at 60 °C has exhibited high electrical conductivity than the sample synthesized with 2 Cu equivalents, MeOH at R.T. In disordered materials, electrical transport occurred via localized states near the band edges by hopping conduction mechanism. At high temperatures, carriers are thermally activated and overcome the energy barrier resulting high electrical conductivity. [99] In figure 34 when increasing only the number of Cu equivalents, Cu-ETT sample synthesized with 2 Cu equivalents, MeOH at 60 °C has exhibited low electrical conductivity than the sample synthesized with 1 Cu equivalents, MeOH at 60 °C. CuCl_2 contains Cu^{2+} which can act as a p type dopant in semiconductor materials.[100] Koopmans et al. in their article have shown that when increasing doping density can enhance the electrical conductivity into a certain limit. But after a certain limit of adding dopant result reducing electrical conductivity due to structural dopant induced disorders.[101] This can be a reason for reduced electrical conductivity with high number of Cu equivalents may be having disorders in structure.

Figure 35 shows temperature dependence of Seebeck coefficient of synthesized Cu-ETT samples.

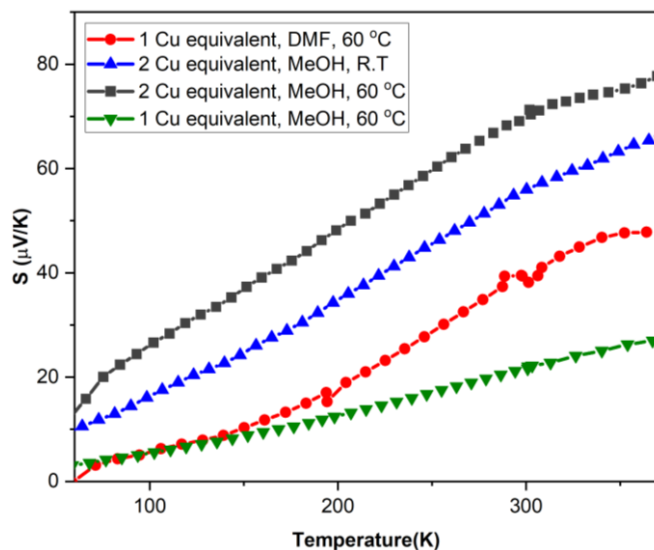


Figure 35. Temperature dependence of Seebeck coefficient of synthesized Cu-ETT samples

In figure 35, Seebeck coefficient has increased when increasing the temperature and the positive sign of Seebeck coefficient indicate the p type charge carriers in the Cu-ETT polymer. When the temperature increases carrier concentration and mobility also increase while decreasing the Seebeck coefficient.[102] Sheng et al. have reported the p type semiconductor behaviour of Cu-ETT with the graphs of positive sign in their article.[1]

The Seebeck coefficient indicates the thermoelectric power generation efficiency of a material. Materials with high Seebeck coefficient generates high voltage in a particular temperature gradient making it more efficient in converting heat energy to electricity.[103] In figure 35, highest Seebeck coefficient can be observed with Cu-ETT sample synthesized with 2 Cu equivalents, MeOH at 60 °C which is the sample with highest thermoelectric power generation.

6.2 ALD/MLD

6.2.1 Deposition process optimization for Cu-ETT

In this thesis, two ALD and MLD processes have been carried out with different precursors to fabricate Cu-ETT thin films. Identification of optimized process parameters for chosen precursors is important to ensure reliable and effective ALD and MLD processes. Under process parameter optimization, pulse length was optimized for 3 precursors which were Li-HMDS, Cu(acac)₂ and TPD.

LiO^tBu and Li-HMDS were used as bases for fabricating Cu-ETT thin films. Among these 2 different bases, Li-HMDS was chosen for process optimization over LiO^tBu because of comparatively low pulse length saturation time of Li-HMDS. For different ALD processes pulse saturation time for Li-HMDS is around 3-4 s.[104],[105] Madadi et al. and Pearse et al. proved that the pulse length saturation time of LiO^tBu in different ALD processes is around 20 seconds which can be due to reactor system and time take to reach precursor molecules to substrate.[106],[107] In the Cu-ETT process, GPC values indicate the possible saturation behaviour of Li-HMDS is around 3-4 seconds. Pulse length optimization for Li-HMDS at 220 °C is shown in Figure 36(a).

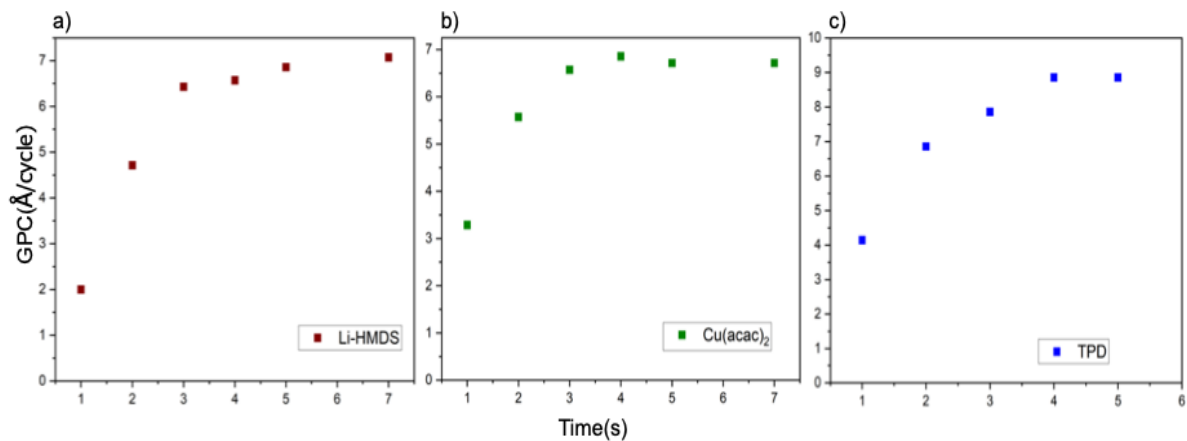


Figure 36. Pulse length optimization for (a) Li-HMDS when pulse/purge lengths were 2 s/8s, 3 s/12s for TPD, Cu(acac)₂, (b) Cu(acac)₂ when pulse/purge lengths were 2 s/8 s, 4 s/16 s for TPD, Li-HMDS and, (c) TPD when pulse/purge lengths were 4 s/16 s for Cu(acac)₂ and Li-HMDS at 220 °C

For different ALD processes pulse length saturation of $\text{Cu}(\text{acac})_2$ has been reported in the range of 2-3 seconds.[108], [109] In our Cu-ETT process, GPC values indicate the possible saturation behaviour of $\text{Cu}(\text{acac})_2$ around 3-4 seconds. Figure 36(b) shows the pulse length optimization curve of $\text{Cu}(\text{acac})_2$.

According to Figure 36(c), possible saturation behaviour of TPD is around 4-5 seconds. There is no literature available on TPD as a precursor for ALD and/or MLD process. TPD is a bulky molecule as shown in Figure 23. It slowly diffuses to the active sites on the substrate resulting longer pulse time to saturate. According to Sønsteby et al., there is a possibility of varying pulse saturation lengths of air/moisture sensitive precursors in ALD process. TPD is recognised as an air sensitive precursor. During ALD process, TPD was shortly exposed to ambient air when transferring to the ALD reactor. Also, between 2 depositions, reactor opened for next substrate, and this can help to expose precursor to ambient air. This might affect the saturation behaviour of TPD, and saturation pulse length can be varied from what we got during our Cu-ETT process. [110]

Figure 37(a) shows linear dependency of thin film thickness with number of ALD/MLD cycles at 220 °C. Pulse and purge lengths of $\text{Cu}(\text{acac})_2$, Li-HMDS and TPD were fixed to 3 /12 s, 3/12 s and 2/ 8 s, respectively. The thickness controllability of Cu-ETT ALD/MLD process can be observed by the linear behaviour of film thickness while increasing number of ALD/MLD cycles. Linearity of thickness is a key characteristic of ALD/MLD technique.

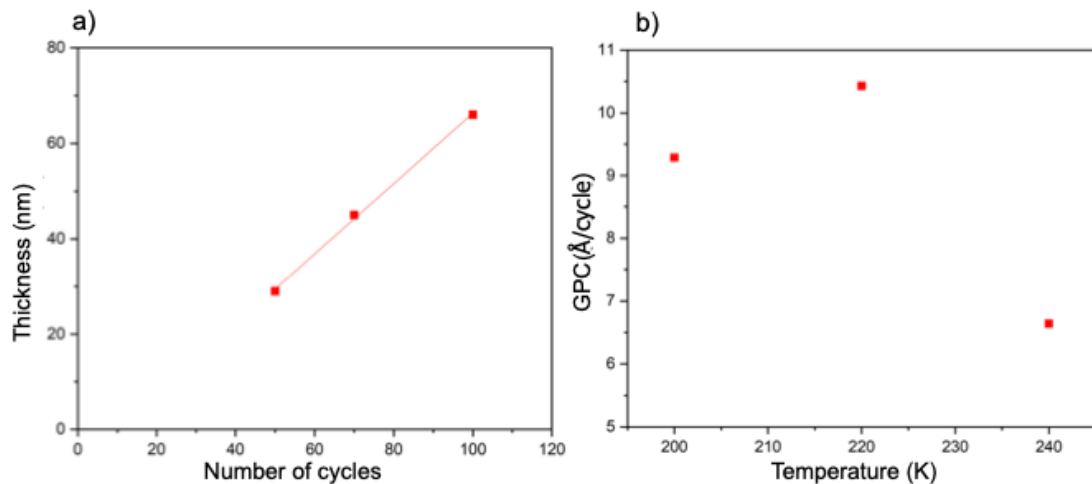


Figure 37. (a) Film thickness as a function of deposition number of cycles at 220 °C, (b) The GPC as a function of deposition temperature in Cu-ETT process

Figure 37(b) shows temperature dependency of GPC of Cu-ETT ALD process. Fluctuation of GPC can be observed in our Cu-ETT process. Although it is expected to have a high GPC value at 240 °C, it resulted in a low GPC value. One of a reason for this may be, the thermal decomposition of precursors leading to incomplete surface coverage during prolonged time in high temperatures. The deposition temperature was chosen as 220 °C to ensure the electrical conductivity of Cu-ETT thin films and to avoid possible precursor decomposition.

6.2.2 Chemistry of fabricated thin films

8.2.2.1 FT-IR of fabricated thin films

Cu-ETT is an important material due to its potential capability of used as a thermoelectric material for various applications. Functional groups and relative stoichiometry of each functional group of Cu-ETT can be analysed with FT-IR. Figure 38 shows FT-IR spectrum of deposited Cu-ETT thin film at 220 °C.

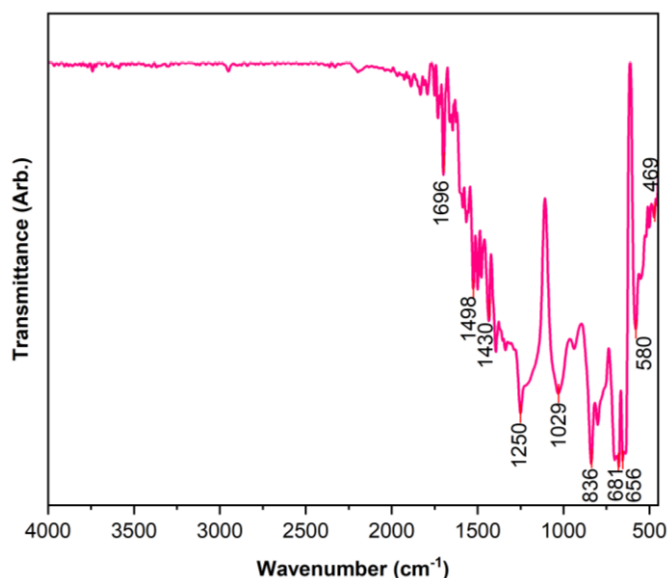


Figure 38. FT-IR spectrum of deposited Cu-ETT thin film with pulse/purge time of TPD, Li-HMDS and Cu(acac)₂ are 7/28 s, 4/16 s and 4/16 s, respectively. The deposition temperature was 220 °C.

In Figure 38, the characteristic peak at 469 cm⁻¹ and 656 cm⁻¹ is attributed to Cu-S stretching. [111] The peak at 1696 cm⁻¹ is due to C=O(ketone) stretching indicating availability of unreacted TPD molecules in the Cu-ETT thin films. The reason for it can be insufficient purge length of TPD. Peak at 681 cm⁻¹ due to aromatic out of plane =C-H bending. The peak at 1501 cm⁻¹ belongs to C=C stretching vibration. The peak at 580 cm⁻¹ and 836 cm⁻¹ belongs to C-S stretching.[91] Peak at 1430 cm⁻¹ due to -CH₂ scissoring. Peak at 1029 cm⁻¹ is from S=O stretching and peak at 1250 cm⁻¹ is from C-O stretching vibration.[112], [92] These S=O and C-O functional groups may be from byproducts or unreacted precursors. C-O functional group can be observed in Cu(acac)₂. Remaining of unreacted precursors and byproducts realize the importance of purge length optimization which we could not carry out within a limited time.

As a proof of concept, Ni(acac)₂ was used instead of Cu(acac)₂ with TPD and Li-HMDS to deposit Ni-ETT thin films. FT-IR spectrum of fabricated Ni-ETT thin film with these precursors is shown in Figure 39.

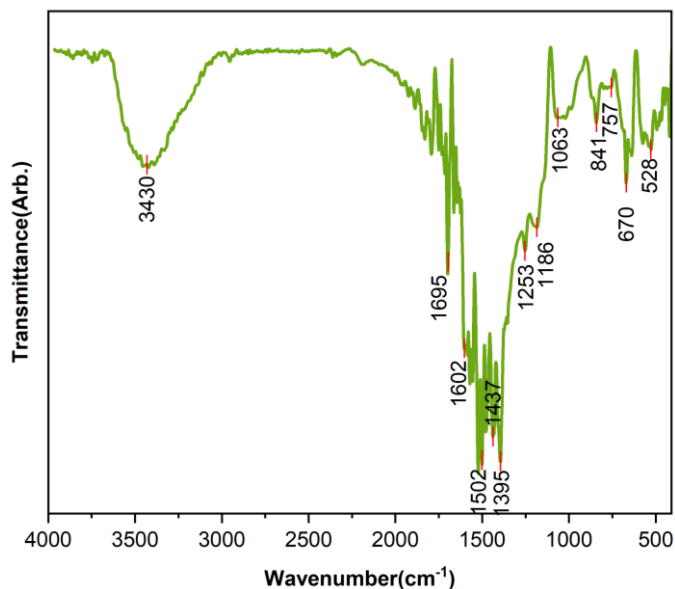


Figure 39. FT-IR spectrum of deposited thin film with pulse/purge time of TPD, Li-HMDS and Ni(acac)₂ are 2/8 s, 3/12 s and 3/12 s, respectively with 200 cycles. The deposition temperature was 220 °C.

In Figure 39, other than common peaks to Cu-ETT, few peaks can be observed. Characteristic peaks at 528 cm⁻¹ and 757 cm⁻¹ are attributed to Ni-S symmetric bond stretching and 1063 is attributed to Ni-S asymmetric bond stretching.[90], [113] Peak at 3430 cm⁻¹ is due to OH group stretching and peak at 1395 cm⁻¹ is due to OH bending of H₂O or OH group containing compound.[114]

Figure 40 shows FT-IR spectra of Two Cu-ETT ALD processes with different lithium precursors LiO^tBu and Li-HMDS.

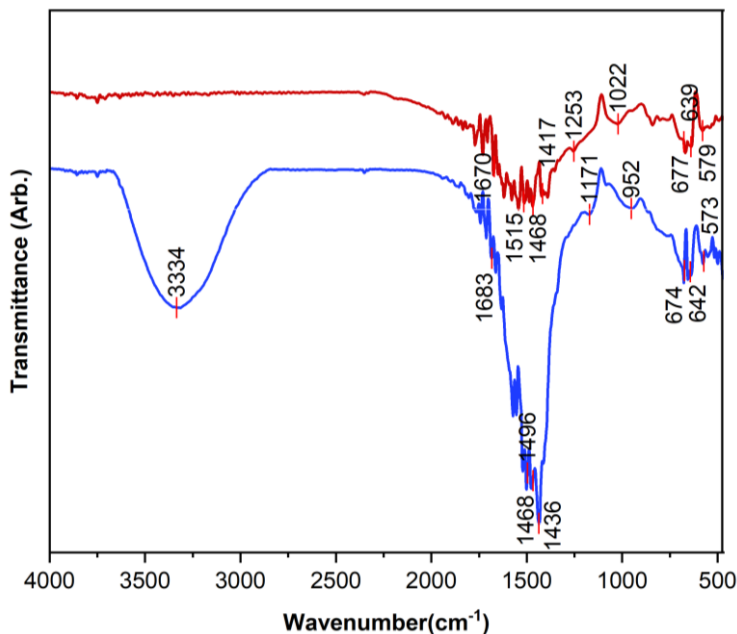


Figure 40. Two Cu-ETT ALD processes with different lithium precursors Li-O^tBu and Li-HMDS, both deposited at 220 °C. Pulse/purge length for Cu(acac)₂, LiO^tBu and Li-HMDS is 3/12 s and for TPD is 2/8 s.

In Figure 40, two ALD processes have compared by using different lithium precursors to deposit Cu-ETT thin films. The deposition temperature was same for both processes which is 220 °C. Precursor temperature of Li-HMDS, Li-O^tBu, TPD and Cu(acac)₂ are 60 °C, 130 °C, 90 °C and 120 °C, respectively. Cu-S stretching peaks around wavenumber 670 cm⁻¹ is observed in both spectra. There is a stoichiometry difference of Cu-S bond between 2 spectra. Peaks around 1430-1470 cm⁻¹ belong to C-H bending in alkanes. There is a high stoichiometry difference of C-H(alkanes) functional group in 2 depositions. Another worth to mention difference between these two IR spectra is the peak at 3339 cm⁻¹ belongs to O-H stretching which can be observed in the deposition with LiO^tBu.[91] This peak cannot be observed in the FT-IR belongs to the deposition of Cu-ETT with Li-HMDS. The reason for appearing moisture peak is, high reactivity of LiO^tBu towards moisture compared to Li-HMDS. As shown in chapter 4.2.1, Li-HMDS is more sterically hindered compared to Li-O^tBu. Steric effect in Li-HMDS avoid reacting with water molecules. But as a strong base, LiOtBu readily react with moisture and result lithium hydroxide and tert-butanol.[110]

6.2.2.2 GI-XRD of fabricated thin films

To analyse the structural properties of fabricated thin film, GIXRD was used. GIXRD pattern of thin film fabricated at at 220 °C with 200 cycles pulse/ purge lengths of Cu(acac)₂, Li-HMDS and TPD are 3/12 s, 3/12 s and 2/8 s, respectively is shown in Figure 41.

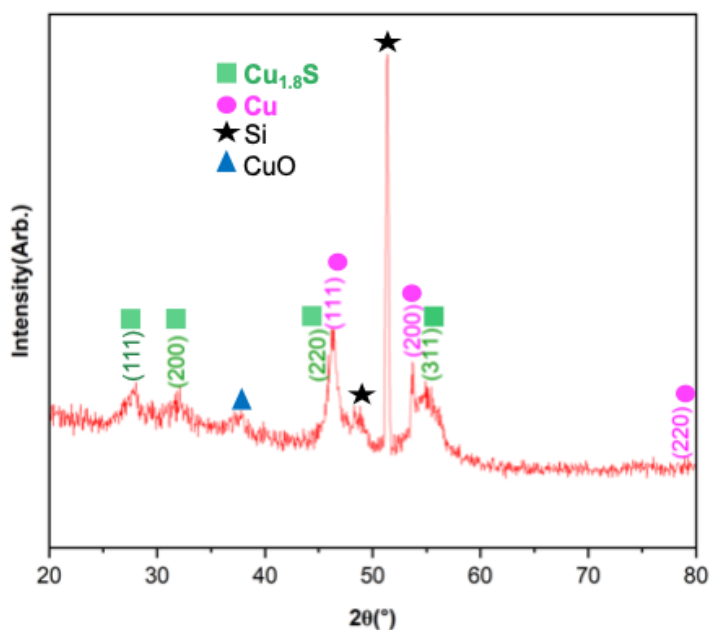


Figure 41. GIXRD of synthesized thin film at 220 °C with 200 cycles pulse/ purge lengths of Cu(acac)₂, Li-HMDS and TPD are 3/12 s, 3/12 s and 2/8 s, respectively.

In Figure 41, there are sharp peaks indicating crystallinity of the sample. According to analysed results with Highscore software, peaks around 46, 53 and 79 match with XRD pattern of Cu (ICDD-04-028-0148). Peaks at 28, 32, 45 and 55 match with XRD pattern of Cu_{1.8}S (ICDD-04-007-9851). These Highscore matching results show that the sample consists of Cu and Cu_{1.8}S. The peak around 47 is due to Si, because Cu-ETT films deposited on Si substrate.[115] The peak around 37 is due to CuO.[116]

8.2.2.3 Morphology of fabricated thin films

To observe the surface morphology of synthesized Cu-ETT thin film, SEM images were taken at 220 °C, for 300 cycles from 2 kx to 40.2 kx magnification. These SEM images are shown in Figure 42. The image with 40.2x magnification clearly shows dents and highly textured areas on thin film indicating roughness of the surface.

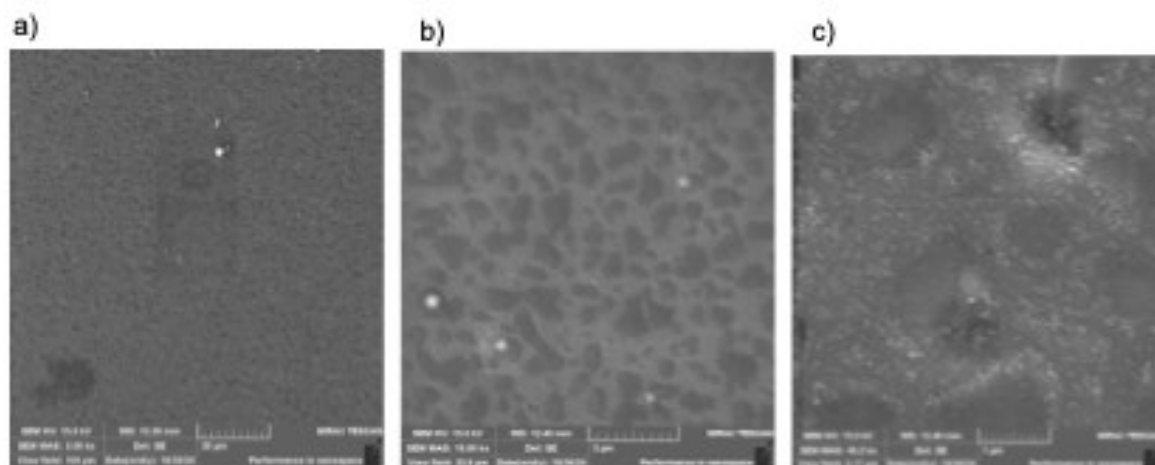


Figure 42. SEM images of synthesized Cu-ETT thin films at 220 °C, 300 cycles with 2 kx(left side), 10 kx(middle) and 40.2 kx(right side) magnification.

Macroscopic view of fabricated thin film on silicon substrate and borosilicate glass substrate at 220 °C with 300 cycles are shown in Figure 43. Deposition on silicon substrate has bluish purple colour and glass substrate has pale brown colour. High conformality of ALD technique exhibited by depositing film back side (less exposed region) of the substrate.

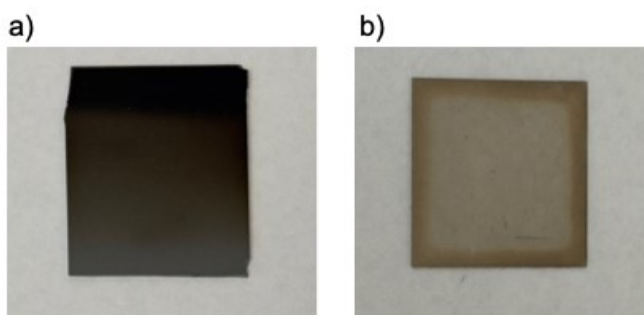


Figure 43. Macroscopic view of synthesized Cu-ETT thin film at 220 °C, 300 cycles (a) on silicon substrate and (b) on borosilicate glass substrate

6.2.3 Thermoelectric properties of Cu-ETT thin films

Electrical resistivity of deposited Cu-ETT thin films on borosilicate glass substrate was measured because electrical resistivity directly affects the thermoelectric efficiency. Figure 44 shows temperature dependence of electrical resistivity of synthesized Cu-ETT thin film with 200 cycles deposited at 220 °C and the pulse/purge times were 4 s/16 s for Li-HMDS and Cu(acac)₂ and 7 s/28 s for TPD.

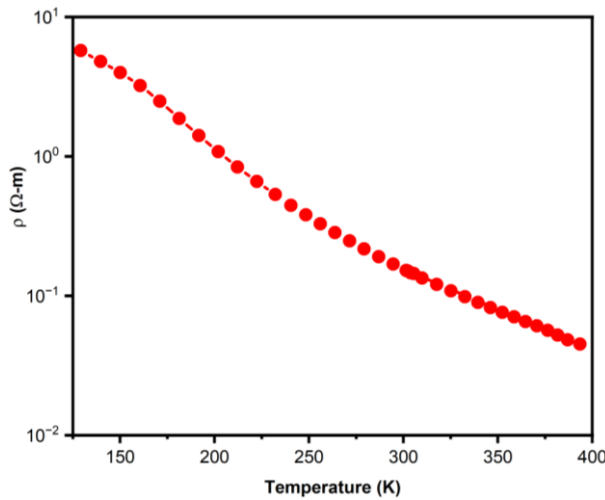


Figure 44. Temperature dependence of electrical resistivity of synthesized Cu-ETT thin film with 200 cycles, deposited at 220 °C and the pulse/purge times were 4 s/16 s for Li-HMDS and Cu(acac)₂ and 7 s/28 s for TPD

In figure 44, electrical resistivity of deposited thin film was measured by PPMS technique. Electrical resistivity has decreased when increasing the temperature due to increasing charge carrier (holes) concentration. As electrical resistivity inversely proportional to electrical conductivity it shows the increment of electrical conductivity when increasing temperature which is a typical behaviour for semiconductor.[83],[1]

Electrical resistivity of Cu-ETT thin films deposited during process optimization was measured with multi meter. During the pulse length optimization of Cu(acac)₂ precursor, pulse/purge lengths of TPD, Li-HMDS were set at 2 s/8 s, 4 s/16 s for, respectively at 220 °C. Until 7 s pulse length of Cu(acac)₂ no electrical resistivity was observed. But at 7 S pulse length electrical resistivity on borosilicate glass was observed. One of a possible reason for it is, not having O-H containing chemical species in the film which could observed in the FT-

IR spectrum. If the deposited thin film containing chemically less stable/unstable compounds, these compounds can react with H₂O molecules in the air to form stable compounds. Different thin films containing Cu compounds have shown reduction in electrical conductivity after exposing to moisture.[117],[118] Cu containing compounds can react with H₂O and result Cu(OH)₂ (which is not electrical conductive) or they can physically adsorb water molecules to form hydrated phase on thin film which can act as an insulating layer inhibiting charge carrier mobility.[119] Another possible reason for electrical resistivity at 7 s pulse length may be, considerable amount of metallic Cu or CuS or electrically conductive Cu compounds resulted from decomposition/reduction of Cu(acac)₂ which can be detected by multi meter. Although 1 s, 2 s, 3 s, 4 s and 5 s pulse time depositions result metallic Cu/electrically conductive Cu compounds, the amount may not be sufficient to generate comparatively high electrical resistivity which can monitor by multi meter (as electrical resistance). Tripathi et al. have deposited metallic Cu films by ALD with Cu(acac)₂ and hydroquinone/water as reductants.[109]

During pulse length optimization of TPD and Li-HMDS, electrical resistivity was not observed in the deposited Cu-ETT thin films. As discussed above the possible reason may be presence of O-H containing species in Cu-ETT thin films which could observe in FT-IR spectra.

During the temperature optimization of Cu-ETT process, electrical resistivity was observed only at 220 °C and not observed at 200 °C or 240 °C. The reason for not showing electrical resistivity at 240 °C may be the thermal decomposition of precursors due to high temperature. At 200 °C, low deposition temperature can lead to partially adsorb or react precursors on the substrate of the thin film resulting incomplete reactions and thereby no electrical resistivity in the film.

Figure 45 shows temperature dependence of Seebeck coefficient of synthesized Cu-ETT thin film with 200 cycles deposited at 220 °C and the pulse/purge times were 4 s/16 s for Li-HMDS and Cu(acac)₂ and 7 s/28 s for TPD.

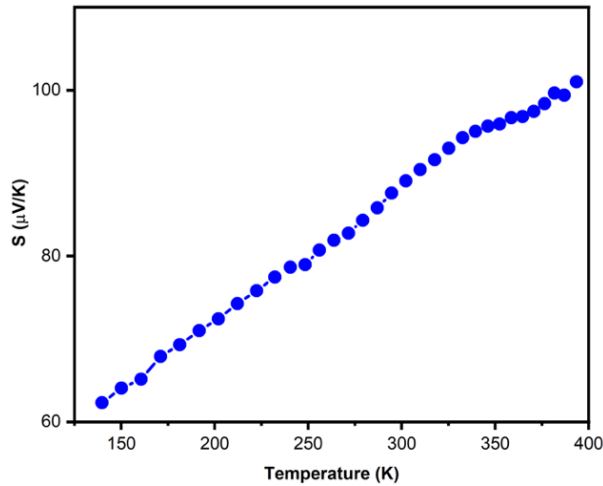


Figure 45. Temperature dependence of Seebeck coefficient of synthesized Cu-ETT thin film with 200 cycles, deposited at 220 °C and the pulse/purge times were 4 s/16 s for Li-HMDS and Cu(acac)₂ and 7 s/28 s for TPD

Seebeck coefficient of deposited Cu-ETT thin film was measured with PPMS technique. In figure 45, Seebeck coefficient has increased when increasing the temperature and the positive sign of Seebeck coefficient indicate the p type charge carriers in the Cu-ETT polymer. When the temperature increases carrier concentration and mobility also increase while decreasing the Seebeck coefficient.[102]

6.2.4 Stability of Cu-ETT thin films

The stability of synthesized Cu-ETT films were analysed using FT-IR. Cu-ETT thin films of 200 cycles were deposited at 220 °C and the pulse/purge times were 4 s/16 s for Li-HMDS and Cu(acac)₂ and 7 s/28 s for TPD. Couple of silicon wafer and borosilicate glass substrate were kept in ambient air, humid conditions and a desiccator. Samples were measured right after deposition (0 hour), 1 hour after deposition and then 1 day, 4 days, 8 days and 14 days after deposition. The FT-IR measurements are shown in Figure 46 and electrically conductive behaviour of borosilicate glass substrates shown in Table 05.

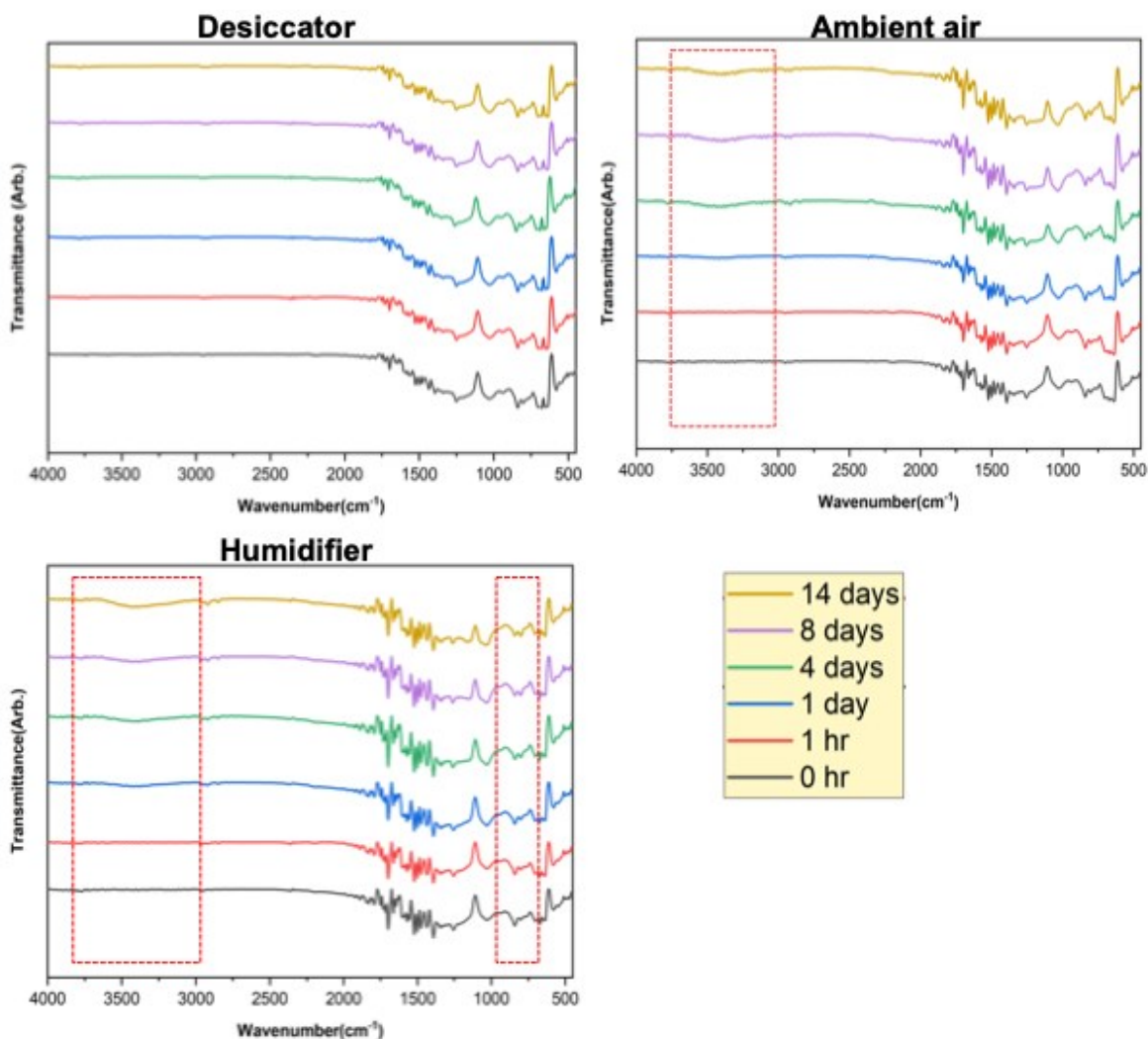


Figure 46. The variations of FT-IR spectra with time for Cu-ETT thin films under 3 different conditions, ambient air, humidifier and desiccator

Table 05. Electrical conductivity of borosilicate glasses kept at ambient air, humidifier and desiccator right after deposition (0 minute), 1 hour after deposition and then 1 day, 4 days, 8 days and 14 days after deposition.

Condition	After 0 minute (MΩ)	After 1 hour (MΩ)	After 1 day (MΩ)	After 4 days (MΩ)	After 8 days (MΩ)	After 14 days (MΩ)
Ambient air	0.6-35	0.6-35	0.3-35	0.3-35	0-35	0-35
Humidifier	2-30	2-30	-	-	-	-
Desiccator	4-38	4-38	4-38	4-38	4-38	4-38

The stability of M-ETT bulk material has discussed in the literature, although there is no literature available for Cu-ETT thin film fabrication so far. According to literature, M-ETT is a stable material in the ambient air.[84] After 0

minute (just after the deposition) the different areas of the glass substrate shows various electrical resistivity values due to high gradient of the synthesized Cu-ETT thin film.

In Figure 46, FT-IR spectra of Cu-ETT show good stability in the desiccator. There is no intensity variation of characteristic peaks over time. The electrical conductivity measurements of film kept in the desiccator do not show any variation with time. It remains in the range of 4-38 M Ω throughout 14 days. In the ambient air, it can observe slight growth of peak around 3500 cm⁻¹ indicating the amount of moisture or hydroxyl functional group containing compound is increasing from day 4. Electrical conductivity of the thin film sample kept in ambient has shown 0.6-35 M Ω until 1 hour and electrical conductivity has reduced from day 1. There can be Cu containing compounds in the film which can react with H₂O and result Cu(OH)₂ or physically adsorb water and form hydrated phase in the thin film over time which can act as an insulating layer inhibiting charge carrier mobility.[119] Cheng et al. and Dhonge et al have reported reduction of electrical conductivity of Cu compounds containing thin films with increasing moisture content.[117], [118]

The most interesting results for chemical stability can be observed in the sample kept in the humidifier. In FT-IR spectrum, the peak around 3500 cm⁻¹ and 800 cm⁻¹ are growing from day 1. Enhancing intensity of peak at 3500 cm⁻¹ indicates increasing the amount of adsorbed water/hydroxyl group containing compound. Enhancing the intensity of peak at 800 cm⁻¹ indicates increasing the amount of C-H group containing aromatic compound. Electrical conductivity was 2-30 M Ω until 1 hour and from day 1 no electrical conductivity was observed. As discussed above, the possible reason for this may be forming an insulating layer on the surface of the film by reacting Cu containing compounds with moisture.

7 Conclusions and research suggestions

In this thesis, copper containing metal organic polymer, copper-ethylene-tetrathiolate (Cu-ETT) which is a thermoelectric material was synthesized with two different synthesis methods. Bulk material of Cu-ETT synthesized with chemical synthesis method. Experimental conditions were varied to study the thermoelectric properties of synthesized Cu-ETT samples. Cu-ETT thin films were deposited via ALD/MLD technique and process parameter optimization was carried out. The electrical resistivity of deposited thin films was studied.

The literature section of this thesis was written and linked to the experimental section to understand the synthesized methods and their importance. Although there is no literature available about electrically conductive MOF (EC-MOF) thin films deposited with ALD/MLD technique, the literature section gives a broad idea about this technique. Also, literature section explains an overview of MOFs and EC-MOFs. Electrically conductive mechanisms and the approaches to designing EC-MOFs were discussed in detail. Understanding electrically conductive mechanisms is crucial in MOFs with high electrical conductivity. Because electrical conductivity directly impacts the efficiency of thermoelectric performance. It is evident that the presence of π conjugated organic linker, mixed valency in SBU or organic linker, coordinating atom, 2-dimensionality, and guest molecule introduction into the inner pore of MOF help to enhance or introduce conductivity in MOFs.

The experimental section of this thesis aimed to synthesize thermoelectric material, Cu-ETT as bulk material and thin films. For this purpose, Cu-ETT bulk material was synthesized with chemical synthesis method by using 1,3,4,6-tetrathiapentalene-2,5-dione (TPD) as the organic linker source, copper chloride dihydrate ($\text{CuCl}_2 \cdot 2\text{H}_2\text{O}$) as secondary building unit (SBU) source and sodium methoxide (NaOMe) as the base. The effect of several reaction parameters on thermoelectric behaviour was studied by varying the number of Cu equivalents, temperatures and solvents. Cu-ETT thin film was deposited with two different ALD/MLD processes that had different bases lithium *tert*-butoxide (Li-O t Bu) and lithium bis(trimethylsilyl)amide(Li-HMDS). Other

precursors, TPD and copper acetylacetonate ($\text{Cu}(\text{acac})_2$) were same for both ALD/MLD processes. In this thesis, ALD/MLD processes of Cu-ETT were compared by varying pulse/ purge lengths and thus changing the exposure time of precursors. Electrical resistivity was measured with each deposition to study the effect of deposition parameter variation on electrical resistivity.

When considering bulk synthesis results, powder XRD results showed that Cu-ETT is an amorphous material. Because of the amorphous nature of Cu-ETT, the XRD pattern gave broad peaks and thus could not assign the peaks to find the composition or crystal structure of synthesized material.

ICP-OES and elemental analyser results showed that synthesized sample contains C, Cu, S, H and Na. Although the elemental ratio of the sample is determined from the weight percentage of these elements, the chemical formula could not be found. The reason for this was, the possibility of centre metal ion becoming counter ion and polymerizing the compound as a low molecular weight polymer with a high fraction of terminal groups. In this thesis, ATR equipped FT-IR was used to identify the functional groups present in the sample. But when analysing amorphous materials with ATR equipped with FT-IR, it gave broad peaks due to the lack of long-range order. Hence for precise determination of chemical composition and formula, characterization techniques such as X-ray photoelectron spectroscopy (XPS), X-ray Absorption Near Edge Structure (XANES) and Extended X-ray Absorption Fine Structure (EXAFS) are required.

Thermoelectric properties such as thermal conductivity, electrical resistivity and Seebeck coefficient of synthesized four different Cu-ETT samples were analysed with PPMS. Low electrical resistivity and low thermal conductivity were expected in the sample with the highest thermoelectric performance. However, the lowest thermal conductivity and lowest electrical resistivity were recorded in two different samples. Annealing of Cu-ETT sample is one of a solution for it. Annealing can improve the thermoelectric properties and make the consistency of multiple samples by relieving the internal stress of the samples and refining the microstructure. Another option is to apply a high and equal level

of pressure for all samples when preparing sample pellets for PPMS measurements. It makes dense and compact structures reducing voids and grain boundaries. Voids can disrupt the charge transport pathways increasing electrical resistivity and, vibrational mode scattering can occur at grain boundaries lowering thermal conductivity. The Cu-ETT sample with the highest thermoelectric performance can be identified by plotting the graphs of temperature vs power factor ($1/\rho.S^2$) which quantifies the ability to convert heat into electricity. Graphs of Seebeck coefficient exhibit the p-type semiconductor behaviour of synthesized Cu-ETT samples indicating charge carriers in the material are holes.

In the results from ALD/MLD technique, chemical composition and stoichiometry of Cu-ETT thin films were analysed in detail by FT-IR technique. Due to the overlapping of peaks in the FT-IR spectra, it was difficult to identify the exact functional groups present in the samples. Because of that, more precise means such as XPS, energy dispersive electron probe X-ray microanalysis (ED-EPMA) are required to find the chemical composition and stoichiometry

Thermoelectric properties of Cu-ETT thin films showed that the fabricated films are electrically conductive. Thermal conductivity of Cu-ETT thin films deposited on borosilicate glass substrate was not measured due to thermal contact resistance which can lead to inaccurate measurements. Graph of Seebeck coefficient exhibited the p-type semiconductor behaviour of deposited Cu-ETT film indicating charge carriers in the sample are holes. According to the electrical resistivity and FT-IR results, there is a correlation observed between having O-H groups in the film and electrical resistivity that is, O-H group in the Cu-ETT film inhibit the electrical conductivity. The reasons could be the formation of hydroxide of Cu which is not electrically conductive.

SEM images of Cu-ETT thin films showed the roughness of deposited Cu-ETT films. Due to the roughness, it was hard to analyse the film thickness by ellipsometer. Roughness of the film surface causes it to scatter light into multiple directions instead of reflecting light in a well-defined specular direction. This roughness may be due to instability of film under ambient conditions with

time. Other than the visible gradient of Cu-ETT film, wide ranged electrical resistivity evidence of a significant gradient across the film.

GI-XRD results of deposited thin film showed the crystallinity of sample and the sample contains $\text{Cu}_{1.8}\text{S}$, Cu and with trace amount of CuO. Because of these reasons it is important to consider other organic linker source to deposit electrically conductive thin films. As discussed in the literature section, high electrical conductivity of the metal organic polymer can be achieved by selecting an organic linker mainly with π conjugated system, 2-dimension. $\text{Cu}(\text{acac})_2$ or $\text{Ni}(\text{acac})_2$ still can be used as SBU because unpaired electrons of Cu^{2+} and Ni^{2+} can participate to form an extended π conjugated system with organic linker and thereby enhance the overall electrical conductivity. Selection of chelating atom affects the electrical conductivity of the metal organic polymer. According to hard and soft acid and bases (HSAB) classification Cu^+ has been identified as a softer metal ion. Cu^{2+} and Ni^{2+} have identified as intermediate metal ions. If the SBU contains Cu^+ organic linker, with N or S as chelating atoms, this can enhance the electrical conductivity of resulted metal organic polymer. HHTP, HATP and HITP are 2-D organic linker sources with extended π conjugated system and S or N as chelating atoms. If $\text{Cu}(\text{acac})_2$ or $\text{Ni}(\text{acac})_2$ are used as SBU sources then organic linkers with S, N or O chelating atom can be used. Also, HHTP, HATP, HITP or HHTP are 2-D organic linkers with extended π conjugated system suitable for SBU sources.

References

- [1] P. Sheng, Y. Sun, F. Jiao, C. Liu, W. Xu, and D. Zhu, "Optimization of the thermoelectric properties of poly[Cu_x(Cu-ethylenetetra-thiolate)]," *Synth Met*, vol. 188, pp. 111–115, Feb. 2014, doi: 10.1016/j.synthmet.2013.12.004.
- [2] J. Multia and M. Karppinen, "Atomic/Molecular Layer Deposition for Designer's Functional Metal–Organic Materials," May 01, 2022, *John Wiley and Sons Inc.* doi: 10.1002/admi.202200210.
- [3] L. S. Xie, G. Skorupskii, and M. Dincă, "Electrically Conductive Metal–Organic Frameworks," Aug. 26, 2020, *American Chemical Society*. doi: 10.1021/acs.chemrev.9b00766.
- [4] M. F. Silva, J. F. Ribeiro, J. P. Carmo, L. M. Gonçalves, and J. H. Correia, "Thin Films for Thermoelectric Applications", doi: 10.1007/978-3-642-25414-7__17.
- [5] Z. Zhou *et al.*, "Atomic layer deposition meets metal–organic frameworks," *Prog Mater Sci*, vol. 138, p. 101159, Sep. 2023, doi: 10.1016/j.pmatsci.2023.101159.
- [6] L. Jiao, J. Y. R. Seow, W. S. Skinner, Z. U. Wang, and H.-L. Jiang, "Metal–organic frameworks: Structures and functional applications," *Materials Today*, vol. 27, pp. 43–68, Jul. 2019, doi: 10.1016/j.mat-tod.2018.10.038.
- [7] J. Fonseca, T. Gong, L. Jiao, and H. L. Jiang, "Metal-organic frameworks (MOFs) beyond crystallinity: amorphous MOFs, MOF liquids and MOF glasses," May 07, 2021, *Royal Society of Chemistry*. doi: 10.1039/d1ta01043c.
- [8] Yaghi O.M, Li Guangming, and Li Hailian, "Selective binding and removal of guests in a microporous metal-organic framework," *Nature*, vol. 378, pp. 703–706, 1995.
- [9] Li Hailian, Eddaoudi Mohamed, O'Keeffe M, and Yaghi O.M, "Design and synthesis of an exceptionally stable and highly porous metal-organic framework," *Nature*, vol. 402, pp. 276–279, 1999.
- [10] Q. Li and T. Thonhauser, "A theoretical study of the hydrogen-storage potential of (H₂)₄ CH₄ in metal organic framework materials and carbon nanotubes," *Journal of Physics: Condensed Matter*, vol. 24, no. 42, p. 424204, Oct. 2012, doi: 10.1088/0953-8984/24/42/424204.
- [11] V. F. Yusuf, N. I. Malek, and S. K. Kailasa, "Review on Metal–Organic Framework Classification, Synthetic Approaches, and Influencing Factors: Applications in Energy, Drug Delivery, and Wastewater Treatment," *ACS Omega*, vol. 7, no. 49, pp. 44507–44531, Dec. 2022, doi: 10.1021/acsomega.2c05310.

- [12] Y. An *et al.*, “The stability of MOFs in aqueous solutions—research progress and prospects,” *Green Chemical Engineering*, vol. 5, no. 2, pp. 187–204, Jun. 2024, doi: 10.1016/j.gce.2023.07.004.
- [13] A. Schoedel and S. Rajeh, “Why Design Matters: From Decorated Metal Oxide Clusters to Functional Metal–Organic Frameworks,” *Top Curr Chem*, vol. 378, no. 1, p. 19, Feb. 2020, doi: 10.1007/s41061-020-0281-0.
- [14] H. Furukawa, K. E. Cordova, M. O’Keeffe, and O. M. Yaghi, “The chemistry and applications of metal-organic frameworks.,” *Science*, vol. 341, no. 6149, p. 1230444, Aug. 2013, doi: 10.1126/science.1230444.
- [15] T. Saeed *et al.*, “Structure, nomenclature and viable synthesis of micro/nanoscale metal organic frameworks and their remarkable applications in adsorption of organic pollutants,” *Microchemical Journal*, vol. 159, p. 105579, Dec. 2020, doi: 10.1016/j.microc.2020.105579.
- [16] H. Deng *et al.*, “Large-Pore Apertures in a Series of Metal-Organic Frameworks,” *Science (1979)*, vol. 336, no. 6084, pp. 1018–1023, May 2012, doi: 10.1126/science.1220131.
- [17] N. C. Burtch, J. Heinen, T. D. Bennett, D. Dubbeldam, and M. D. Allendorf, “Progress Report manuscript to Mechanical Properties in Metal-Organic Frameworks: Emerging Opportunities and Challenges for Device Functionality and Technological Applications.”
- [18] C. Xiao, J. Tian, Q. Chen, and M. Hong, “Water-stable metal-organic frameworks (MOFs): rational construction and carbon dioxide capture,” Jan. 10, 2024, *Royal Society of Chemistry*. doi: 10.1039/d3sc06076d.
- [19] Z. Cao *et al.*, “Metal–Organic Framework Materials for Electrochemical Supercapacitors,” *Nanomicro Lett*, vol. 14, no. 1, p. 181, Dec. 2022, doi: 10.1007/s40820-022-00910-9.
- [20] G. Férey, “Hybrid porous solids: Past, present, future,” *Chem Soc Rev*, vol. 37, no. 1, pp. 191–214, Dec. 2008, doi: 10.1039/b618320b.
- [21] J. Ru, X. Wang, F. Wang, X. Cui, X. Du, and X. Lu, “UiO series of metal-organic frameworks composites as advanced sorbents for the removal of heavy metal ions: Synthesis, applications and adsorption mechanism,” *Ecotoxicol Environ Saf*, vol. 208, p. 111577, Jan. 2021, doi: 10.1016/j.ecoenv.2020.111577.
- [22] H. Liu *et al.*, “Electrically Conductive Coordination Polymers for Electronic and Optoelectronic Device Applications,” Feb. 18, 2021, *American Chemical Society*. doi: 10.1021/acs.jpcclett.0c02988.
- [23] S. Takaishi *et al.*, “Electroconductive Porous Coordination Polymer Cu[Cu(pdt)₂] Composed of Donor and Acceptor Building Units,” *Inorg Chem*, vol. 48, no. 19, pp. 9048–9050, Oct. 2009, doi: 10.1021/ic802117q.

- [24] L. Sun, M. G. Campbell, and M. Dincă, “Elektrisch leitfähige poröse Metall-organische Gerüstverbindungen,” *Angewandte Chemie*, vol. 128, no. 11, pp. 3628–3642, Mar. 2016, doi: 10.1002/ange.201506219.
- [25] J. H. Dou *et al.*, “Signature of metallic behavior in the metal-organic frameworks $M_3(\text{hexaminobenzene})_2$ ($M = \text{Ni}, \text{Cu}$),” *J Am Chem Soc*, vol. 139, no. 39, pp. 13608–13611, Oct. 2017, doi: 10.1021/jacs.7b07234.
- [26] A. Walsh, K. T. Butler, and C. H. Hendon, “Chemical principles for electroactive metal-organic frameworks,” *MRS Bull*, vol. 41, no. 11, pp. 870–876, Nov. 2016, doi: 10.1557/mrs.2016.243.
- [27] S. S. Park *et al.*, “Cation-dependent intrinsic electrical conductivity in isostructural tetrathiafulvalene-based microporous metal-organic frameworks,” *J Am Chem Soc*, vol. 137, no. 5, pp. 1774–1777, Feb. 2015, doi: 10.1021/ja512437u.
- [28] C. Li, X. Sun, Y. Yao, and G. Hong, “Recent advances of electrically conductive metal-organic frameworks in electrochemical applications,” Mar. 01, 2021, *Elsevier Ltd*. doi: 10.1016/j.mtnano.2020.100105.
- [29] L. E. Darago, M. L. Aubrey, C. J. Yu, M. I. Gonzalez, and J. R. Long, “Electronic Conductivity, Ferrimagnetic Ordering, and Reductive Insertion Mediated by Organic Mixed-Valence in a Ferric Semiquinoid Metal-Organic Framework,” *J Am Chem Soc*, vol. 137, no. 50, pp. 15703–15711, Dec. 2015, doi: 10.1021/jacs.5b10385.
- [30] Y. Kobayashi, B. Jacobs, M. D. Allendorf, and J. R. Long, “Conductivity, doping, and redox chemistry of a microporous dithiolene-based metal-organic framework,” *Chemistry of Materials*, vol. 22, no. 14, pp. 4120–4122, Jul. 2010, doi: 10.1021/cm101238m.
- [31] R. Kato, “Conducting metal dithiolene complexes: Structural and electronic properties,” Nov. 2004. doi: 10.1021/cro30655t.
- [32] H. Dong, X. Fu, J. Liu, Z. Wang, and W. Hu, “25th Anniversary Article: Key Points for High-Mobility Organic Field-Effect Transistors,” Nov. 20, 2013. doi: 10.1002/adma.201302514.
- [33] R. Saha, K. Gupta, and C. J. Gómez García, “Strategies to Improve Electrical Conductivity in Metal-Organic Frameworks: A Comparative Study,” Mar. 06, 2024, *American Chemical Society*. doi: 10.1021/acs.cgd.3c01162.
- [34] J. Li, A. Kumar, B. A. Johnson, and S. Ott, “Experimental manifestation of redox-conductivity in metal-organic frameworks and its implication for semiconductor/insulator switching,” *Nat Commun*, vol. 14, no. 1, Dec. 2023, doi: 10.1038/s41467-023-40110-6.
- [35] M. Dincă and F. Léonard, “Metal-organic frameworks for electronics and photonics,” *MRS Bull*, vol. 41, no. 11, pp. 854–857, Nov. 2016, doi: 10.1557/mrs.2016.240.

- [36] M. E. Ziebel, L. E. Darago, and J. R. Long, "Control of Electronic Structure and Conductivity in Two-Dimensional Metal-Semiquinoid Frameworks of Titanium, Vanadium, and Chromium," *J Am Chem Soc*, vol. 140, no. 8, pp. 3040–3051, Feb. 2018, doi: 10.1021/jacs.7b13510.
- [37] C. Wu, P. Geng, G. Zhang, X. Li, and H. Pang, "Synthesis of Conductive MOFs and Their Electrochemical Application," Apr. 25, 2024, *John Wiley and Sons Inc.* doi: 10.1002/sml.202308264.
- [38] S. Feng, H. Duan, C. Wang, F. Hu, and W. Yan, "High electrical conductivity in a mixed-valence metal-organic framework," *Radiation Physics and Chemistry*, vol. 218, May 2024, doi: 10.1016/j.radphyschem.2024.111580.
- [39] M. G. Campbell, D. Sheberla, S. F. Liu, T. M. Swager, and M. Dincă, "Cu₃(hexaiminotriphenylene)₂: An Electrically Conductive 2D Metal–Organic Framework for Chemiresistive Sensing," *Angewandte Chemie*, vol. 127, no. 14, pp. 4423–4426, Mar. 2015, doi: 10.1002/ange.201411854.
- [40] T. Kambe *et al.*, "π-Conjugated nickel bis(dithiolene) complex nanosheet," *J Am Chem Soc*, vol. 135, no. 7, pp. 2462–2465, Feb. 2013, doi: 10.1021/ja312380b.
- [41] L. Sun, C. H. Hendon, M. A. Minier, A. Walsh, and M. Dincă, "Million-fold electrical conductivity enhancement in Fe₂(DEBDC) versus Mn₂(DEBDC) (E = S, O)," *J Am Chem Soc*, vol. 137, no. 19, pp. 6164–6167, May 2015, doi: 10.1021/jacs.5b02897.
- [42] L. Sun, T. Miyakai, S. Seki, and M. Dincă, "Mn₂(2,5-disulfhydrylbenzene-1,4-dicarboxylate): A microporous metal-organic framework with infinite (-Mn-S-)∞ chains and high intrinsic charge mobility," *J Am Chem Soc*, vol. 135, no. 22, pp. 8185–8188, Jun. 2013, doi: 10.1021/ja4037516.
- [43] E. M. Johnson, S. Ilic, and A. J. Morris, "Design Strategies for Enhanced Conductivity in Metal-Organic Frameworks," *ACS Cent Sci*, vol. 7, no. 3, pp. 445–453, Mar. 2021, doi: 10.1021/acscentsci.1c00047.
- [44] H. T. B. Pham *et al.*, "Imparting Functionality and Enhanced Surface Area to a 2D Electrically Conductive MOF via Macrocyclic Linker," *J Am Chem Soc*, vol. 144, no. 23, pp. 10615–10621, Jun. 2022, doi: 10.1021/jacs.2c03793.
- [45] R. W. Day *et al.*, "Single Crystals of Electrically Conductive Two-Dimensional Metal-Organic Frameworks: Structural and Electrical Transport Properties," *ACS Cent Sci*, vol. 5, no. 12, pp. 1959–1964, Dec. 2019, doi: 10.1021/acscentsci.9b01006.
- [46] J. Park *et al.*, "Two-Dimensional Conductive Ni-HAB as a Catalyst for the Electrochemical Oxygen Reduction Reaction," *ACS Appl Mater Interfaces*, vol. 12, no. 35, pp. 39074–39081, Sep. 2020, doi: 10.1021/acsami.0c09323.

- [47] D. Kim, D. W. Kim, W. G. Hong, and A. Coskun, "Graphene/ZIF-8 composites with tunable hierarchical porosity and electrical conductivity," *J Mater Chem A Mater*, vol. 4, no. 20, pp. 7710–7717, 2016, doi: 10.1039/c6ta01899h.
- [48] R. Saha and C. J. Gomez Garcia, "Extrinsically conducting MOFs: guest-promoted enhancement of electrical conductivity, thin film fabrication and applications," 2024, *Royal Society of Chemistry*. doi: 10.1039/d4cs00141a.
- [49] Z. C. Zhang, Z. G. Gu, and J. Zhang, "Host–Guest Metal–Organic Frameworks-Based Long-Afterglow Luminescence Materials," Jul. 01, 2024, *Multidisciplinary Digital Publishing Institute (MDPI)*. doi: 10.3390/molecules29132989.
- [50] D. K. Panda, K. Maity, A. Palukoshka, F. Ibrahim, and S. Saha, "Li + Ion-Conducting Sulfonate-Based Neutral Metal-Organic Framework," *ACS Sustain Chem Eng*, vol. 7, no. 5, pp. 4619–4624, Mar. 2019, doi: 10.1021/acssuschemeng.8b06254.
- [51] C. Lu, T. Ben, S. Xu, and S. Qiu, "Electrochemical Synthesis of a Microporous Conductive Polymer Based on a Metal–Organic Framework Thin Film," *Angewandte Chemie*, vol. 126, no. 25, pp. 6572–6576, Jun. 2014, doi: 10.1002/ange.201402950.
- [52] L. Sun *et al.*, "A Microporous and Naturally Nanostructured Thermoelectric Metal-Organic Framework with Ultralow Thermal Conductivity," *Joule*, vol. 1, no. 1, pp. 168–177, Sep. 2017, doi: 10.1016/j.joule.2017.07.018.
- [53] K. Epp, I. Luz, W. R. Heinz, A. Rapeyko, F. X. Llabrés i Xamena, and R. A. Fischer, "Defect-Engineered Ruthenium MOFs as Versatile Heterogeneous Hydrogenation Catalysts," *ChemCatChem*, vol. 12, no. 6, pp. 1720–1725, Mar. 2020, doi: 10.1002/cctc.201902079.
- [54] I. Periyaiyah *et al.*, "Facile synthesis of Co-Cu metal organic framework as efficient non-noble bifunctional electrocatalysts for overall water splitting," *Applied Surface Science Advances*, vol. 21, Jun. 2024, doi: 10.1016/j.apsadv.2024.100593.
- [55] K. Wada, K. Sakaushi, S. Sasaki, and H. Nishihara, "Multielectron-Transfer-based Rechargeable Energy Storage of Two-Dimensional Coordination Frameworks with Non-Innocent Ligands," *Angewandte Chemie*, vol. 130, no. 29, pp. 9024–9028, Jul. 2018, doi: 10.1002/ange.201802521.
- [56] D. Sheberla, J. C. Bachman, J. S. Elias, C. J. Sun, Y. Shao-Horn, and M. Dincă, "Conductive MOF electrodes for stable supercapacitors with high areal capacitance," *Nat Mater*, vol. 16, no. 2, pp. 220–224, Feb. 2017, doi: 10.1038/nmat4766.
- [57] B. Wang, Y. Luo, B. Liu, and G. Duan, "Field-Effect Transistor Based on an in Situ Grown Metal-Organic Framework Film as a Liquid-Gated

- Sensing Device,” *ACS Appl Mater Interfaces*, vol. 11, no. 39, pp. 35935–35940, Oct. 2019, doi: 10.1021/acsami.9b14319.
- [58] H. Nagatomi, N. Yanai, T. Yamada, K. Shiraishi, and N. Kimizuka, “Synthesis and Electric Properties of a Two-Dimensional Metal-Organic Framework Based on Phthalocyanine,” *Chemistry - A European Journal*, vol. 24, no. 8, pp. 1806–1810, Feb. 2018, doi: 10.1002/chem.201705530.
- [59] J. Wang, T. Chen, J. J. Oppenheim, M. Jeon, B. Tan, and M. Dincă, “Superior charge transport in Ni-diamine conductive MOFs”, doi: 10.26434/chemrxiv-2024-vfd45.
- [60] W. H. Li *et al.*, “Conductive Metal–Organic Framework Nanowire Array Electrodes for High-Performance Solid-State Supercapacitors,” *Adv Funct Mater*, vol. 27, no. 27, Jul. 2017, doi: 10.1002/adfm.201702067.
- [61] J. Park *et al.*, “Synthetic Routes for a 2D Semiconductive Copper Hexahydroxybenzene Metal-Organic Framework,” *J Am Chem Soc*, vol. 140, no. 44, pp. 14533–14537, Nov. 2018, doi: 10.1021/jacs.8b06666.
- [62] L. Mendecki, M. Ko, X. Zhang, Z. Meng, and K. A. Mirica, “Porous Scaffolds for Electrochemically Controlled Reversible Capture and Release of Ethylene,” *J Am Chem Soc*, vol. 139, no. 48, pp. 17229–17232, Dec. 2017, doi: 10.1021/jacs.7b08102.
- [63] A. A. Talin *et al.*, “Tunable Electrical Conductivity in Metal-Organic Framework Thin-Film Devices,” 2014. [Online]. Available: <https://www.science.org>
- [64] D. Sheberla *et al.*, “High electrical conductivity in Ni₃(2,3,6,7,10,11-hexaiminotriphenylene)₂, a semiconducting metal-organic graphene analogue,” *J Am Chem Soc*, vol. 136, no. 25, pp. 8859–8862, Jun. 2014, doi: 10.1021/ja502765n.
- [65] X. Yang *et al.*, “Wet-Adhesive On-Skin Sensors Based on Metal–Organic Frameworks for Wireless Monitoring of Metabolites in Sweat,” *Advanced Materials*, vol. 34, no. 44, Nov. 2022, doi: 10.1002/adma.202201768.
- [66] H. Jia, Y. Yao, J. Zhao, Y. Gao, Z. Luo, and P. Du, “A novel two-dimensional nickel phthalocyanine-based metal-organic framework for highly efficient water oxidation catalysis,” *J Mater Chem A Mater*, vol. 6, no. 3, pp. 1188–1195, 2018, doi: 10.1039/c7ta07978h.
- [67] X. Sun, K. H. Wu, R. Sakamoto, T. Kusamoto, H. Maeda, and H. Nishihara, “Conducting p-conjugated bis(iminothiolato)nickel nanosheet,” *Chem Lett*, vol. 46, no. 8, pp. 1072–1075, 2017, doi: 10.1246/cl.170382.
- [68] X. Sun *et al.*, “Bis(aminothiolato)nickel nanosheet as a redox switch for conductivity and an electrocatalyst for the hydrogen evolution reaction,” *Chem Sci*, vol. 8, no. 12, pp. 8078–8085, 2017, doi: 10.1039/c7sc02688a.

- [69] C. P. Raptopoulou, “Metal-organic frameworks: Synthetic methods and potential applications,” Jan. 02, 2021, *MDPI AG*. doi: 10.3390/ma14020310.
- [70] P. Mao *et al.*, “Recent advances in synthesis of two-dimensional conductive metal-organic frameworks and their electrochemical energy storage application,” Dec. 01, 2021, *Elsevier B.V.* doi: 10.1016/j.susmat.2021.e00354.
- [71] Y. R. Lee, J. Kim, and W. S. Ahn, “Synthesis of metal-organic frameworks: A mini review,” Sep. 2013. doi: 10.1007/s11814-013-0140-6.
- [72] M. Hmadeh *et al.*, “New porous crystals of extended metal-catecholates,” *Chemistry of Materials*, vol. 24, no. 18, pp. 3511–3513, Sep. 2012, doi: 10.1021/cm301194a.
- [73] M. H. Hassan *et al.*, “Electrically Conductive, Monolithic Metal-Organic Framework-Graphene (MOF@G) Composite Coatings,” *ACS Appl Mater Interfaces*, vol. 11, no. 6, pp. 6442–6447, Feb. 2019, doi: 10.1021/acsami.8b20951.
- [74] X. Wu *et al.*, “Rapid microwave synthesis of Ru-supported partially carbonized conductive metal-organic framework for efficient hydrogen evolution,” *Chemical Engineering Journal*, vol. 431, Mar. 2022, doi: 10.1016/j.cej.2021.133247.
- [75] H. Jeong, G. Park, J. Jeon, and S. S. Park, “Fabricating Large-Area Thin Films of 2D Conductive Metal-Organic Frameworks,” *Acc Chem Res*, vol. 57, no. 16, pp. 2336–2346, Aug. 2024, doi: 10.1021/acs.accounts.4c00292.
- [76] M. Choe *et al.*, “Chemical Vapor Deposition of Edge-on Oriented 2D Conductive Metal-Organic Framework Thin Films,” *J Am Chem Soc*, vol. 144, no. 37, pp. 16726–16731, Sep. 2022, doi: 10.1021/jacs.2c07135.
- [77] H. Van Bui, F. Grillo, and J. R. Van Ommen, “Atomic and molecular layer deposition: off the beaten track,” *Chemical Communications*, vol. 53, no. 1, pp. 45–71, 2017, doi: 10.1039/c6cc05568k.
- [78] P. Sundberg and M. Karppinen, “Organic and inorganic-organic thin film structures by molecular layer deposition: A review,” 2014, *Beilstein-Institut Zur Forderung der Chemischen Wissenschaften*. doi: 10.3762/bjnano.5.123.
- [79] A. J. Karttunen, T. Tynell, and M. Karppinen, “Atomic-level structural and electronic properties of hybrid inorganic-organic ZnO:Hydroquinone superlattices fabricated by ALD/MLD,” *Journal of Physical Chemistry C*, vol. 119, no. 23, pp. 13105–13114, Jun. 2015, doi: 10.1021/acs.jpcc.5b03433.
- [80] Y. Liu *et al.*, “Electrochemical Synthesis of Large Area Two-Dimensional Metal-Organic Framework Films on Copper Anodes,”

Angewandte Chemie - International Edition, vol. 60, no. 6, pp. 2887–2891, Feb. 2021, doi: 10.1002/anie.202012971.

- [81] M. Yao *et al.*, “Layer-by-Layer Assembled Conductive Metal–Organic Framework Nanofilms for Room-Temperature Chemiresistive Sensing,” *Angewandte Chemie*, vol. 129, no. 52, pp. 16737–16741, Dec. 2017, doi: 10.1002/ange.201709558.
- [82] M. d’Angelo, C. Galassi, and N. Lecis, “Thermoelectric Materials and Applications: A Review,” Sep. 01, 2023, *Multidisciplinary Digital Publishing Institute (MDPI)*. doi: 10.3390/en16176409.
- [83] Y. Sun *et al.*, “Organic thermoelectric materials and devices based on p- and n-type poly(metal 1,1,2,2-ethenetetrathiolate)s,” *Advanced Materials*, vol. 24, no. 7, pp. 932–937, Feb. 2012, doi: 10.1002/adma.201104305.
- [84] A. K. Menon, R. M. W. Wolfe, S. R. Marder, J. R. Reynolds, and S. K. Yee, “Systematic Power Factor Enhancement in n-Type NiETT/PVDF Composite Films,” *Adv Funct Mater*, vol. 28, no. 29, Jul. 2018, doi: 10.1002/adfm.201801620.
- [85] P. Sheng, Y. Sun, F. Jiao, C. Di, W. Xu, and D. Zhu, “A novel cuprous ethylenetetrathiolate coordination polymer: Structure characterization, thermoelectric property optimization and a bulk thermogenerator demonstration,” *Synth Met*, vol. 193, pp. 1–7, 2014, doi: 10.1016/j.synthmet.2014.03.024.
- [86] Y. Sun *et al.*, “Organic thermoelectric materials and devices based on p- and n-type poly(metal 1,1,2,2-ethenetetrathiolate)s,” *Advanced Materials*, vol. 24, no. 7, pp. 932–937, Feb. 2012, doi: 10.1002/adma.201104305.
- [87] Y. Sun *et al.*, “Flexible n-Type High-Performance Thermoelectric Thin Films of Poly(nickel-ethylenetetrathiolate) Prepared by an Electrochemical Method,” *Advanced Materials*, vol. 28, no. 17, pp. 3351–3358, May 2016, doi: 10.1002/adma.201505922.
- [88] R. Tkachov *et al.*, “Polyethenetetrathiolate or polytetrathiooxalate? Improved synthesis, a comparative analysis of a prominent thermoelectric polymer and implications to the charge transport mechanism,” *Polym Chem*, vol. 9, no. 36, pp. 4543–4555, Sep. 2018, doi: 10.1039/c8py00931g.
- [89] D. K. Gupta *et al.*, “Trace level monitoring of Cu(II) ion using CuS particles based membrane electrochemical sensor,” *Heliyon*, vol. 7, no. 6, Jun. 2021, doi: 10.1016/j.heliyon.2021.e07167.
- [90] S. Nachimuthu, K. Kannan, S. Thangavel, and K. Gurushankar, “Electrochemical and magnetic properties of 3D porous NiS/CuS nanocomposites,” *Applied Surface Science Advances*, vol. 7, Feb. 2022, doi: 10.1016/j.apsadv.2022.100209.

- [91] D. L. . Pavia, G. M. . Lampman, G. S. . Kriz, and J. R. . Vyvyan, *Introduction to spectroscopy*. Brooks/Cole, Cengage Learning, 2009.
- [92] A. B. D. Nandiyanto, R. Ragadhita, and M. Fiandini, “Interpretation of Fourier Transform Infrared Spectra (FTIR): A Practical Approach in the Polymer/Plastic Thermal Decomposition,” *Indonesian Journal of Science and Technology*, vol. 8, no. 1, pp. 113–126, 2023, doi: 10.17509/ijost.v8i1.53297.
- [93] Brian C. Smith, “Spectroscopic solutions for material analysis,” Nov. 2020. [Online]. Available: www.milestonesci.com/digestion|866.995.5100
- [94] B. Li, F. DeAngelis, G. Chen, and A. Henry, “The importance of localized modes spectral contribution to thermal conductivity in amorphous polymers,” *Commun Phys*, vol. 5, no. 1, Dec. 2022, doi: 10.1038/s42005-022-01103-x.
- [95] Y. Ren, K. Wu, D. F. Coker, and N. Quirke, “Thermal transport in model copper-polyethylene interfaces,” *Journal of Chemical Physics*, vol. 151, no. 17, Nov. 2019, doi: 10.1063/1.5123616.
- [96] V. Singh *et al.*, “High thermal conductivity of chain-oriented amorphous polythiophene,” *Nat Nanotechnol*, vol. 9, no. 5, pp. 384–390, 2014, doi: 10.1038/nnano.2014.44.
- [97] R. Muthaiah and J. Garg, “Temperature effects in the thermal conductivity of aligned amorphous polyethylene - A molecular dynamics study,” *J Appl Phys*, vol. 124, no. 10, Sep. 2018, doi: 10.1063/1.5041000.
- [98] M. Z. Rajab and K. M. Ziadan, “The effect of the solvents on electrical properties of pot conducting polymer,” *Mechanics of Advanced Composite Structures*, vol. 8, no. 2, pp. 283–289, Jun. 2021, doi: 10.22075/MACS.2021.21274.1302.
- [99] K. Shrestha, D. Whitfield, V. C. Lopes, A. J. Syllaios, and C. L. Littler, “Electrical conductivity and structural order of P-type amorphous silicon thin films,” in *Materials Research Society Symposium Proceedings*, Materials Research Society, 2015, pp. 1–6. doi: 10.1557/opl.2014.962.
- [100] S. Pak, “Controlled p-Type Doping of MoS₂ Monolayer by Copper Chloride,” *Nanomaterials*, vol. 12, no. 17, Sep. 2022, doi: 10.3390/nano12172893.
- [101] M. Koopmans *et al.*, “Electrical Conductivity of Doped Organic Semiconductors Limited by Carrier-Carrier Interactions,” *ACS Appl Mater Interfaces*, vol. 12, no. 50, pp. 56222–56230, Dec. 2020, doi: 10.1021/acsami.0c15490.
- [102] X. Guan and J. Ouyang, “Enhancement of the Seebeck Coefficient of Organic Thermoelectric Materials via Energy Filtering of Charge

Carriers,” Oct. 01, 2021, *Chinese Chemical Society*. doi: 10.31635/ccschem.021.202101069.

- [103] A. C. Iyasara *et al.*, “Seebeck Coefficient, Electrical Conductivity and Thermal Conductivity as Veritable Tools for Measuring the Thermoelectric Performance of Engineering Materials Osonwa Nobert Okechinyere Akanu Ibiam Federal Polytechnic, Unwana Isiaka Olajide Odewale Akanu Ibiam Federal Polytechnic, Unwana Seebeck Coefficient, Electrical Conductivity and Thermal Conductivity as Veritable Tools for Measuring the Thermoelectric Performance of Engineering Materials.” [Online]. Available: www.accegate.com/papers@accegate.com1 | page
- [104] J. Hennessy and S. Nikzad, “Atomic Layer Deposition of Lithium Fluoride Optical Coatings for the Ultraviolet,” *Inorganics (Basel)*, vol. 6, no. 2, p. 46, May 2018, doi: 10.3390/inorganics6020046.
- [105] V. Sallaz *et al.*, “Dual Storage Mechanism in Nanoscale Solid-State Lithium-Ion Supercapacitors,” *ACS Electrochemistry*, Oct. 2024, doi: 10.1021/acselectrochem.4c00022.
- [106] M. Madadi, M. Heikkinen, A. Philip, and M. Karppinen, “Conformal High-Aspect-Ratio Solid Electrolyte Thin Films for Li-Ion Batteries by Atomic Layer Deposition,” *ACS Appl Electron Mater*, vol. 6, no. 3, pp. 1574–1580, Mar. 2024, doi: 10.1021/acsaelm.3c01565.
- [107] A. J. Pearse *et al.*, “Nanoscale Solid State Batteries Enabled by Thermal Atomic Layer Deposition of a Lithium Polyphosphazene Solid State Electrolyte,” *Chemistry of Materials*, vol. 29, no. 8, pp. 3740–3753, Apr. 2017, doi: 10.1021/acs.chemmater.7b00805.
- [108] G. Bartholazzi, M. M. Shehata, D. H. Macdonald, and L. E. Black, “Atomic layer deposition of Cu₂O using copper acetylacetonate,” *Journal of Vacuum Science & Technology A*, vol. 41, no. 2, Mar. 2023, doi: 10.1116/6.0002238.
- [109] T. S. Tripathi *et al.*, “Atomic Layer Deposition of Copper Metal Films from Cu(acac)₂ and Hydroquinone Reductant,” *Adv Eng Mater*, vol. 23, no. 10, Oct. 2021, doi: 10.1002/adem.202100446.
- [110] H. H. Sønsteby *et al.*, “tert-butoxides as Precursors for Atomic Layer Deposition of Alkali Metal Containing Thin Films.”
- [111] S. I. Raj, A. Jaiswal, and I. Uddin, “Ultrasmall aqueous starch-capped CuS quantum dots with tunable localized surface plasmon resonance and composition for the selective and sensitive detection of mercury(ii) ions,” *RSC Adv*, vol. 10, no. 24, pp. 14050–14059, Apr. 2020, doi: 10.1039/c9ra09306k.
- [112] D. Shao and Q. Wei, “Microwave-assisted rapid preparation of nano-ZnO/Ag composite functionalized polyester nonwoven membrane for improving its UV shielding and antibacterial properties,” *Materials*, vol. 11, no. 8, Aug. 2018, doi: 10.3390/ma11081412.

- [113] E. Darezereshki, A. B. Vakylabad, A. Hassanzadeh, T. Niedoba, A. Surowiak, and B. Koohestani, "Hydrometallurgical synthesis of nickel nano-sulfides from spent lithium-ion batteries," *Minerals*, vol. 11, no. 4, Apr. 2021, doi: 10.3390/min11040419.
- [114] A. Gahtar, S. Benramache, A. Ammari, A. Boukhachem, and A. Zi-ouche, "Effect of molar concentration on the physical properties of NiS thin film prepared by spray pyrolysis method for supercapacitors," *Inorganic and Nano-Metal Chemistry*, vol. 52, no. 1, pp. 112–121, 2022, doi: 10.1080/24701556.2020.1862225.
- [115] Matthew. Laudon and Bart. Romanowicz, *Nanotech conference and expo 2010 : an interdisciplinary integrative forum on nanotechnology, biotechnology and microtechnology*. Nano Science and Technology Institute, 2010.
- [116] J. Kaur, A. Khanna, R. Kumar, and R. Chandra, "Growth and characterization of Cu₂O and CuO thin films," *Journal of Materials Science: Materials in Electronics*, vol. 33, no. 20, pp. 16154–16166, Jul. 2022, doi: 10.1007/s10854-022-08506-0.
- [117] Y. L. Cheng, K. W. Leon, J. F. Huang, W. Y. Chang, Y. M. Chang, and J. Leu, "Effect of moisture on electrical properties and reliability of low dielectric constant materials," *Microelectron Eng*, vol. 114, pp. 12–16, 2014, doi: 10.1016/j.mee.2013.08.018.
- [118] B. P. Dhonge, S. S. Ray, and B. Mwakikunga, "Electronic to protonic conduction switching in Cu₂O nanostructured porous films: The effect of humidity exposure," *RSC Adv*, vol. 7, no. 35, pp. 21703–21712, 2017, doi: 10.1039/c7ra00383h.
- [119] M. Kristl, B. Dojer, S. Gyergyek, and J. Kristl, "Synthesis of nickel and cobalt sulfide nanoparticles using a low cost sonochemical method," *Heliyon*, vol. 3, no. 3, Mar. 2017, doi: 10.1016/j.heliyon.2017.e00273.